EXAMINING THE RELATIONSHIP BETWEEN BOLD FMRI AND INFRASLOW EEG SIGNALS IN THE RESTING HUMAN BRAIN

A Thesis
Presented to
The Academic Faculty

By

Joshua Koehler Grooms

In Partial Fulfillment
Of the Requirements for the Degree
Master of Science in Biomedical Engineering

Georgia Institute of Technology
and Emory University

August, 2015

Examining the Relationship between BOLD fMRI and Infraslow EEG Signals in the Resting Human Brain

Approved By:

Dr. Shella D. Keilholz, Advisor
Department of Biomedical Engineering
Georgia Institute of Technology and Emory University

Dr. Charles Epstein
Department of Neurology
The Emory Clinic

Dr. Xiaoping Hu
Department of Biomedical Engineering
Georgia Institute of Technology and Emory University

Date Approved: June 19th, 2015

ACKNOWLEDGMENTS

The work that went into creating this thesis was performed in the Magnetic Imaging of Neural Dynamics (MIND) Laboratory at the Georgia Institute of Technology and Emory University. None of this would have been possible without everyone's kindness, wisdom, patience, and willingness to introduce me to the wonderfully interesting yet incredibly difficult field of neuroscience and neuroimaging. To current and former lab members Jacob Billings, Matthew Magnuson, Michael Merritt, Sadia Shakil, Garth Thompson, and Wenju Pan, I especially thank you for all of your help with this project. Your contributions to collecting and analyzing data, as well as your critiques and insights, have been invaluable. To Dr. Shella Keilholz, who served as my advisor, mentor, and friend over the past several years, I thank you most of all. I will be forever grateful for all of your guidance throughout my studies, and will always remember my time with the lab fondly.

I would also like to thank other contributors for their roles in this project. Dr. Eric Schumacher and his lab at Georgia Tech provided much needed help in the acquisition and analysis of our human data. Dr. Charles Epstein lent us his considerable expertise in acquiring and analyzing all of our data, particularly with EEG, and was also a valued member of my thesis committee. Dr. Xiaoping Hu also served on my committee and contributed his insights to this work. Other contributors include: Nytavia Wallace at the Center for Advanced Brain Imaging, Dr. Alessio Medda at the Georgia Tech Research Institute, and the United States Air Force Center of Excellence, who provided the funding for this project. My deepest thanks to you all.

Lastly, I would like to thank my family and friends: Mom, Dad, Matt, Jen, and in particular Vanessa for everything that you all have done for me. I would not have been able to do this without you!

TABLE OF CONTENTS

LIST OF FIGURES

LIST OF COMMON ABBREVIATIONS

BOLD	Blood Oxygen-Level Dependent
DMN	Default Mode Network
IC	Independent Component
ICA	Independent Component Analysis
EEG	Electroencephalography
FWER	Family-Wise Error Rate
fMRI	Functional Magnetic Resonance Imaging
LFP	Local Field Potential
MRI	Magnetic Resonance Imaging
RSN	Resting State Network
SGoF	Sequential Goodness of Fit
SMN	Sensorimotor Network
SWC	Sliding Window Correlation
TPN	Task-Positive Network
TR	Repetition Time

SUMMARY

Resting state functional magnetic resonance imaging (fMRI) is currently at the forefront of research on cognition and the brain's large-scale organization. Patterns of hemodynamic activity that it records have been strongly linked to certain behaviors and cognitive pathologies. These signals are widely assumed to reflect local neuronal activity but our understanding of the exact relationship between them remains incomplete. Researchers often address this using multimodal approaches, pairing fMRI signals with known measures of neuronal activity such as electroencephalography (EEG). It has long been thought that infraslow (< 0.1 Hz) fMRI signals, which have become so important to the study of brain function, might have a direct electrophysiological counterpart. If true, EEG could be positioned as a low-cost alternative to fMRI when fMRI is impractical and therefore could also become much more influential in the study of functional brain networks. Previous works have produced indirect support for the fMRI-EEG relationship, but until recently the hypothesized link between them had not been tested in resting humans. The objective of this study was to investigate and characterize their relationship by simultaneously recording infraslow fMRI and EEG signals in resting human adults. We present evidence strongly supporting their link by demonstrating significant stationary and dynamic correlations between the two signal types. Moreover, functional brain networks appear to be a fundamental unit of this coupling. We conclude that infraslow electrophysiology is likely playing an important role in the dynamic configuration of the resting state brain networks that are well-known to fMRI research. Our results provide new insights into the neuronal underpinnings of hemodynamic activity and a foundational point on which the use of infraslow EEG in functional connectivity studies can be based.

CHAPTER 1

INTRODUCTION

1.1 – Functional Magnetic Resonance Imaging (fMRI)

Functional magnetic resonance imaging (fMRI) is a relatively recent development in the field of neuroimaging (Belliveau et al., 1990; Ogawa and Lee, 1990). In the past 25 years, its use has undergone an explosive growth (Friston, 2011; Raichle, 2011) that today places it in the forefront of neuroscience research, particularly in the study of large-scale brain organization. The reason behind its popularity is simple: fMRI is capable of non-invasively producing very spatially resolved mappings of *in vivo* brain activity. In this endeavor, there are no currently known alternatives capable of matching both its safety and spatial resolution in living subjects.

The topic of fMRI, from its theoretical foundations to its practical applications, is an entire science unto itself. There are tomes of literature in existence covering this field in exquisite detail that we simply cannot replicate or even adequately summarize in the allotted space here. As such, we refer interested readers to some selected examples of these (Buxton, 2009; Faro and Mohamed, 2010; Huettel et al., 2009; Logothetis and Wandell, 2004; Logothetis et al., 2001; Nair, 2005; Sharma, 2012) and resort to considering only the barest essentials that directly relate to our study as an introduction.

1.1.1 – Blood Oxygenation Level Dependent (BOLD) fMRI

As its name implies, fMRI is actually a specific application of magnetic resonance imaging (MRI), which has been in use since the 1970s (Lauterbur, 1973) and is routinely invoked to produce high contrast, high resolution *in vivo* tissue images. fMRI measures brain activity through MRI using special contrast mechanisms, perhaps the most popular of which is blood oxygenation level dependent (BOLD) contrast. BOLD fMRI relies on the circulatory system's oxygenated and deoxygenated hemoglobin content as an endogenous contrast agent to produce images (Belliveau et al., 1991; Kwong et al., 1992; Ogawa et al., 1992). Fluctuations in the BOLD signal amplitude arise from localized changes in oxyhemoglobin-to-deoxyhemoglobin ratios, which themselves are often the result of changes in local metabolic demands. When using fMRI to image the brain, we ascribe a majority of these changes to fluctuating levels of neuronal activity.

BOLD fMRI is typically used to record four-dimensional images of the brain. Each recording is comprised of *voxels*, or volumetric elements, that occupy a position in three-dimensional space at a single point in time. Thus, one 4D image is actually an array of signals that detail the ongoing changes in blood oxygenation throughout the vasculature supplying the brain. Modern fMRI equipment allows us to digitize BOLD activity across the entire volume of a participant's skull at spatial resolutions of only a few cubic millimeters, and even higher resolutions are possible using state-of-the-art technologies (Bianciardi et al., 2009; Hyde and Li, 2014; Neuner et al., 2013). Combined with its non-invasiveness and lack of ionizing radiation exposure, such a well-resolved window into the living brain volume makes fMRI the preeminent neuroimaging modality that it is today.

Unfortunately, the temporal resolution afforded by BOLD fMRI is rather poor by comparison, which introduces difficulties in reconciling functional signals with true brain activity. To make matters worse, this problem is not merely a technological limitation. The hemodynamics that BOLD signals reflect fluctuate very slowly relative to the rapid electrical activity that is thought to underpin cognitive processing. To provide some perspective, a hypothetical neuronal event might take place across 100 milliseconds of time while the hemodynamic response to it would require approximately 10 seconds to evolve (Huettel et al., 2009; Poldrack et al., 2011). Thus, regardless of how fast the scanning equipment is, it can only capture fluctuations that are low-pass filtered representations of the brain activity that caused them (Logothetis et al., 2001).

1.1.2 – The Neural Basis of the BOLD Signal

By their nature, BOLD signals are a proxy measure of neuronal activity. Their dependence on changes in blood oxygenation means that communication throughout the brain's extensive neuronal networks is not directly observed. Instead, we observe the influence that such communications have on a circulatory system that is constantly adapting to serve metabolic needs. This poses problems when trying to interpret BOLD signals in terms of brain function; our ability to make sense of fMRI data relies heavily on how well we understand the link between their so-called *hemodynamics* and neuronal activities.

The neuroimaging community has expended considerable effort in pursuit of understanding this link. As a result, we now widely accept that BOLD signals generally reflect neuronal communications. Supporting evidence comes from several early studies

that demonstrated a clear relationship between changes in brain activity and changes in blood flow and oxygenation (Belliveau et al., 1991; Kwong et al., 1992; Ogawa et al., 1992), both of which are captured by BOLD signals. Additional evidence is provided by studies utilizing multiple imaging modalities. These combine the recording of hemodynamics with the recording of direct measures of brain activity (typically electrophysiology) and then attempt to describe relationships between the two. To cite one important example, Logothetis et al. showed an excellent correspondence between BOLD fluctuations and regional electrical activity from groups of neurons by simultaneously recording both signal types in non-human primates (Logothetis et al., 2001). Others have since reported similar findings (Goense and Logothetis, 2008; Rauch et al., 2008; Shmuel et al., 2006).

Despite these advances, we do not yet possess a comprehensive description of the neurovascular coupling mechanism. Many questions remain unanswered that will likely have a profound impact on the way we interpret fMRI data. For example, it is still unclear whether or not various neuronal processes contribute equally or disproportionately to BOLD responses. We mentioned earlier that researchers have been addressing this very question through multimodal studies. However, their findings to date indicate that the relationship is complex and not always straightforward to characterize. As we shall see throughout this text, one of the major goals of our study is to provide some additional information about the neural basis of BOLD signals by using a method that, until recently, has been relatively unexploited.

1.2 – Functional Connectivity

Understanding how cognition and behavior emerges from the interactions of widespread brain structures requires a thorough knowledge of how these structures are organized. Some of that knowledge can be obtained by studying how large-scale brain regions cooperate with one another and coordinate their activities over time in order to perform tasks or give rise to seemingly spontaneous events. Although not exclusively, this is the domain of functional connectivity research, and it is a central topic that pervades the coming chapters of this study.

The term *functional connectivity* refers to a tendency for certain separate brain regions to behave similarly to one another over time. To say that two regions are functionally connected is to say that they have well-correlated measures of their underlying neuronal activities (Friston et al., 1993; Horwitz, 2003), which in turn suggests that they serve related functions. As a topic of investigation, functional connectivity is a specialization of broader research efforts that are attempting to understand the organization, or connectivity, of the brain. The specificity of the term is intended to disambiguate it from separate but related concepts, which together include brain areas connected by anatomy (*anatomical* connectivity), by function (*functional* connectivity), or by causal influence (*effective* connectivity).

The brain's functionally connected nature was first documented using electrophysiology (Gerstein, 1970) and it has been shown that neuronal electrical activities can be coherent between both local clusters of neurons (Frostig et al., 1983) and distant regions on opposing

brain hemispheres (French and Beaumont, 1984). Shortly thereafter, this phenomenon was observed using other measures of neuronal activity, such as the glucose metabolic rate (Clark et al., 1984; Horwitz et al., 1984; Metter et al., 1984) and regional cerebral blood flow (Friston et al., 1993; Horwitz et al., 1995, 1992; Zeki et al., 1991) data recorded by positron emission tomography (PET).

The first application of fMRI to functional connectivity research came not long after the inception of the imaging technology and quickly superseded the use of PET in this capacity. In that landmark study, strong correlations were found between hemodynamic signals originating from the bilateral sensorimotor cortices and other remote areas in resting humans (Biswal, 1995). Additionally, it was noted that this connectivity tended to occur in the very slowly oscillating components (<0.1 Hz) of the signals from these areas, which later would be shown to be of particular importance for these apparently synchronized regions (Cordes et al., 2000).

These initial results had a profound impact on the field. By establishing fMRI as a viable tool for the study of functional connectivity, Biswal et al set the stage for two decades of subsequent research that would extensively chart and characterize the large-scale functional organization of the brain. Moreover, their research helped shift attention to the *infraslow* (<0.1 Hz) activity occurring throughout the brain, which is now thought to play a role in long-range communications between remote but functionally connected areas (Buzsáki, 2006; Elbert, 1993; Khader et al., 2008).

1.2.1 – Static Functional Connectivity

The discovery of functional connectivity in fMRI recordings fueled an effort to map a complete set of functionally connected brain networks. Researchers have applied many different methods over the years in pursuit of this goal, but many of them share a common important detail; they were applied to data acquired from test subjects that were at rest. Typically, a resting state is defined as one in which volunteers remain awake but are relaxed and thinking freely. By this approach it is expected that recordings reflect spontaneous brain activity that is unique to the individual or scanning trial. This outcome contrasts with that of a task state, during which subjects perform an activity while being imaged. Task states are often employed to elicit a prescribed or predictable sequence of brain activity across multiple trials, facilitating comparisons across many individuals.

The fact that the first and many subsequent networks were discovered from resting subjects has led to them being called *resting state functional networks* (RSNs). Such networks are by definition collections of nodes, or brain regions, whose hemodynamic activities are similar over the entire measurement duration. Their existence and number demonstrates that the brain does not idle, even in relaxed individuals, but instead is constantly maintaining a complex organizational scheme (Buckner and Vincent, 2007; Buckner et al., 2008; Greicius, 2008) that is likely involved in continuous information processing and cognition (Biswal et al., 1997; Cordes et al., 2000; Greicius et al., 2003; Lowe et al., 2000)

In order to identify RSNs, many researchers (Biswal, 1995; Biswal et al., 1997; Cordes et al., 2001, 2000; Fox et al., 2006, 2005; Fransson, 2005; Greicius et al., 2003; Jiang et al.,

2004; Laufs et al., 2003a; Lowe et al., 1998) have followed approaches similar to those that Biswal et al. laid out in their initial fMRI study, whereby a candidate network node is manually selected from the brain and all other nodes that are significantly correlated with it are identified. Although easy to understand and apply, this method requires *a priori* knowledge of an interesting candidate node and is not easily applied to the study of functional connectivity across the entire brain (van den Heuvel and Hulshoff Pol, 2010). Other studies have employed more data-driven approaches that cluster functionally connected areas and overcome that particular shortcoming. Among these is independent component analysis (ICA), which has become a popular and extensively used tool to simultaneously identify multiple RSNs across the whole brain (Calhoun and Adali, 2001; Calhoun et al., 2001; Damoiseaux et al., 2006; De Luca et al., 2006; Mantini et al., 2007; McKeown et al., 1997; van de Ven et al., 2004). We will discuss ICA in more detail in Section 3.4.1 as it was applied to data from our study.

Regardless of the approach used, a number of RSNs have been mapped using fMRI that are robustly consistent across trials, individuals, and studies (Biswal et al., 1997; Damoiseaux et al., 2006; De Luca et al., 2006; Fox and Raichle, 2007; Ganzetti and Mantini, 2013; Greicius et al., 2003; M. H. Lee et al., 2013; Lowe et al., 2000; Rosazza and Minati, 2011; Van Dijk et al., 2010; Veer et al., 2010). Figure 1.1 contains examples of some well-studied networks. Although discoveries are still ongoing, a large body of literature now exists that supports their neurophysiological importance by linking them to both normal and pathological brain function (Greicius, 2008; Greicius et al., 2007; M. H. Lee et al., 2013; Rosazza and Minati, 2011).

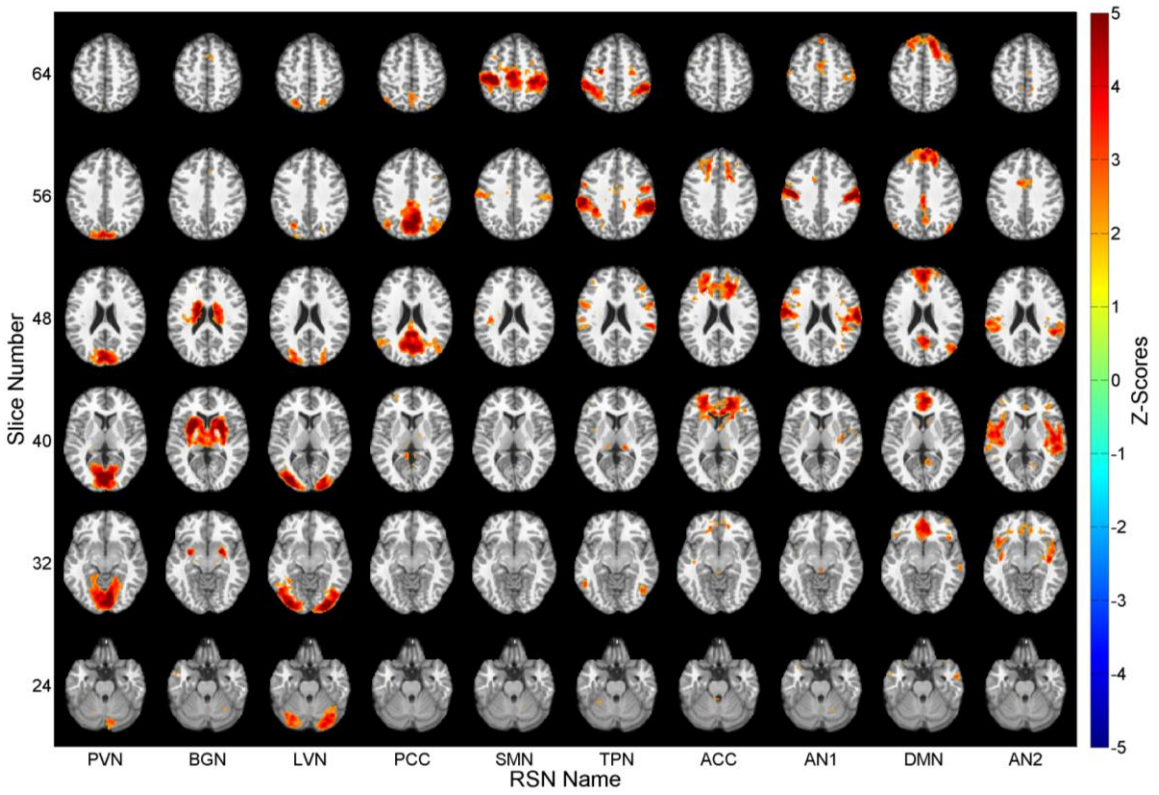

Figure 1.1: Some examples of resting state networks (RSNs). Each is labeled by an acronym of its commonly used name: primary visual network (PVN), basal ganglia network (BGN), lateral visual network (LVN), posterior cingulate cortex (PCC), sensorimotor network (SMN), task positive network (TPN), anterior cingulate cortex (ACC), first auditory (AN1), default mode network (DMN), and second auditory (AN2).

Unfortunately, an in-depth coverage of known RSN functions and behaviors would be quite extensive and thus outside the scope of this brief review. There are, however, two particular networks that we will witness throughout the coming chapters and are worth mentioning in more detail here. One of these is the known as the default mode network (DMN). It was one of the first RSNs discovered after Biswal et al. documented the sensorimotor network (SMN) at rest, and tends to be more active between tasks or during periods of quiet introspection (Raichle et al., 2001). The other is the task positive network (TPN). This RSN

becomes more active during performance of certain tasks (Fox et al., 2005; Fransson, 2005).

The apparently inverted behaviors of these two networks are especially noteworthy. This well-documented feature is often summarized by saying that DMN and TPN activities are anticorrelated to one another (Chai et al., 2012; Fox et al., 2009, 2005; Fransson, 2005; Kelly et al., 2008; Uddin et al., 2009). Thus, as one of the networks becomes more active, the other tends to become more inactive. The DMN-TPN anticorrelation has been shown to have physiological relevance as well. For example, its characteristics have been found to be predictive of both performance in certain tasks (Hampson et al., 2010; Kelly et al., 2008; Prado and Weissman, 2011) and some disease states (Castellanos et al., 2008; Chai et al., 2011; Wang et al., 2007; Whitfield-Gabrieli et al., 2009).

Static functional connectivity has offered a wealth of insight into the brain's inner workings, especially regarding its large-scale networks. But we have not yet discussed what is meant by the term *static*. The studies referenced in this section all share a common trait. Namely, they estimate functional connectivity using whole signals that span the entire duration of a scanning session, which typically last around 10 minutes. This has long been a popular approach and has some appealing advantages. Calculating functional connectivity metrics between long signals is easy to perform and computationally undemanding. The process also yields summary statistics for an entire scan that are easy to interpret and are readily comparable throughout groups of test subjects.

However, the use of whole time series for these calculations carries an implicit assumption of temporal stationarity, meaning that the functional connectivity metrics are not allowed to change as a function of time. Thus, static functional connectivity generally reflects only the predominant or average relationships between brain regions over longer periods of time. Any variations in connectivity that occur at time scales much less than the scan duration can easily be obscured and unobservable.

1.2.2 – Dynamic Functional Connectivity

Interest has recently been shifting away from static examinations like those reviewed in the previous section. Instead, researchers are increasingly focused on the study of *dynamic* functional connectivity, which is attempting to document the evolving relationships within and between functional networks on smaller time intervals. Whereas static analyses utilize an entire scanning trial (perhaps 10 minutes or so), dynamic analyses report on functional interactions at time scales of approximately 10-100 seconds.

One of the first demonstrations of fMRI-based functional connectivity dynamics came from earlier work done by our group (Majeed et al., 2009). In that study a characteristic repeating pattern of brain activity was found in the cortices of anesthetized rats. These were referred to as *quasiperiodic patterns* (QPPs) because they appeared to be periodic but were not always active. Importantly, their existence suggested that functional connectivity exhibits a temporal organization on the scale of seconds rather than minutes as is typically assumed by stationary analyses.

A potentially homologous pattern was later observed in awake humans (Chang et al., 2013; Grigg and Grady, 2010; Majeed et al., 2011) and took on the appearance of an alternation between DMN and TPN activations. Earlier studies had already linked activity in these networks to subject task performance (Drummond et al., 2005; Hampson et al., 2010; Kelly et al., 2008; Prado and Weissman, 2011), even on time scales shorter than a typical scan duration (Singh and Fawcett, 2008), and it was suspected that simultaneous co-activation of both networks would degrade performance (Eichele et al., 2008b). Taken together, this all suggests that QPPs have a very specific behavioral relevance; alternations between the DMN and TPN may represent a cycling of brain states between information processing and readiness to take action. Support for this hypothesis came from another study performed by this group, which found that the strength of DMN-TPN anticorrelations just before task onset is predictive of performance (Thompson et al., 2013a). Stronger anticorrelations (i.e. less co-activation) predicted better performance.

Others have observed that functional connectivity varies over time within the networks originally defined by static analyses (Allen et al., 2014; Chang and Glover, 2010; Handwerker et al., 2012; Hutchison et al., 2013b). Similar findings have also been reported using non-human species (Hutchison et al., 2013b; Keilholz and Magnuson, 2013). Another study found significant variability in the spatial extents of traditional RSNs within the same individual (Kiviniemi et al., 2011). Although their physiological significance is still being unraveled, these results indicate that the popular assumption of temporal stationarity is invalid for functional connectivity phenomena.

Researchers have already investigated dynamic functional connectivity with a variety of methods, often building upon approaches that proved useful to static analyses. Some have applied ICA to windowed segments of BOLD data (Esposito et al., 2003; Karvanen and Theis, 2004; Kiviniemi et al., 2011; Smith et al., 2012) while others have pursued pattern finding algorithms to isolate repetitive occurrences of activity (Liu and Duyn, 2013; Majeed et al., 2011, 2009). One study has also applied wavelet transforms (Chang and Glover, 2010), which is a promising approach that analyses the coherence between signals across multiple temporal and frequency scales (Torrence and Compo, 1998). However, the most prevalent technique to date has been to calculate *sliding window correlations* (SWC) between time series (Allen et al., 2014; Handwerker et al., 2012; Hutchison et al., 2013a, 2013b; Keilholz, 2014; Leonardi and Ville, 2015; Thompson et al., 2013a, 2013b). This method will be discussed more fully in Section 4.2.1, but in summary SWC calculates a time series of correlation coefficients between windowed segments of neurophysiological signals.

1.3 – Electrophysiology

Unlike fMRI or even MRI technologies, the science of recording electrical activity in the brain has a long history that extends back nearly a century in humans (Berger, 1929) and even further in animals (Caton, 1875). Over the years, a wide variety of methods have been developed to study electrophysiological activity in the central nervous system, but by far the most common of these in humans is called *electroencephalography* (EEG). Recording EEG signals typically entails placing electrically conductive sensors (i.e. electrodes) across

the surface a subject's scalp and recording the changes in electrical potential over time relative to a chosen reference.

The popularity of EEG today can be attributed to several factors. One is the large body of supporting literature that has resulted from its extensive lifespan, which makes it an especially appealing modality for clinical applications (Møller, 2011) and provides a sound basis on which investigators can base their experiments. EEG recording equipment is also generally non-invasive, widely available, and cheap. It is especially inexpensive and accessible when compared with some other neuroimaging modalities, such as MRI.

In the context of this and related studies, however, EEG possesses other particularly noteworthy advantages. Firstly, the signals that it records are known to directly reflect neuronal electrical activity. Even when the distance between electrodes and brain tissue is on the order of centimeters, as it is when recording through the scalp, spontaneous EEG waveforms primarily represent activity from large segments of gray matter (Shah et al., 2004). The major contributor to this activity are the oscillatory dendritic polarizations found on cortical pyramidal neurons (Bollimunta et al., 2008; Murakami and Okada, 2006). A second advantage of this recording modality is its high temporal resolution; EEG equipment is capable of sampling brain potentials tens of thousands of times of times per second. Considering the fastest physiologically relevant activities that are commonly studied (Buzsáki and Silva, 2012), this means that the temporal resolution of EEG is practically unlimited.

Oscillatory brain activity is classically subdivided into separate frequency bands based on associations with various brain states (Buzsáki, 2006; Engel et al., 2001; Klimesch, 1999). Named by Greek letters in order of their discovery, they range as follows: δ (<4 Hz), θ (4-7 Hz), α (8-12 Hz), β (13-30 Hz), and γ (30-100 Hz). Although still in use, the tendency to classify EEG activity according to this scheme has declined somewhat due to the ambiguity that it introduces. For example, complex interactions have been known to occur between separate bands (Steriade, 2006, 2001) and two instances of the same activity can be classified differently depending on the age or species of the subject from which they were recorded (Buzsáki, 2006). Additionally, oscillations whose frequencies are outside of those bands have been shown to have physiological relevance (for reviews see Buzsáki and Silva, 2012; Vanhatalo et al., 2005).

Of course, while EEG is exceedingly popular in human studies and is a focus of this document, it is far from the only means of recording electrical activity from living brain tissue. This is true in humans but applies particularly to non-human species, for which invasive electrophysiology becomes a much more feasible approach. Invasive methods are advantageous in that they circumvent the confounding effects of intermediate tissue between the brain and the recording electrodes and can offer much better localization of source activity (Buzsáki et al., 2012; Laufs et al., 2008).

Studies utilizing animal models often report on *local field potentials* (LFPs), which are shifts in electrical potentials arising from neuronal activity that are acquired through microelectrodes directly implanted into brain tissue. In contrast, when invasive methods are used on human subjects, *electrocorticography* (ECoG) is the modality of choice. ECoG

involves placing a mesh of recording electrodes in direct contact with exposed cortical tissue and, as a result, is exclusively used in surgical patient populations. Importantly, ECoG typically does not invade the brain tissue itself, unlike LFP recording. These alternative approaches are given mention in order to provide some familiarity with methods used in several of the prior works that are referenced throughout this study.

1.3.1 – Infraslow Electrophysiology

As we mentioned in the previous section, frequencies of EEG activity below about 4 Hz are grouped together into what is known as the δ-band. However, the inclusion of frequencies below approximately 1 Hz in EEG recordings is comparatively uncommon. These slowly oscillating components constitute a band of frequencies that include *slow* (<1 Hz) and *infraslow* (<0.1 Hz) electrophysiological activity (Khader et al., 2008), the latter of which is of special importance to our study here because it exactly matches the frequencies of spontaneous BOLD signals that are commonly used to study functional connectivity.

Although the majority of EEG-related studies do not investigate slow signals, their existence has nevertheless been documented for more than 50 years in both humans (Aladjalova, 1964; Birbaumer et al., 1990; Monto et al., 2008; Trimmel et al., 1990; Vanhatalo et al., 2005) and animals (Aladjalova, 1957; Filippov et al., 2002; Norton and Jewett, 1965; Pan et al., 2013). Throughout this time, researchers have repeatedly noticed that potentials at this frequency scale are strongly linked to cognitive processing and consistently occur in conjunction with certain stimuli or neural events. Perhaps the best-

known examples include *contingent negative variation*, which is a potential deflection that occurs when individuals are anticipating but have not yet experienced a stimulus (Walter et al., 1964), and the so-called *readiness potential* that can be found prior to voluntary movement (Kornhuber and Deecke, 1965). Many studies have also found correspondences between infraslow potentials and task performances involving attention, memory, mental imagery, and mental calculations (for reviews, see Khader et al., 2008; Palva and Palva, 2012; Rösler et al., 1997).

Compared to these behavioral or event-related potentials, less is known about spontaneous infraslow electrophysiology. Evidence shows that spontaneous waveforms at these frequencies are a feature of recordings made in preterm neonates (Vanhatalo et al., 2005, 2002) and in sleeping adults (Vanhatalo et al., 2005, 2004). They have also been linked to both task performance (Born et al., 1982; Monto et al., 2008; Stamm et al., 1987; Trimmel et al., 2001, 1990) and attentional disorders (Helps et al., 2008, 2010, 2009). One of the most interesting discoveries, however, concerns their relationship with higher frequency electrophysiology. Specifically, it has been found that the phases of infraslow fluctuations are well-correlated with the amplitudes of faster activity (Aladjalova, 1957; Monto et al., 2008; Vanhatalo et al., 2004). This phenomenon is an example of *phase-amplitude* or *cross-frequency coupling* (Canolty and Knight, 2010), a topic that has been gaining increasing attention in the study of brain networks. Such a relationship between the EEG bands suggests that infraslow activity could be reflecting large-scale cortical excitability (Elbert, 1993).

All together, these findings indicate that infraslow electrophysiology is a useful marker of neuronal activity. Why, then, does this scale of EEG activity receive so much less attention than its higher frequency counterparts? The answer is largely one of practicality. Infraslow activity in particular is usually filtered out of recordings due to concerns over data quality. In order to record very slowly oscillating activity with high fidelity, special constraints on preparation and hardware are required beyond those that are necessary for higher frequency recording (Khader et al., 2008; Tallgren, 2006; Tallgren et al., 2005; Vanhatalo et al., 2005). A DC-capable amplifier with high input impedance and wide dynamic range is required, especially when recording over longer intervals. This is likely the principal obstacle to capturing infraslow EEG signals because many existing amplifiers are AC-coupled and are therefore incapable of accurately recording long segments of nearly constant potential (Bauer et al., 1989). Furthermore, non-polarizable Ag/AgCl electrodes and a chloride-containing gel are required (Tallgren et al., 2005), which precludes nearly all alternative electrode materials and electrolyte-free gels. Lastly, special considerations must made for the galvanic skin response, which can introduce artifacts that are indistinguishable from neuronal activity (Birbaumer et al., 1990). This entails abrading the scalp beneath each electrode recording site (Vanhatalo et al., 2005). Given the existing challenges of recording EEG at any frequency (especially in conjunction with fMRI, see Sections 1.4 and 2.1), it is often more practical to use widely available amplifiers, electrodes, and gels while simply removing infraslow signals via filtering, thus avoiding these additional problems altogether.

1.4 – Simultaneous fMRI and EEG Recording

So far we have given a modest introduction to EEG and fMRI as neuroimaging modalities and have very briefly discussed how each can be leveraged to learn more about the brain. We also covered some of the strengths and weaknesses of each: fMRI affords remarkable spatial resolution but suffers in the temporal domain while EEG records signals with excellent temporal resolution that cannot be easily localized in space. Soon after fMRI was discovered, researchers noticed that these qualities are quite complementary to one another (Ives et al., 1993) and therefore began to conduct experiments that simultaneously utilized EEG and fMRI. Ultimately, they hoped that the different recordings could be reconciled to produce non-invasive activity mappings with both high spatial *and* temporal resolution.

1.4.1 – Technical Challenges of Simultaneous Recording

Concurrent EEG and fMRI recording is a challenging proposition for several reasons (for reviews, see Gutberlet, 2010; Huster et al., 2012). Among the most important are the additional considerations that must be made in the name of safety and in particular impose constraints on EEG equipment options. Materials used inside of the scanner suite cannot contain ferromagnetic components that could become weaponized by the extreme magnetic fields present and injure the participant or damage the scanner itself. Additionally, any electrodes and their associated wiring must be properly shielded and carefully arranged so that electromagnetic excitation pulses emitted from the scanner do not result in burns to the participant or equipment. To alleviate some of these burdens, manufacturers today

produce EEG equipment that is specifically designed for simultaneous use with MRI and is tested for safety.

Beyond just material concerns, concurrent recording presents unique challenges to data processing as well. Operating EEG and fMRI equipment in tandem introduces artifacts into the recordings of both that must be addressed before the data can be used (for reviews, see Eichele et al., 2010; Mullinger and Bowtell, 2010). Of special concern are the gradient switching artifacts imposed on EEG data by MRI (Eichele et al., 2010; Huster et al., 2012; Niazy et al., 2005). These manifest as extremely large deflections that span a wide range of frequencies and mar the underlying real electrophysiology. Another concern is the so-called *ballistocardiographic* (BCG) artifact. This is a much more subtle artifact than that introduced by gradient switching and is always present in EEG recordings that are made inside of a scanner. The BCG manifests as a low frequency fluctuation that is related to the cardiac cycle instead of the brain's neurophysiology. In truth, the exact origins of this signal are not yet known, but the prevailing theory holds that it is related to a pulsatile motion occurring throughout the body as a result of cardiac activity (Debener et al., 2008; Eichele et al., 2010; Mullinger et al., 2013). Fortunately, software solutions are available that help compensate for these artifacts during preprocessing (Debener et al., 2008; Eichele et al., 2010; Harrison et al., 2014).

1.4.2 – Electrophysiological Correlates of Functional Connectivity

Despite the challenges of simultaneous recording, investigators have spent close to two decades applying this technique to learn more about the neuronal origins of the fMRI

signals and, by extension, BOLD functional connectivity. Nearly all of their studies to date have focused on finding a relationship between BOLD signals and higher-frequency (>1 Hz) electrophysiology. This approach has been popular for at least three reasons. Firstly, faster EEG activity is thought to be more closely related to rapid cognitive processes (Fries et al., 2001; Koch, 2009; Palva et al., 2010, 2005; VanRullen and Koch, 2003; VanRullen et al., 2007; Womelsdorf et al., 2006). Slower signals, in contrast, are currently believed to be involved in more generalized coordination of large-scale brain states and integration of information (Elbert, 1993; He and Raichle, 2009; Monto et al., 2008; Steriade, 2001). Secondly, recording slower EEG signals can be difficult on its own (see Section 1.3.1) and is only made more difficult by the presence of an MR scanner. Thirdly, higher-frequency EEG is currently better understood than slower activity, making the results of studies on the former easier to interpret in a meaningful way.

Although the ultimate goal of recording high spatiotemporal resolution brain activity has not yet been achieved, combining fMRI and EEG modalities has led to a number of discoveries that have helped shape an early understanding of the relationship between functional connectivity and electrophysiology. One of the most interesting findings to emerge is that BOLD activity is associated with certain spectral signatures of EEG. Some of the earliest experiments to utilize continuous acquisition in both modalities found that BOLD signals are well-correlated with α-band EEG power fluctuations in specific brain regions (Goldman et al., 2002; Laufs et al., 2003a; Moosmann et al., 2003). Similar relationships were shown to exist in other bands too, including β and θ (Laufs et al., 2003b; Scheeringa et al., 2008).

These results eventually led researchers to suspect that entire functional brain networks might be contributed to by several frequency bands of electrophysiology (Laufs et al., 2006). In a well-known study, Mantini et al. provided direct support for this hypothesis by showing that several BOLD RSNs are associated with unique combinations of EEG frequencies ranging from δ through γ. (Mantini et al., 2007). Indirect support has been produced as well. Studies utilizing ECoG have shown that electrophysiological power fluctuations exhibit interregional correlations that resemble BOLD RSNs (He et al., 2008; Jerbi et al., 2010; Nir et al., 2008).

However, there are inconsistencies within this body of evidence that have not yet been resolved. For example, one early simultaneous fMRI-EEG study found high levels of inter-subject variability in their results when correlating BOLD and α-band EEG signals (Gonçalves et al., 2006). Such variability would not be expected if functional connectivity phenomena are indeed statically and uniquely tied to various electrophysiological frequency bands. Following on those experiments, Meyer et al. were unable to reproduce the group-wide statistical significance that Mantini et al. had reported, although some of the same trends in correlation were observed (Meyer et al., 2013). They argued that the lack of group-level significance, caused by large inter-subject correlation variability, may point to a temporally dynamic relationship existing between the imaging modalities. This is an interesting notion that has not yet been thoroughly explored, but supportive results have been accumulating recently. We will return to this idea for a much more thorough treatment in Chapter 4.

Other studies have documented links between functional brain networks and the *microstates* of high-frequency EEG data, which are defined as quasi-stable configurations of electrical potential that exist across the scalp for brief periods of ~100 ms (Koenig et al., 2002; Michel et al., 2004). Microstates are currently thought to play a critical role in the formation of spontaneous thoughts and rapid cognition (Koenig et al., 2005; Lehmann et al., 1998) and, interestingly, both their topographies and time series have been shown to be highly specific to those of BOLD RSNs (Britz et al., 2010; Musso et al., 2010; Yuan et al., 2012). This suggests that microstates could be the higher-frequency EEG counterparts of BOLD functional networks. If true, developing a better understanding of them would be of the utmost importance to achieving high spatiotemporal resolution in simultaneous fMRI-EEG recordings.

1.4.3 – Infraslow Electrophysiological Correlates of Functional Connectivity

Soon after the discovery of fMRI, theories began to emerge concerning the existence of an infraslow electrophysiological counterpart to BOLD signals. These theories can actually be traced back to the very beginnings of fMRI (Birbaumer et al., 1990), but really began to gain traction once the importance of infraslow hemodynamics to functional connectivity had been established (Drew et al., 2008; He et al., 2008; Khader et al., 2008; Palva and Palva, 2012). Specifically, they hypothesize that spontaneous infraslow electrophysiology is a correlate of BOLD activity and therefore could represent a neuronal basis for BOLD functional connectivity.

Researchers have only recently conducted direct tests of this theory. After a considerable body of indirect supporting evidence had accumulated (for a review, see Palva and Palva, 2012), the first experiments to examine the relationship between infraslow hemodynamic and electrophysiological signals were performed in anesthetized rat models (Pan et al., 2013). In their publication, Pan et al reported significant temporal correlations between simultaneously recorded BOLD and infraslow LFP signals, indicating that the two are indeed related by a common mechanism. Correlations were also well-localized to cortical tissue, suggesting that gray matter neuronal processing is relevant to the relationship. Furthermore, correlations were observed at signal delays approximating the hemodynamic response interval, which is consistent with the notion of a causal relationship between electrophysiology and hemodynamics.

These results were quickly reproduced in resting human subjects using simultaneously recorded BOLD and EEG data (Hiltunen et al., 2014). In this study, Hiltunen et al. confirmed that the infraslow relationship existed across mammalian species and could be observed using scalp-recorded electrophysiology instead of invasive LFPs. Additionally, by using human participants, they were able to show that infraslow EEG signals are statically related to the time courses of BOLD RSNs themselves, lending strong support to the hypothesis that, at least in part, functional connectivity arises from equivalently slow electrophysiological activity.

1.5 - Project Objectives

The principal objective of this project was to investigate for the presence of a relationship between BOLD and EEG signals in humans at equivalent infraslow passbands. Healthy adult human subjects were to undergo simultaneous fMRI and EEG imaging during a state of resting wakefulness in order to compare signals of both modalities. It was expected that this approach would allow for direct tests of the longstanding hypotheses suggesting that BOLD signals are a reflection of infraslow electrophysiological fluctuations in humans. If evidence supporting the existence of this relationship were found, then we intended to characterize some of its behaviors and document whether or not they could be linked to functional connectivity measures.

The recent publication by Hiltunen et al. found that the independent components of infraslow EEG are correlated with BOLD in spatial patterns that match the signatures of well-known functional networks in resting humans (Hiltunen et al., 2014), providing the first direct evidence that infraslow BOLD and EEG signals share a common mechanism. Our results, as described in subsequent chapters, both confirm those findings and extend our understanding of the infraslow BOLD-EEG relationship as it relates to correlation time shifts, the spatial layout of electrodes, and spatiotemporal dynamics within a single trial.

In the early stages of this project, there was already considerable evidence that an infraslow BOLD-EEG relationship does exist in humans and the study by Hiltunen et al. had not yet been published. We therefore hypothesized that we would find markers of the link in the form of significant linear correlations between hemodynamic and scalp

electrophysiological signals. Strong correlations would indicate that both recorded signal types are influenced by the same or related processes in the brain, which would in turn provide evidence favoring the view that functional connectivity phenomena are driven at least in part by infraslow neuronal dynamics (Birbaumer et al., 1990; He et al., 2008; Khader et al., 2008).

The immediate impacts of a demonstrable infraslow relationship would be significant for functional connectivity researchers. From a purely academic perspective, it would provide crucial information that may be necessary to completely describe the neuronal origins of the BOLD signal. One current theory suggests that neurovascular coupling links multiple frequency scales of electrical activity with slow hemodynamic fluctuations, and if that holds true then this study may help characterize a relatively unexplored band of that scheme.

The ultimate outcomes of this and related studies may be much more far-reaching. From a practical standpoint, new avenues for clinical- and research-related brain imaging may become available. For example, it may eventually be possible to use infraslow or full-band EEG as an alternative to fMRI recording while examining certain BOLD or functional connectivity phenomena. This scenario could be particularly advantageous where fMRI is impractical or impossible to use because EEG equipment is much more portable, much less expensive, and has fewer exclusion factors. Additionally, the use of EEG in lieu of fMRI might help bring the study of functional connectivity to a much wider scientific body that currently does not have access to fMRI scanners.

To offer a contrasting example, it may also become possible to map infraslow electrophysiology to fMRI signals. EEG is the current standard for directly and non-invasively imaging brain activity in humans, but is only capable of recording from large patches of surface cortex. Fully characterizing the BOLD-EEG relationship could afford us the opportunity to image infraslow neuronal activity throughout the entire brain with unprecedented spatial resolution. This could have a powerful impact on research related to behavior and certain disorders.

CHAPTER 2

DATA ACQUISITION AND PREPROCESSING

2.1 - Introduction

Data preprocessing is a critical prerequisite for studies on functional brain connectivity, regardless of the recording modality or modalities used. This is especially apparent for functional brain images acquired through fMRI, which often undergo a lengthy procedure to prepare and standardize the data for analysis. In no particular order, this procedure typically includes: corrections for subject movements, corrections for delays between acquisitions of volume slices, functional-to-anatomical image coregistration, and spatiotemporal filtering (Faro and Mohamed, 2010). Additional or fewer steps may be warranted, depending on study requirements, but those listed here are frequently observed in publications on the topic. EEG preprocessing steps are somewhat less prescribed and will often depend on the goals of the study, but temporal filtering is commonly performed.

This chapter describes the experimental paradigm under which the data for this study were acquired. It also outlines the preprocessing methods that were applied prior to conducting any of the analyses presented in later chapters. Lastly, measures taken to ensure reasonable data quality and their results are covered. Simultaneously recording EEG and fMRI data presents a superset of preprocessing requirements. In addition to the steps that would be performed for each one individually, the influences that each modality have on the other must also be taken into account.

2.2 - Acquisition

2.2.1 - Experimental Protocol

Ten healthy adult human subjects (4 female and 6 male) of ages ranging between 18-39 years were recruited. Informed consent was obtained from all individuals. All studies were approved by the Georgia Institute of Technology Institutional Review Board. Data acquisition for every subject was performed at the joint Georgia Institute of Technology/Georgia State University Center for Advanced Brain Imaging.

Subjects participated in a single session that included four individual scans lasting approximately ten minutes each. Every scan consisted of simultaneously recording both functional images and electrophysiological signals from the brain using fMRI and EEG technology. Of the four scans that were acquired per session, the first two were recorded while the subject was in a resting state. The last two scans were recorded while subjects performed a task. The ordering of this sequence was never changed.

A resting state for test subjects is characterized here as lying motionless in the scanner with eyes open and forwardly fixated on a small dot projected onto a screen directly above them. Subjects were instructed to remain awake but to otherwise let their minds wander freely. In contrast, the task state that took place during the latter two scans consisted of subjects performing a psychomotor vigilance task (Dinges and Powell, 1985). This task involves watching for randomly occurring color changes in the projected dot and pushing a button immediately after the change is perceived.

Although mentioned briefly here for the sake of completeness in documenting this study, it must be noted that the task data from the final two scans have never been analyzed. The psychomotor vigilance task trials were included because it is a measure of sustained attention for which performance is predictable using activity in nodes of the default mode and task positive networks (Drummond et al., 2005; Thompson et al., 2013a). We originally intended to test whether or not the infraslow EEG data could be linked to activity in those nodes and if it could be used to offer similarly reliable performance predictions. However, difficulties with the software that administered the task and an abrupt severance of project funding meant that very little useable task data were ultimately collected. Therefore, data from these scans are not discussed further.

2.2.2 - Functional Neuroimaging

Images were acquired using a Siemens Trio 3T whole body MRI scanner. A three-plane localizer was first used to determine body positioning. Structural images with 1mm isotropic voxels were then acquired for each participant using a T1-weighted MP RAGE 3D sequence. Finally, the functional data were recorded for two consecutive resting state scans. Functional scanning was performed using an echo-planar imaging (EPI) sequence with an echo time (TE) of 30ms. One complete brain volume was produced per every 2s interval (TR), and each consisted of 64x64x33 voxels measuring approximately 3.4mm isotropic.

2.2.3 - Electroencephalography (EEG)

While functional imaging took place, continuous direct current EEG was simultaneously recorded from 68 sintered Ag/AgCl electrodes for each participant. Electrodes were positioned according to the standard International 10-10 System montage and were permanently affixed to a cap that subjects wore while inside the scanner. Prior to the start of a scanning session, the cap itself was aligned on the scalp using common skull landmarks. Throughout the session, electrode data was transmitted from the cap to a DC-capable SynAmps2 amplifier (Neuroscan Systems, Charlotte, NC, USA) located outside of the scanner room. Signals were digitized at a passband of 0-300 Hz, a 24 bit amplitude resolution, and a sampling frequency of 10 kHz. Infraslow data recording was possible due to the sintered Ag/AgCl electrode interface and the lack of any hardware highpass filter in the amplifier. Additionally, cardiac pulse timing was recorded using a custom optical detector placed on each subject's left index finger in eight out of ten subjects.

2.3 - Preprocessing

2.3.1 - Functional Image Preprocessing

fMRI data preprocessing followed procedures that are typical of functional connectivity studies (Faro and Mohamed, 2010; Poldrack et al., 2011). All steps were performed using the freely available toolbox SPM8 for MATLAB (Wellcome Department of Cognitive Neurology, London, UK), except where noted otherwise. A summary of each specific stage is provided as follows.

T1-weighted structural images were first segmented into gray matter, white matter, and cerebrospinal fluid mappings. These were used to generate corresponding masks that could be applied to the BOLD volumes. Slice-timing corrections and functional image realignment were then performed using AFNI (Cox, 1996). Next, images were registered to their anatomical counterparts and normalized to MNI spatial coordinates in order to facilitate comparisons between individuals.

From this point forward, custom-written MATLAB routines were responsible for finalizing the preprocessed data. BOLD data sets were spatially blurred using a 3D Gaussian kernel (sized 3x3x1 voxels, σ = (2, 2, 1) voxels**).** The time series of each voxel was then FIR filtered to a passband of 0.01-0.08 Hz. Following this step, the first 22 volumes of each scanning trial were discarded. This was done to account for both MR stabilization effects and the phase delay that filtering imposed. Quadratic detrending was also performed in order to remove drift artifacts. The final preprocessing step was to z-score each voxel over time. This re-expresses voxel signal amplitude as a fraction of its standard deviation and centers it about zero.

2.3.2 - EEG Preprocessing

EEG data were preprocessed through the open source MATLAB toolbox EEGLab (Delorme and Makeig, 2004). MRI gradient switching artifacts were first removed using the Bergen EEG-fMRI Toolbox (Moosmann et al., 2009). EEG signals were then synchronized with the functional imaging data using the known temporal locations of MRI gradient switching artifacts. Ballistocardiographic artifacts were removed next by the

FMRIB plug-in for EEGLab. This tool operates by subtracting a template from each channel time series that is constructed using QRS events detected in the optical cardiac signal (Iannetti et al., 2005; Niazy et al., 2005). EEG signals were then FIR filtered to a final passband of 0.01-0.08 Hz and downsampled to match the BOLD sampling rate. As was done for the functional data, the first 22 samples were discarded to account for phase delay and maintain synchronicity with BOLD signals. Quadratic detrending was also performed here to eliminate drift artifacts. Finally, each EEG signal was z-scored across time, scaling it to zero mean and unit variance.

2.4 - Quality Assurance

2.4.1 - Data Exclusion

Data were to be excluded from this study if any head movements were detected that covered a single voxel's width (3.4mm) or greater distance. Fortunately, no trials were lost to this criterion. However, a total of four participants (eight trials) were ultimately excluded for different reasons. For one participant, corrupted EEG data files discovered after the scanning session resulted in exclusion. A second participant was excluded upon discovering that an irregular electrode ordering scheme was used while recording EEG data. In this case, the true scalp electrodes from which the recorded signals originated could not be determined with certainty. Two additional participants (four trials) were excluded due to the presence of large artifacts in the EEG data that could neither be explained nor adequately removed. These artifacts were found across all electrodes and effectively obscured any neurophysiological data that might have been acquired.

2.4.2 - EEG Volume Conduction at Infraslow Frequencies

Volume conduction is a well-known phenomenon in electrophysiology that is characterized by a near-instantaneous spread of current from a single source throughout the brain. It is particularly troublesome to the task of source-localizing neuronal activity from EEG recordings, and in that context it has been studied and modeled extensively (Darvas et al., 2004; Michel et al., 2004; Peraza et al., 2012; Wendel et al., 2009). As its definition implies, volume conduction is often observed in the tendency for nearby EEG channels to be strongly correlated with one another, reflecting their recording of a common source (Stam et al., 2007) that may or may not be remote relative to the electrode site (Khader et al., 2008). Put simply, the problem is then this: for any given spatial pattern of EEG electrode activity, there are many possible neuronal source configurations that would explain it.

As we shall see in later chapters, the presence of volume conduction in our data would greatly complicate the interpretation of results and the goals of this study. Fortunately, simulations of electrical activity throughout human head models suggest that this phenomenon is not a major contributor to infraslow scalp-recorded signals (Birbaumer et al., 1990). Basic tests conducted on our EEG data lend support to this assertion.

If volume conduction were substantially affecting our data, then we would expect it to manifest as large clusters of electrodes that are most similar to one another without delay. We tested our infraslow EEG data against this criterion by cross-correlating pairs of signals and determining the temporal offset at which the maximum value was achieved (see

Section 3.3.2 for details on calculation cross-correlation functions). We repeated the test for all possible channel pairings across all trials and constructed color-coded maps of the offsets to visualize the results.

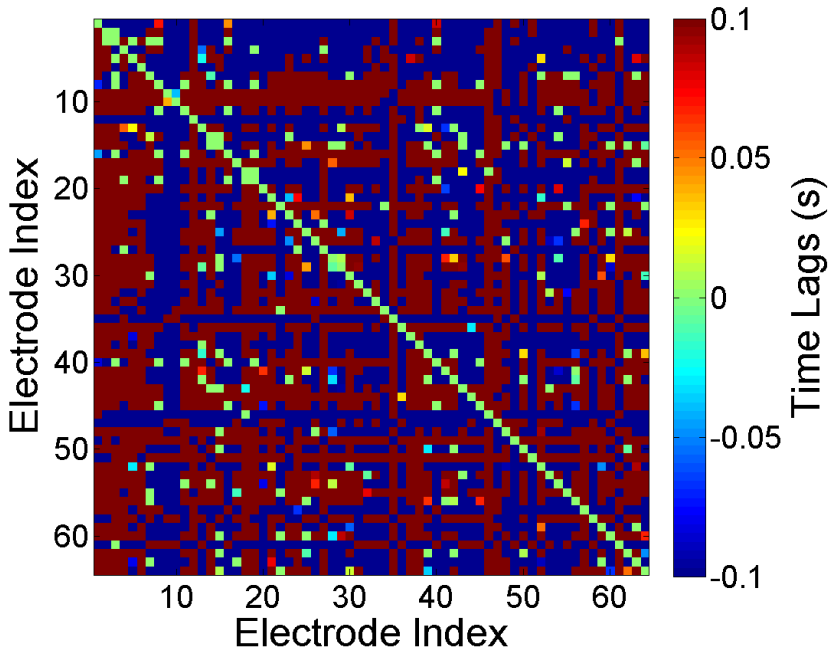

Figure 2.1: Time delays of maximum correlation between EEG signals as a test for volume conduction from a single representative trial. Colors span an offset range of 200ms, and most channel pairings require delays outside of this range to achieve maximum correlation. Few channels correlate most strongly near 0s, which would indicate the presence of volume conduction.

The offsets that result in maximal correlation between infraslow EEG signals are visualized in Figure 2.1 for one typical trial. A select few channel pairings are most strongly correlated at approximately 0s offset, but the vast majority require delays in excess of 100ms to achieve maximum covariance. These and similar findings across all trials led us to

conclude that volume conduction was not being observed in our infraslow electrophysiological data. Consequently, it was decided that corrective actions were unwarranted.

2.5 - EEG Electrode Subset Selection

Ideally, the relationship between infraslow BOLD and EEG signals could be examined using all available data. Such a comprehensive approach would afford the best possible view on the nature of this relationship and would decrease the likelihood of missing critical details and misinterpreting results. However, a comparison between all 68 channels of EEG data and all voxels of a functional image volume over multiple analyses would impose extreme computational demands and would generate pools of results that would be impractical to inspect manually.

We avoid this problem here through the use of only a subset of electrodes spanning the available montage. In doing so we not only lessen the computational and inspection burdens but we also take advantage of an otherwise negative feature of scalp-recorded EEG data in order to retain some of the detail that is being lost. EEG recordings from nearby locations tend to be quite similar to one another, a result of the filtering effects from tissues that lie between the neuronal electrical source and the recording site (Laufs et al., 2008). By choosing regionally representative electrodes across the scalp, we preserve much of the available spatial information.

The electrodes that we chose to examine in detail throughout this study were: FPz, FT7, FCz, FT8, TP9, CPz, TP10, PO9, POz, and PO10 (see the blue highlighted electrodes in

Figure 2.2 for the spatial layout of this subset). This set of ten electrodes provided evenly distributed brain coverage in the anterior-to-posterior and left-to-right directions. Additionally, these particular electrodes contained healthy-looking data that were free of any obvious artifacts across all scans that were used.

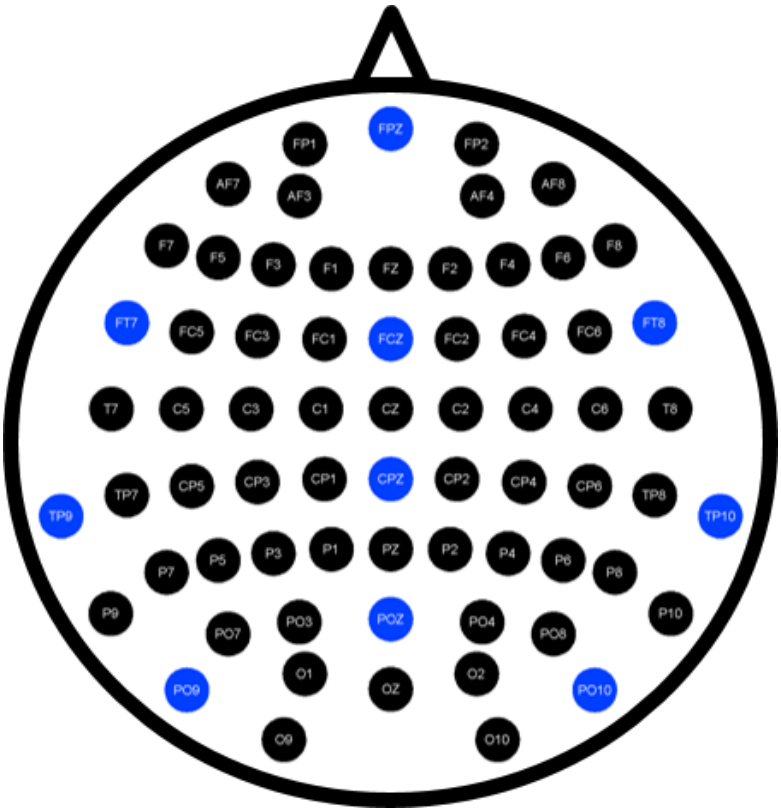

Figure 2.2: 10 EEG channels (highlighted in blue) forming a subset of the complete montage that were chosen for direct comparisons with BOLD data throughout this project. Subset channels were chosen such that they evenly covered the scalp and contained valid electrophysiological data in every trial. This step was performed to reduce computational demands as well as the amount of analysis output data that would require inspection. All EEG mappings throughout this document are oriented identically to this figure. Starting from the top (nasion direction) and moving left-to-right towards the bottom (inion direction), the highlighted channels are: FPz, FT7, FCz, FT8, TP9, CPz, TP10, PO9, POz, and PO10.

CHAPTER 3

TIME-INVARIANT DATA RELATIONSHIPS

3.1 - Introduction

This chapter describes our initial investigation of the relationships between infraslow BOLD and EEG data sets. As detailed in Sections 1.2 and 1.4, many functional connectivity and multimodality studies have provided valuable insights on the brain's inner workings using the assumption of temporal stationarity. To reiterate, this assumption posits that certain properties of the data being examined do not change as a function of time or change only over periods longer than the recording duration. All analyses discussed over the coming sections implicitly assume that the relationships between data sets are constant over time.

At the time of this project's launch, no direct comparisons between infraslow signals of the BOLD and EEG recording modalities had yet been made in awake humans. Drawing on a limited body of prior works regarding this relationship and on other higher-frequency simultaneous fMRI-EEG studies, we reasoned that the static analyses well known to investigators of functional connectivity provided a logical first step towards accomplishing our project goals. Despite foreknowledge that temporal stationarity assumptions would limit our ability to fully characterize any discovered links, we expected that it would offer valuable insight into time- and group-averaged relationship tendencies. These could then in turn be used to inform more advanced and nuanced examinations of our data.

3.2 - Statistical Significance Testing

Throughout this chapter, certain results are presented after having been thresholded for statistical significance. In all cases, the statistical significance of results was assessed using permutation tests (Poldrack et al., 2011). This is a nonparametric approach that estimates confidence intervals for hypothesis tests by empirically constructing a null distribution against which real data sets can be compared. Specifically, the null distribution is made by shuffling the data sets that are being analyzed in such a way that the result is expected to be insignificant (i.e. the null hypothesis). This is done repeatedly, typically as many times as the available data will allow, until a sufficiently complete distribution of null values are attained.

Permutation tests are perhaps best understood by example. Consider the process of conducting some arbitrary analysis that compares BOLD and EEG data sets. We first run this analysis as it is ordinarily indicated, which would likely involve comparing the EEG data from a trial with the BOLD data from that same trial. The result of this first step is a set of observations, or values, that we wish to test for significance. A set of null values is then constructed in much the same manner except that data are shuffled first. This frequently means that the EEG data from one trial will be compared with the BOLD data from a *different* trial using the same analysis method as before. This process can then be repeated until all possible inappropriate pairings of data have been analyzed and a full distribution of null values has been populated.

When conducted properly, data permutations build effective null distributions. They are especially useful when the parametric sampling distribution of the real observations is complex or unknown. The latter condition is often the case when working with BOLD and EEG data. Although some analyses may produce results that belong to a classical parametric distribution, it is usually more convenient to just create one, especially when working with groups of data over multiple trials. Empirical null distributions can also more easily account for data manipulations that universally affect data or have complicated influences on their statistics, such as certain preprocessing steps (see Section 3.3.4).

Permutation tests for this study were performed using all possible inappropriate pairings of trial data, amounting to $66 = \binom{12}{2}$ sets of data per null distribution. This was expected to break any existing temporal synchronization between neural events in the BOLD and EEG data sets. Control of family-wise error rate (FWER) for the large numbers of comparisons being made per analysis was accomplished using sequential goodness of fit (SGoF) (Carvajal-Rodríguez et al., 2009). This method corrects against Type I errors and has been shown to increase in statistical power with increasing numbers of comparisons. It operates by querying a binomial distribution for the probability of observing certain numbers of positive results given a total number of comparisons that were made, and then adjusts the CDF cutoff value using the probabilities that are beneath a designated FWER. For this study, FWER was fixed at 0.05.

3.3 - Mapping Correlations between Infraslow BOLD and EEG Signals

3.3.1 - Pearson Product-Moment Correlation Coefficients

The Pearson product-moment correlation coefficient, referred to as the correlation coefficient henceforth, is frequently employed to test for the existence of linear relationships between ordered data sets. In the context of this and related studies, it is used as a quantitative measure of how similar two signals are to one another. A correlation coefficient is often symbolized by the variable *r* and is calculated between two signals *X* and *Y* through the following formula (Shiavi, 2007):

$$r = \sum_i \frac{(x_i - \overline{x})(y_i - \overline{y})}{s_x s_y} \tag{3.1}$$

where x_i and y_i are the i^{th} elements of the two signals, $\overline{x}$ and $\overline{y}$ are the time averaged signal amplitudes, and s_x and s_y are the sample standard deviations of the signals. Values of *r* always fall in the range [-1, 1]. Technically speaking, an *r* magnitude of unity indicates that one signal can be exactly defined as a linear function of the other. The sign of *r* then dictates whether or not the line that connects the amplitude values is positive or negative in slope. Intermediate *r* values describe inexact linear relationships and an *r* value of zero indicates that no linear relationship exists between the signals.

However, when dealing with signals that are already z-scored, such as those used throughout this study, it is perhaps more useful to think of the correlation coefficient as a measure of how similar the waveforms are in shape. This is true because z-scoring is actually part of the formula in equation 3.1, and thus what is truly being measured is signal

covariance. In that case, an *r* value of positive unity indicates that two signals are identical to one another, while negative unity indicates that one signal is inverted (i.e. it's amplitude is multiplied by -1) with respect to the other but is otherwise identical in shape. An *r* value of zero still indicates that one signal cannot linearly describe the other.

3.3.2 - Cross-Correlation Functions

The correlation coefficient as defined in the previous section is useful for estimating waveform similarity when related events in both signals occur simultaneously. However, it cannot account for any temporal offsets that may be present between related events. Considering delays between events becomes critical when comparing two very different neural activity measures. To wit, neuronal activity triggers electrophysiological events that are essentially simultaneous in time, but corresponding hemodynamic events may be delayed by a period of several seconds.

Delays between related events in separate signals may be accounted for by estimating a cross-correlation function. This entails estimating the correlation coefficient between signals whose samples have been shifted in time relative to one another. Mathematically, this operation takes the form:

$$r(t) = \frac{1}{n}\sum_{t}\frac{(x(t)-\overline{x})(y(t+\tau)-\overline{y})}{s_x s_y} \tag{3.2}$$

where all variables retain their definitions from equation 3.1 and t is time, τ is some time shift between the two signals, and n is the number of samples in x and y. Note that this formula computes normalized correlation coefficients ranging between [-1, 1], which for

the purposes of this study are the only kind of interest because non-normalized coefficients cannot readily be compared when calculated using different data sets.

3.3.3 - Fisher's r-to-z Transform

Statistical significance testing for correlation coefficients is complicated by the fact that coefficient values are bound within a finite range. One direct consequence of this is that the variance of a distribution of *r*-values depends upon the mean of the distribution; the closer the mean is either boundary, the smaller the variance tends to become. Fortunately, a simple transformation is available that stabilizes the variance of an *r*-value distribution and allows for straightforward significance testing using a normal distribution. This transformation, called Fisher's Transform after the statistician that introduced it (Fisher, 1915), is as follows:

$$z = \frac{1}{2}\ln\left(\frac{1 + r}{1 - r}\right) = \operatorname{arctanh}(r) \tag{3.3}$$

When applied to a distribution of correlation coefficients derived from data that are not correlated beyond chance (i.e. the null distribution), the resulting z-scores approximate a standard normal distribution: $z \sim N(0, 1)$.

3.3.4 - Correcting Fisher's Transform for Filtered Signals

The Fisher Transform as defined in Equation 3.3 is derived under the assumption that the signal time points used to calculate correlation coefficients are bivariate normal. Stated another way, the derivation assumes that individual time points are independent from one

another and are identically distributed. Certain preprocessing steps that are commonly performed on neurophysiological signals, such as blurring and filtering, can easily violate this assumption and thereby render typical significance tests invalid (Davey et al., 2013; Lenoski et al., 2008; Worsley and Friston, 1995; Zarahn et al., 1997). This fact can readily be observed in low-pass filtered signals, to which filtering can introduce substantial autocorrelations between time points (Davey et al., 2013). In such cases, null z-scored correlation values belong not to a standard normal distribution but to a narrower Gaussian distribution that relies on the degrees of freedom (ν) of the data used to generate them: $z \sim N(0, \nu^{-1})$

One approach to accounting for this effect involves estimating the effective degrees of freedom in a signal. This quantity is then used in any descriptive statistic calculations needed for significance testing that rely on the degrees of freedom of the data. A simple estimator for the effective degrees of freedom of FIR filtered signals was recently derived in (Davey et al., 2013) and is calculated using the following equation:

$$\kappa = 2T_s(f_h - f_l)T \tag{3.4}$$

where κ is the *effective* degrees of freedom, T_s is the sampling period, f_h and f_l are respectively the high- and low-pass cutoff frequencies for the FIR filter, and T is the number of samples in the signal. The corrected Fisher's Transform is then derived by dividing out the standard error of the null distribution from equation 3.3:

$$z = \frac{\arctan(r)}{1/\sqrt{\kappa}} = \sqrt{\kappa} \cdot \operatorname{arctanh}(r) \tag{3.5}$$

After this correction is applied, the null distribution is approximately standard normal and thus the z-scored correlation coefficients can be tested for significance using the usual methods.

3.3.5 - Average Cross-Correlations between Infraslow BOLD and EEG Data Sets

Using the methods just discussed, we calculated the cross-correlation functions between infraslow BOLD and EEG time series across all data sets. For each individual scan, the ten selected EEG channels (see Section 2.5 and Figure 2.2) were cross-correlated with every BOLD voxel signal in order to produce spatial mappings that estimate the linear relationship between them as a function of temporal offset. A total of twenty-one offsets, ranging between [-20s, 20s] in steps of one TR (2s), were tested between the signals.

Every resulting correlation coefficient was then converted to a standard z-score using the corrected Fisher Transform for filtered time series. Finally, coefficients were averaged across all scans in a fixed effects analysis and tested for statistical significance. Through this approach we expected to observe correlation patterns that would indicate strong or stable relationships between the BOLD and EEG signals, if indeed such relationships do generally exist across the human population.

This analysis ultimately produced a series of ten spatiotemporal correlation maps, representative samples of which are shown in Figures 3.1-3.3. Each is a group-wide average of the correlation between a single EEG signal and all BOLD voxel time series at various time shifts. These images have been thresholded for statistical significance and

corrected against multiple comparisons at a FWER of 0.05. Insignificant correlations have been replaced with an anatomical image underlay.

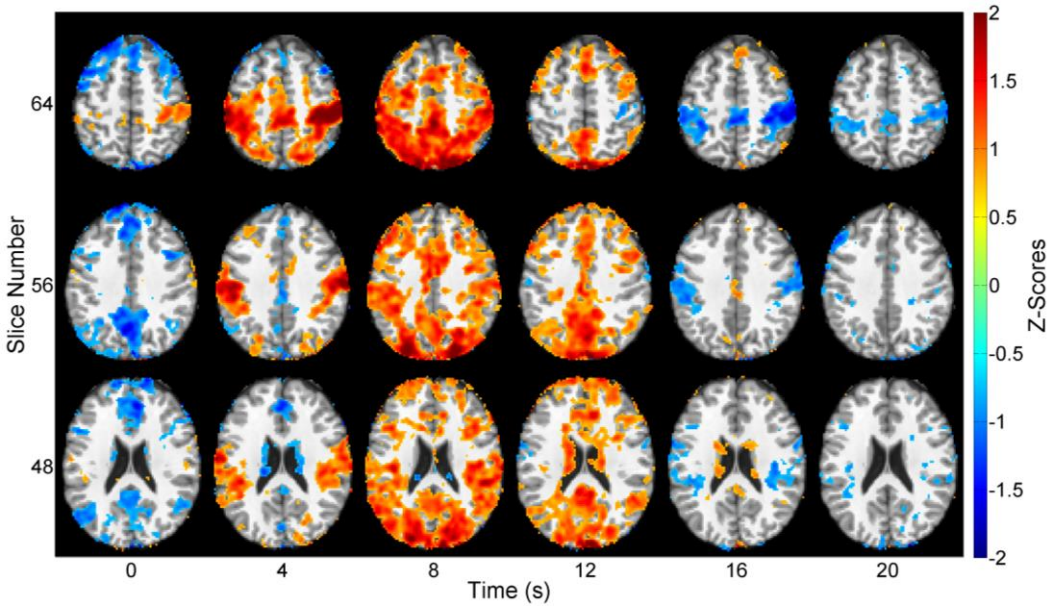

Figure 3.1: Group-averaged correlation between infraslow BOLD and the FPz electrode. Colored results are significant at $p < 0.0372$ corrected for an FWER of 0.05. Time shifts in seconds refer to the delay imposed on the BOLD relative to EEG signals while calculating correlation. Strong positive and negative correlations were observed in BOLD regions belonging to well-known RSNs. At 0s offset, FPz is significantly anticorrelated with nodes of the DMN. Positive correlations with nodes of the SMN and TPN are seen from 4s-8s and later invert in sign between 16s-20s. The sign inversion suggests that both the BOLD and EEG signals contain a common periodic component.

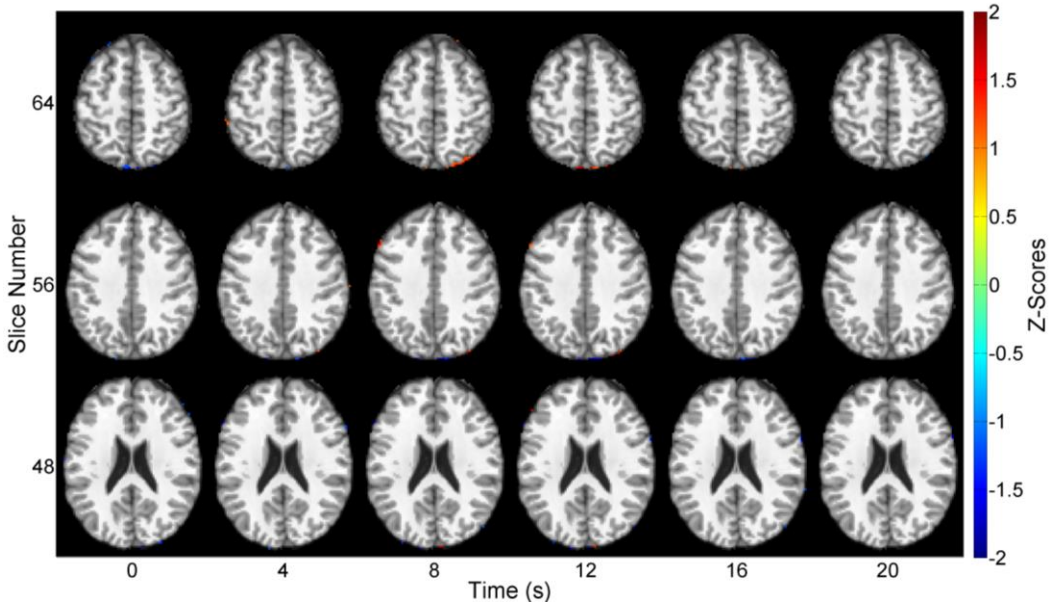

Figure 3.2: Group-averaged correlation between infraslow BOLD and the FT7 electrode. Colored results are significant at $p < 0.01$ corrected for an FWER of 0.05. Time shifts in seconds refer to the delay imposed on the BOLD relative to EEG signals while calculating correlation. Almost no significant correlations are present in this average mapping.

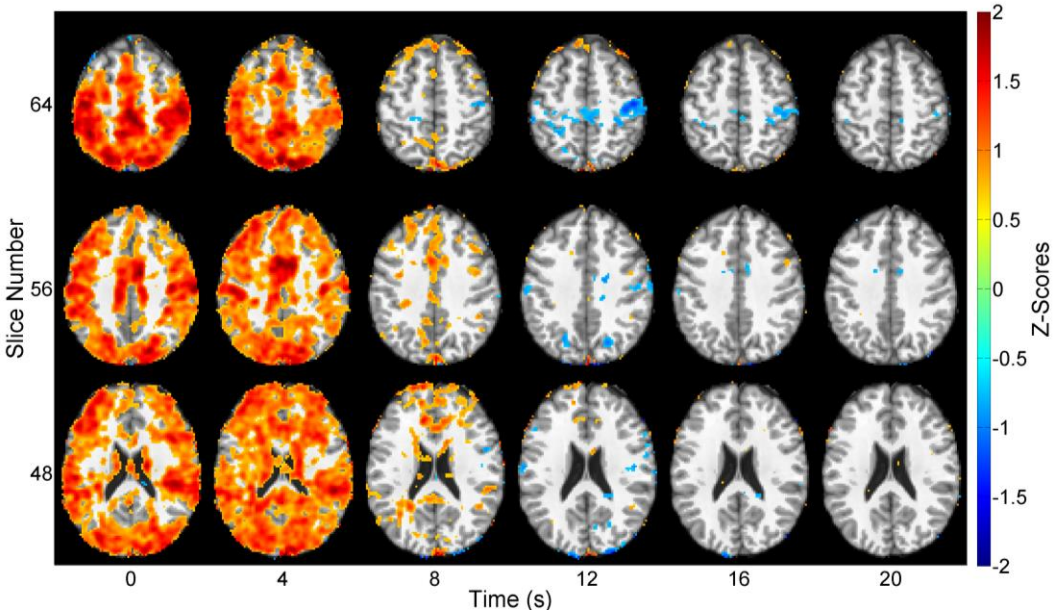

Figure 3.3: Group-averaged correlation between infraslow BOLD and the PO10 electrode. Colored results are significant at $p < 0.0458$ for an FWER of 0.05. Time shifts in seconds refer to the delay imposed on the BOLD relative to EEG signals while calculating correlation. Strong positive correlation is seen throughout gray matter between 0s-4s. Between 12s-16s, PO10 is anticorrelated with regions of the SMN, suggesting involvement of a periodic component that may be related to the one seen in the BOLD-FPz average.

Although only three representative mappings are shown, all other averages exhibit patterns resembling one them. In general, when correlation is present to any large extent, we observed that it almost universally includes both the sensorimotor cortices and intraparietal sulci (IPS). The latter structures are well-known members of the task positive resting state network (TPN) (Fox et al., 2005; Fransson, 2005). In one typical pattern (Figure 3.1), positive correlation in these regions starts as early as the 0s offset, reaches maximal strength at approximately 8s, and then vanishes by about 12s. Negative correlation in these same regions was then observed to follow a similar trend between approximately 12s and 20s. BOLD correlates of FPz, FCz, FT8, CPz, and TP9 all followed this progression of events.

Mappings for the TP10, PO10, and POz electrodes exhibit positive correlations starting at approximately -4s, peaking at 0s, and nearly vanishing by 8s (Figure 3.10). Like the first pattern, there is then a tendency to negatively correlate with these regions at later time shifts. Thus, the two patterns bear a close spatial resemblance to one another, except that one tends to begin earlier and frequently covers larger swaths of gray matter. BOLD correlates of the remaining electrodes (PO9 and FT7) exhibited almost no significant similarities at any shift (Figure 3.2).

The strong, widespread, and significant correlations witnessed between BOLD and EEG throughout the gray matter suggest that there is indeed a direct relationship between them at infraslow frequencies. The apparent similarities between them and the TPN lend additional evidence supporting the link are consistent with the recent findings in (Hiltunen et al., 2014). In their results, they too found that correlation topologies between infraslow

EEG and BOLD resembled functional networks. Furthermore, nodes of the default mode network (Buckner et al., 2008; Raichle et al., 2001) are visible in the BOLD-FPz mappings (Figure 3.1) and display a significant anticorrelated relationship. This provides evidence that electrodes may be correlated with more than just one discrete RSN without blanketing most of the gray matter as was observed in some averages (see Figure 3.3).

It is also interesting to note the shift in sign that tends to occur in most electrodes at later offsets over the sensorimotor cortex and sometimes the IPS. The consistent presence of this shift across several of the averages suggests that the EEG signals contain an oscillating component that is similar to one found in the voxels of those regions. The apparent periods of these shifts are also consistent across the mappings in which they appear, taking on values in the range [16s, 20s]. If these correlation patterns are in fact reflecting a common oscillatory component, it is then possible that we are witnessing the direct electrophysiological correlate of quasiperiodic BOLD patterns (QPPs) that were observed previously by our group (Majeed et al., 2011) and others (Grigg and Grady, 2010; Liu and Duyn, 2013). We will return to this notion for additional considerations in Chapter 4 after discussing the dynamic relationships between infraslow EEG and BOLD signals.

3.3.6 - Single-Trial Cross-Correlations between Infraslow BOLD and EEG Data Sets

Averaging is a common technique in signal processing that can greatly enhance signal-to-noise ratios and has been used to great effect in a number of functional connectivity studies, especially in those that test groups of subjects. However, its explicit purpose in such applications is to remove individual variability in order to enhance group-wide trends. And

to a visible extent, that was indeed accomplished in the previous section; we obtained an approximation of what we might expect from any random trial.

However, we will now present a theme that will pervade every section throughout the remainder of this document. During the course of the BOLD-EEG correlation analysis from the previous section, we noticed that there was a large degree of variability in the correlations between trials. In fact, the single-trial correlation maps exhibited a diverse array of pattern morphologies that the group-wide averaging process was quite effectively hiding. These sometimes included patterns resembling RSNs not seen in Figures 3.1-3.3, patterns occurring at vastly different offsets and even negative offsets (which seem to suggest that BOLD events precede related ones in EEG), and patterns of completely different signs compared to those that the averages were showing.

The images in Figure 3.4 and Figure 3.5 provide an effective example of the variability we are referring to. These show the correlation mappings between BOLD and FT7 for two separate trials and are representative of the kinds of differences that have been observed. FT7 is perhaps a special case because, as was shown in Figure 3.2, its mappings averaged out to an almost entirely insignificant result. With that in mind, the BOLD-FPz correlations are also unique because they displayed the most common tendencies, which is suggested by the results in Figure 3.1. Mappings for other channels typically displayed commonalities in between these extremes.

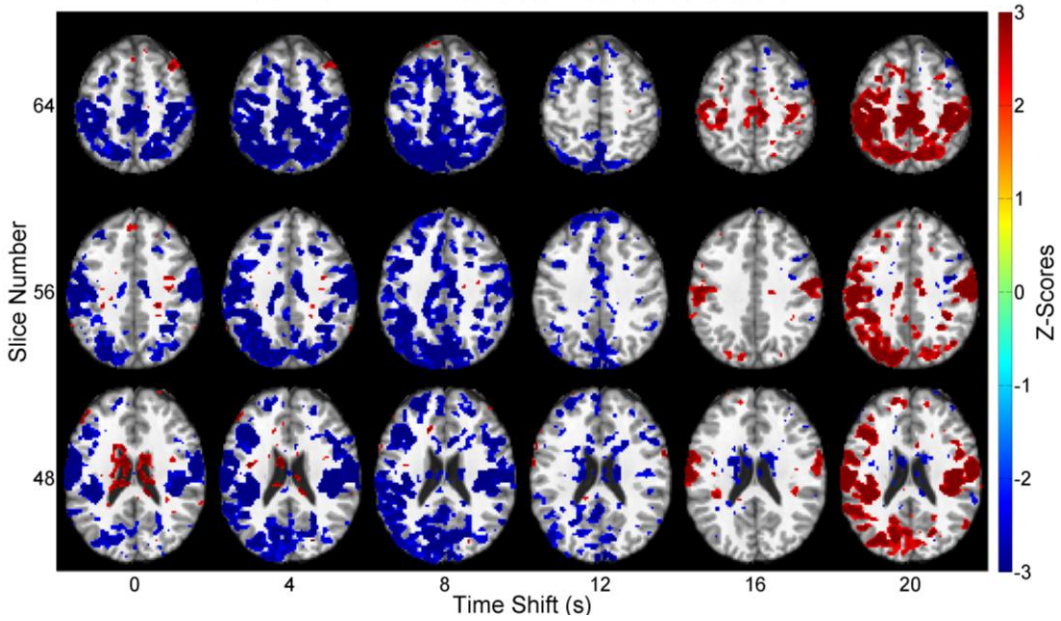

Figure 3.4: Single-trial correlation between infraslow BOLD and the FT7 electrode for one trial. Colored results are significant at $p < 0.0029$ corrected for an FWER of 0.05. Time shifts in seconds refer to the delay imposed on the BOLD relative to EEG signals while calculating correlation.

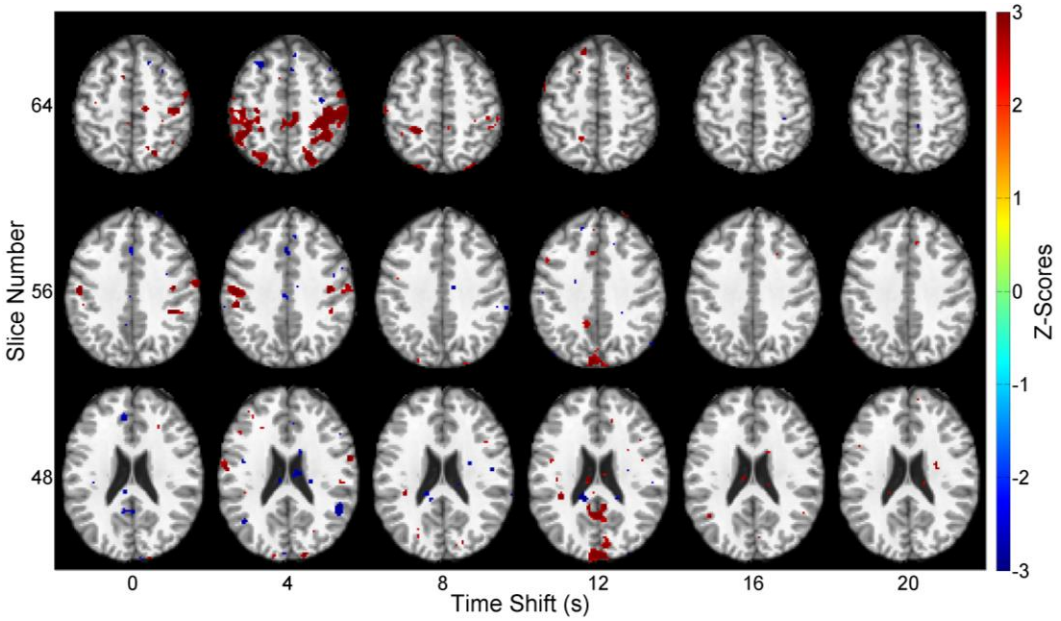

Figure 3.5: Single-trial correlation between infraslow BOLD and the FT7 electrode for a different trial than Figure 3.4 Colored results are significant at $p < 0.0006$ corrected for an FWER of 0.05. Time shifts in seconds refer to the delay imposed on the BOLD relative to EEG signals while calculating correlation.

These single-trial results are consistent with most of the discussion points from the last section. Many of these correlation patterns strongly resemble the TPN, just as the averages suggested, but additional network resemblances were visible that could not be seen in averages. Furthermore, the large variability that is present suggests that the BOLD-EEG relationship is not static across individuals or even trials from the same individual. Assuming that there is truly a relationship between them, this then implies that BOLD-EEG coupling must change over time, a topic that will be investigated in the next chapter.

3.4 - Mapping Correlations between Infraslow RSN and EEG Signals

Cross-correlating the infraslow signals from BOLD voxels and EEG channels regularly produced spatial patterns that resembled RSN topologies in both the single trial and average results. Such a consistent observation implies that RSNs are of critical importance to the link between hemodynamics and electrophysiology. Additionally, both the average and single-trial data showed that these patterns change as a function of the electrode being analyzed and likely involve several networks. The next logical analysis step was therefore to better define which networks are involved and to gain a better understanding of their spatial dynamics with the EEG signals. However, to accomplish all of that, we first needed a way to reliably estimate RSN time courses across individuals.

3.4.1 - Independent Component Analysis (ICA)

Independent component analysis (ICA) is a relatively new statistical approach to the problem of blind source separation (Bell and Sejnowski, 1995; Comon, 1994) and has seen frequent use in functional imaging studies since its first application (McKeown et al.,

1997). Indeed, it has been applied to numerous data sets from both task-state and resting-state experimental paradigms (Allen et al., 2011; Calhoun et al., 2009; Damoiseaux et al., 2006; Hiltunen et al., 2014; Mantini et al., 2007; Meyer et al., 2013; Rytty et al., 2013; Yeo et al., 2011) and has even seen effective use as a preprocessing step (Liao et al., 2005; Thomas et al., 2002; Tohka et al., 2008). ICA's popularity in fMRI studies stems from two major factors (Calhoun and Adali, 2006). Firstly, it is highly flexible; there are several algorithms and extensions that are widely available to tailor and refine its behavior. Secondly, it has the ability to consistently characterize brain activity; ICA is frequently used to decompose fMRI data into RSN activity profiles (Calhoun and Adali, 2001; Calhoun et al., 2001; Damoiseaux et al., 2006; De Luca et al., 2006; Hiltunen et al., 2014; Mantini et al., 2007; van de Ven et al., 2004).

ICA is related to, but should not be confused with, the better-known method *principal component analysis* (PCA). Like its relative, PCA attempts to separate a mixture into a set of constituent source components (i.e. a basis set). Its decomposition process is guided by two important constraints: each derived component must maximally explain the variance in the mixture and must be orthogonal to all other components. In the context of fMRI source separation, these requirements make the components difficult to interpret because there is no reason to expect that brain activity sources are spatially and temporally orthogonal to one another. As a result, the naïve use of PCA can easily produce components that are mixtures of multiple effects (Petersson et al., 1999). Part of ICA's appeal is that it does not rely on that orthogonality assumption and is able to perform separation through constraining either the temporal (tICA) or spatial dimensions (sICA), but not both. It does

this maximizing the statistical independence of components along one or the other dimension.

Although it overcomes some critical shortcomings associated with PCA, ICA does have its own set of limitations that must be considered (McKeown et al., 1997). One such limitation is that the outputted components will be mostly non-overlapping. Consequently, when using sICA to generate RSN patterns from fMRI data, the RSNs will not overlap with one another to any significant degree. This poses a problem when trying to isolate multiple RSNs that share nodes.

Another limitation is the algorithm's assumption that the data being decomposed has been *linearly* mixed; non-linear data mixtures cannot reliably be decomposed using ICA. Additionally, on its own ICA produces unordered outputs; repeatedly invoking the algorithm will result in different output orderings, all inputs held constant. This poses problems when the decomposed components cannot be easily classified or must be reconciled across decompositions of separate data sets. To give a specific example, comparing decompositions of fMRI data from multiple subjects can be difficult. In this case a workaround might involve visual inspection of the components by a researcher.

The final limitation that we discuss involves choosing the number of components to be outputted by ICA. This number is a required parameter and is only constrained to be a positive integer less than the number of time or spatial points available, depending on the dimension over which decomposition occurs. Otherwise, it is free to vary. This particular point can be problematic because the algorithm seems to want *a priori* knowledge about

how to properly separate the data. When decomposing unknown mixtures like fMRI data, such information is rarely known with certainty.

As was mentioned earlier, there have been many ICA algorithms and extensions developed that refine the decomposition behavior and help overcome some of the limitations discussed above. Covering all of them is beyond the scope of this text, but we refer the interested reader to several thorough treatments of the topic (Acharjee et al., 2015; Calhoun and Adali, 2001; Calhoun et al., 2003; Eichele et al., 2009, 2008a; Esposito et al., 2005, 2003; Karvanen and Theis, 2004; Liu and Calhoun, 2007). We will, however, mention one particular extension to ICA that was used in our data called *group ICA*. This is an approach that consistently decomposes data across multiple trials by concatenating them all together along the time dimension (Calhoun et al., 2009, 2001).

3.4.2 - Decomposing BOLD Data with ICA

As was mentioned in the previous section, applying ICA to the spatial dimensions (sICA) of neuroimaging data is a common and data-driven method of isolating RSN activity profiles. We performed this step using the GIFT toolbox for MATLAB (http://mialab.mrn.org/software/), which implements group sICA. We heuristically estimated the number of output components at 20 and selected the Infomax algorithm (Bell and Sejnowski, 1995) as the objective function to maximize independence. The resulting independent components (ICs) were identified by visually inspecting and comparing them to findings in literature.

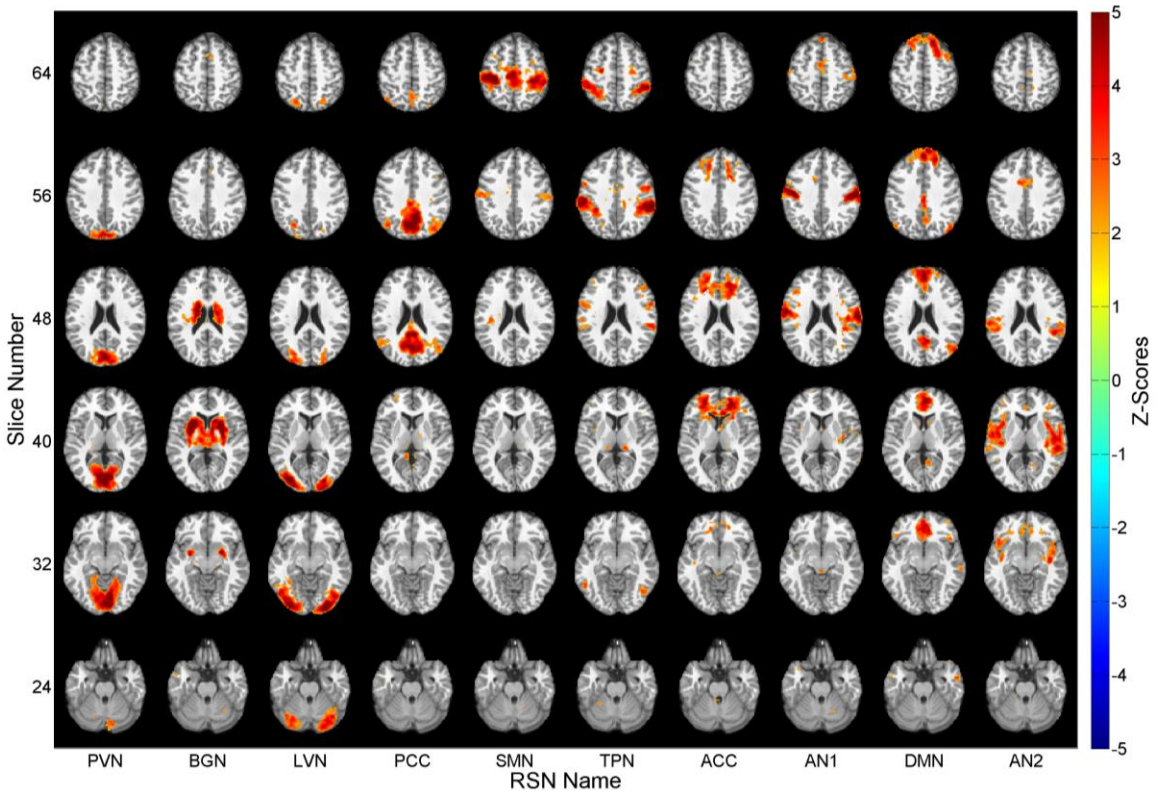

Figure 3.6: Independent spatial components of the resting state BOLD data. Out of 20 total components, the 10 are shown here and are labeled along the horizontal axis with the following acronyms: primary visual (PVN), basal ganglia (BGN), lateral visual (LVN), posterior cingulate cortex (PCC), sensorimotor (SMN), task positive (TPN), anterior cingulate cortex (ACC), first auditory (AN1), default mode (DMN), and second auditory (AN2).

The majority of the ICs are easily recognizable and correspond well with known RSN topographies (Damoiseaux et al., 2006; M. H. Lee et al., 2013; Rosazza and Minati, 2011; Veer et al., 2010) or brain structures. Only one component (not shown) could not be identified with certainty. The comparatively weak intensity and sparse but lateralized distribution of this IC suggest that it arises from over-decomposition, noise, or possibly a combination of the two.

While the spatial profiles outputted by group sICA were useful for identifying and labelling ICs, they held little additional value for this segment of the study. In order to investigate the presence of relationships between the infraslow EEG data and RSNs, a time series for each of the ICs is required. One path to acquiring these data would involve using IC spatial patterns like those shown above as BOLD image masks. Signals could then be constructed by averaging the unmasked voxel signals, similar to what is commonly done for region-of-interest analyses.

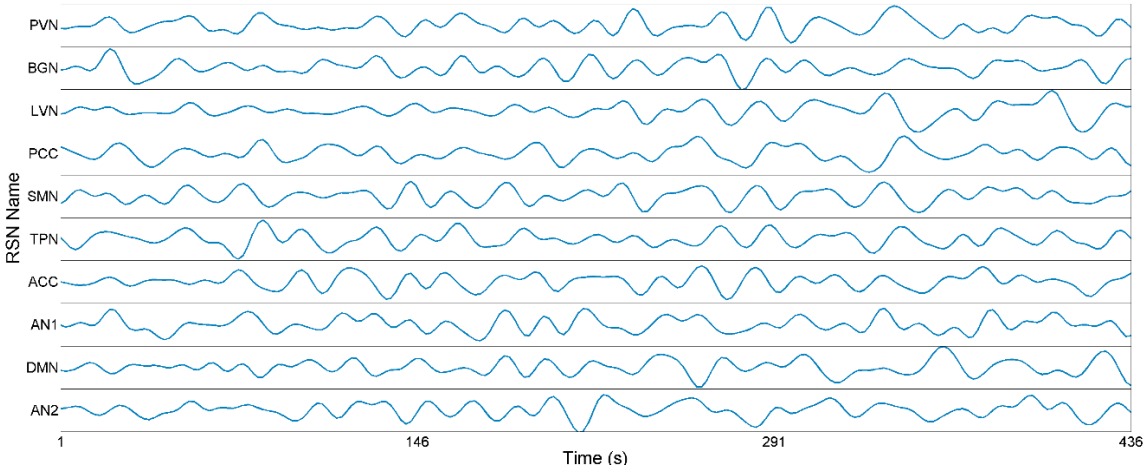

Figure 3.7: Representative RSN time series back-reconstructed by GIFT during decomposition. Of the 20 available ICs, signals from the same 10 shown in Figure 3.6 are displayed here from one single trial as an example. Each row or element of the montage possesses a horizontal axis representing time in seconds and a vertical axis representing z-score values limited between [-3, 3].

Fortunately, a simpler solution is offered by GIFT that avoids the need for constructing and thresholding masks. During the course of decomposition, GIFT automatically back-reconstructs and saves a time series for each resolved IC per individual trial, which are

representative of the regional average BOLD signals (Calhoun et al., 2001). Example time series of from a single trial are shown in Figure 3.7. Validation tests using our data confirm that these signals are very strongly correlated with BOLD in spatial patterns that closely matched the IC profiles they originated from. They were therefore used as the representative RSN time courses during the correlation analysis with EEG discussed next.

3.4.3 - Average Cross-Correlations between Infraslow RSN and EEG Signals

The linear relationship between infraslow electrophysiology and RSN activity was examined by cross-correlating EEG signals with each of the IC time series that were back-reconstructed by GIFT. Correlation coefficients were again converted to z-scores and averaged across all individual trials just like they were in Section 3.3.5. However, unlike that prior analysis, all available EEG electrodes from the full montage were used instead of the 10 channel subset. By this approach, results appear in electrode space mapped to one of the 68 total channels as opposed to the BOLD voxel space that was seen in the previous sections. An abbreviated image containing cross-correlation mappings at positive offsets between 10 ICs and the infraslow EEG data is shown in Figure 3.8.

Averaged correlations between RSN and infraslow EEG signals tend to be weak and no values pass significance thresholding with FWER correction. Coefficients almost universally approximate zero, except for some select RSNs between 0s and 20s signal offsets where they can sparsely achieve higher magnitudes. Although these data are statistically insignificant, they do perhaps offer a glimpse at some patterns and trends that we have already shown and will continue to see throughout later analyses. Namely, there

is a tendency for localized groupings of electrodes to similarly pair with certain RSNs. In some cases, there are also hints of correlation sign inversions occurring at later time shifts (see the primary visual (PVN), posterior cingulate (PCC), sensorimotor (SMN), and the first auditory components (AN1) for examples).

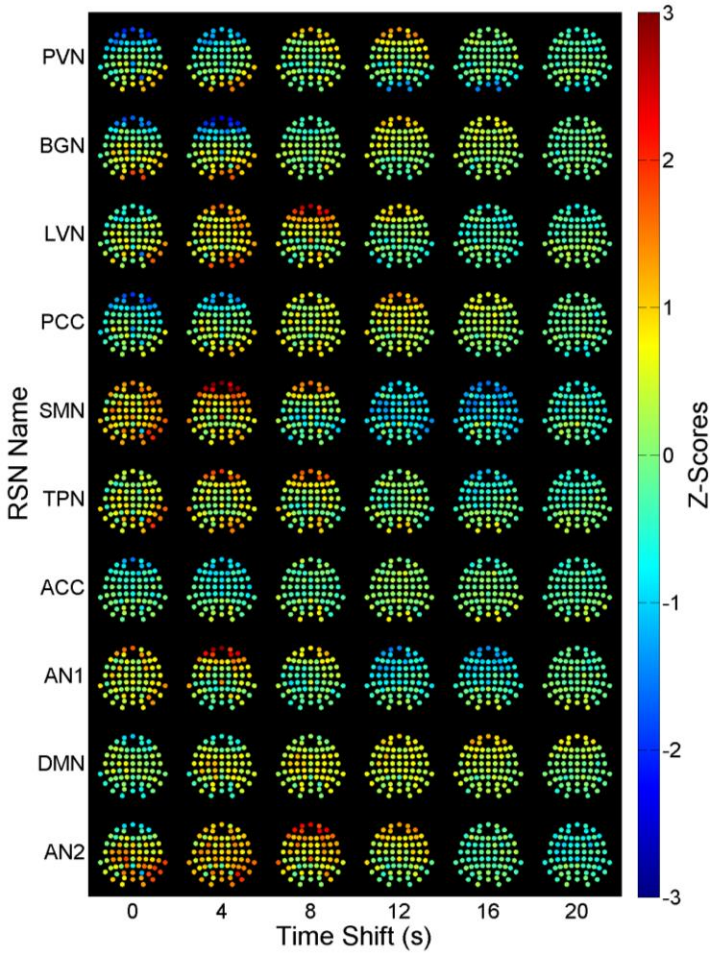

Figure 3.8: Group-averaged cross-correlations between RSN signals and infraslow EEG data. Each of the repeating elements on this montage is a spatial mapping of EEG electrodes (see Figure 2.2 for a complete description of them) that has been colored according to the correlation between EEG and RSN time series. Each row represents the cross-correlation between all EEG channels and one RSN signal at various time shifts. The same 10 RSNs from Figure 3.6 are illustrated here. Correlations from this analysis were mostly of low magnitude and are statistically insignificant after correction for FWER.

These particular observations should seem familiar because they are almost identical to those made earlier with the BOLD-EEG correlations. Those results showed distinct spatiotemporal patterns of correlation that tended to preferentially correspond with either frontal or parietal/occipital electrodes and tended to invert with increasing signal offset. Considering that several of those patterns resembled RSNs, and given the high correspondence between reconstructed RSN signals and their namesake BOLD spatial patterns, it therefore seems likely that we observed related phenomena here despite the failure to attain significance. The patterns seen across several electrodes in Section 3.3.5 are reflected well in the SMN-EEG correlations shown above, where the largest number of electrodes seem to be consistently involved in the relationship. Higher correlations between the SMN and EEG is perhaps not surprising because the vast majority of that RSN is located on the surface of the brain and is therefore close to the recording sites.

The SMN is also one of the only networks showing evidence of coupling with the middle- and temporally-placed EEG channels at any time shift. This is an especially curious finding in light of their proximity to one another and the tendency for remote electrodes to appear more strongly related. It suggests one of two possibilities. One is that these electrodes are mostly uninvolved in the majority of RSN-EEG relationships. The other possibility is that the relationship does exist but is much more variable across trials than it is in other channel groupings. Similar statements can be made regarding the parietal and occipital electrodes. They appear related to some RSNs more often than the middle group but still less often and less strongly than the frontal channels.

The cluster of frontal electrodes visible across several networks and offsets in Figure 3.8 suggest that the most stable relationships between RSNs and infraslow EEG can be found there. However, high magnitude correlations are still far from universally present in those channels. Several ICs, including the ACC, DMN, and others not shown, either correlate poorly with all electrode time series or more strongly correlate with occipital electrophysiology. Nevertheless, consistently high positive or negative correlations across several networks suggests a special importance for frontal EEG signals, although it is unclear what the physiological significance of this might be at present.

It is also worth mentioning that frontal electrodes are only observed to be strongly correlated (either positively or negatively) at offsets of 0s or greater. This provides evidence favoring a direct causal relationship between the RSNs and EEG signals, at least in this region. The parietal and occipital electrodes, in contrast, exhibit high magnitude correlations with certain RSNs at some negative time shifts. If the causality hypothesis is proven true across electrodes, then correlation at negative shifts suggests that electrophysiology is driving periodic or quasiperiodic hemodynamic activity. However, if causality does not exist, then this indicates that RSN and EEG signals share a common component that originates from some other unknown process.

3.4.4 - Single-Trial Cross-Correlations between Infraslow RSN and EEG Data Sets

The correlations from the previous section were almost universally low in magnitude across both networks and signal offsets. When high correlations were observable, they were sparsely distributed among small clusters of frontal and parietal/occipital electrodes.

As was discussed, this suggests that infraslow electrophysiology is either minimally or variably involved in RSN dynamics. These possibilities and the high per-trial variability observed in the BOLD-EEG correlations of Section 3.3.5 led us to examine the non-averaged, single-trial results of the RSN-EEG analysis.

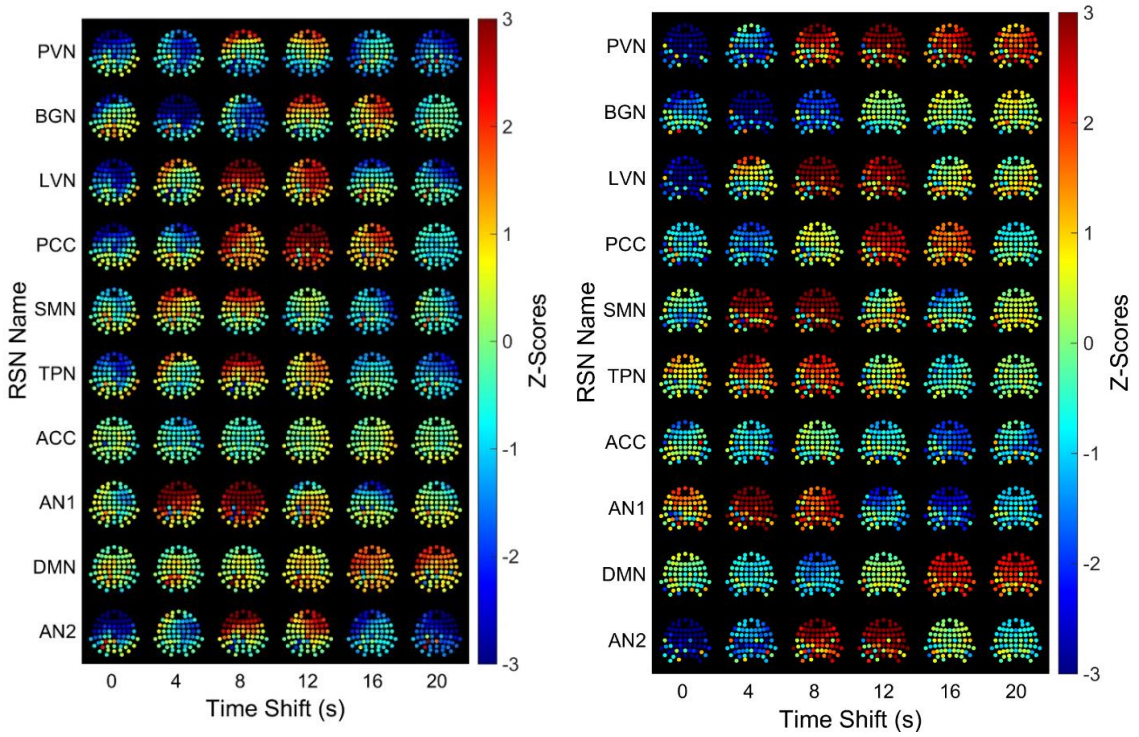

Figure 3.9: Single-trial cross-correlations between RSN signals and infraslow EEG data. Each image is taken from scans performed on two separate individuals, and the same 10 RSNs shown in Figure 3.6 are illustrated here. In contrast with the group-wide average correlations from Figure 3.8, correlations tend to be strong and widespread in data from individual trials. This high variability across trials leads to incoherent averaging.

The correlation mappings between RSN and EEG signals were indeed found to be highly variable between trials. Even in separate trials from the same individual, correlation patterns were found to be quite distinct from one another, which is consistent with the results and discussion in Section 3.3.5. To illustrate the variability that was observed,

Figure 3.9 shows example RSN-EEG cross-correlations at selected time shifts from two separate scans.

A predominant feature across these mappings is the extensive areas of high magnitude correlation values. These were generally observed to be clusters of adjacent electrodes possessing similar values. Although not universally present, such clusters do appear for the vast majority of the 20 total ICs across trials. They also appear to be unstable across time shifts. Sign inversions like those discussed in earlier sections are commonplace and can occur multiple times over offsets within a single network (see Figure 3.9, left). In addition, the topologies of clusters often change as a function of the signal offset, sometimes growing or shrinking in extent and shifting position across electrode space.

The single-trial results of this section provide considerable support for the hypothesized infraslow BOLD-EEG relationship. The strong correlations observed here indicate that RSNs are of central importance to the link; electrophysiological activity very frequently covaries with multiple networks across large sections of the scalp. This consistently observed feature corroborates our findings from Section 3.3.6, where BOLD-EEG stationary correlations were found to frequently resemble RSNs. Additionally, changes in correlation sign across signal offsets provide further evidence of a periodic or quasiperiodic hemodynamic process that is also present in the infraslow EEG data. It could be that these patterns are related to known spatiotemporal dynamics from BOLD (Grigg and Grady, 2010; Liu and Duyn, 2013; Majeed et al., 2011).

If a relationship between these infraslow signals is ultimately proven to exist, the pattern dynamics across time shifts and networks suggest that it is quite complex. Mappings in Figure 3.9 along with others not shown demonstrate that any electrode is capable of coupling with multiple RSNs simultaneously and that specific couplings are not always reproducible between trials. Again, this variability across trials from the same and separate test subjects suggests that the BOLD-EEG relationship changes appreciably with time. It also does not rule out the possibility that the coupling is somehow unique to the individual.

Higher magnitude correlation patterns were never stable across all 40 seconds of tested time shifts. Generally, they persisted unchanged across at least six seconds but their exact durations were inconsistent. In fact, they could sometimes be observed over a range of signal delays spanning more than 20 seconds. Slow pattern changes were visible in conjunction with more rapid changes at later time shifts and in other networks; all results exhibit combinations of the two. Furthermore, pattern duration did not appear to be associated with any particular networks. The variable nature of this feature indicates that the signals most responsible for high correlations are of variable wavelength. This in turn suggests that the BOLD-EEG coupling can take place through several different frequencies of activity, possibly simultaneously.

3.5 - Mapping Frequency Domain Relationships between RSN and EEG Signals

The results shown in the previous section offered some new insights into the purported infraslow BOLD-EEG relationship. Among them were the ideas that coupling between the signals occurs at different frequencies and may even involve multiple frequencies at the

same time. However, cross-correlation analyses are not well suited for identifying which frequencies may be of importance within the data passband. They also cannot easily discern whether or not multiple frequencies are involved simultaneously. Therefore, in order to examine how the BOLD-EEG relationship might change across a spectrum of frequencies, we analyzed the coherence between signals, which estimates the similarities between their constituent frequency components.

3.5.1 - Magnitude Squared Coherence

Magnitude squared coherence, referred to simply as coherence in this study, is frequently employed to test for the existence of linear relationships between data across multiple frequencies. Like the correlation coefficient, it can provide a quantitative measure of how similar two signals are. However, unlike correlation it measures similarity by examining discrete frequency components of a signal. It then reports results across a spectrum of frequencies instead of returning a single summary statistic.

Coherence between two signals x and y is often symbolized as C_{xy} and is calculated through the following formula (Shiavi, 2007):

$$C_{xy}(f) = \frac{\left| P_{xy}(f) \right|^2}{P_x(f)P_y(f)} \tag{3.6}$$

where f is frequency, P_x and P_y are the power spectral densities of x and y, and P_{xy} is the cross-spectral density of x and y. Similar to the behavior of normalized correlation coefficients, coherence values produced through Equation 3.6 are bound within the interval

[0, 1]. A C_{xy} value of zero indicates that there is no linear relationship between the components of the two signals at a particular frequency. A value of positive unity indicates an exact linear relationship between components.

The comparisons drawn between coherence and correlation are useful for interpreting the meaning behind values of the former. However, their comparability is no accident, and now is a good time to point out that they are actually intimately related to one another. The key to this fact is the *cross-spectral density* term P_{xy} of Equation 3.6, which has a special relationship with cross-correlation functions (Shiavi, 2007):

$$P_{xy} = \mathcal{F}\{\gamma(t)\} = \mathcal{F}\{r(t) \cdot s_x \cdot s_y\} \tag{3.7}$$

where $\mathcal{F}$ represents the Fourier transform operation, and $\gamma(t)$ is the cross-covariance function at temporal offset t. As indicated by this equation, cross-covariance is unnormalized cross-correlation (i.e. $r(t)$ from Equation 3.2). Thus, in simpler language, coherence is a normalized measure that reflects cross-covariance in the *frequency* domain while cross-correlation is a normalized measure of cross-covariance in the *temporal* domain. Recall from earlier that normalization is used to allow for comparisons between data with dissimilar signal amplitude characteristics, which we assume across all of our data.

3.5.2 - Average Coherence between RSN and EEG Signals

Magnitude squared coherence was calculated between RSN activities and EEG signals over the frequency range [0.01 Hz, 0.25 Hz]. This range constitutes the maximum frequency

span in which direct comparisons were possible between functional and electrophysiological signals (recall that TR = 2s for our data, thus f_{max} = 0.25 Hz). In order to accommodate this passband, the data being analyzed required special preparations that differed from the standard preprocessing pipeline (see Chapter 2 for more details). First, unfiltered RSN time series were needed. We therefore re-ran group sICA on BOLD data sets that were not temporally filtered but were otherwise fully preprocessed. Parameters used for this task were identical to those from Section 3.4.2. The resulting components closely matched our original infraslow BOLD ICs and were named accordingly. EEG signals were then prepared by downsampling unfiltered but otherwise preprocessed data sets to match the BOLD sampling rate (2s).

Coherence was estimated per trial between each of the 20 newly-acquired IC time series and each of the EEG channels belonging to the subset chosen in Section 2.5. The results were then averaged across all trials to produce mappings of coherence versus electrode and RSN. A sampling of the results are presented in Figure 3.10, showing coherence between ten RSN signals and ten EEG channels. Recalling the findings summarized throughout previous sections of this chapter, it should come as no surprise that average coherence here was observed to be universally low. Across frequencies, values are mostly uniform and tend to fall at approximately 0.3. Averaging coherence spectra across RSNs instead of trials produced similarly low-valued results. No statistical significance was observed in either case. Averaging across EEG resulted in higher values but none that were significant after FWER correction.

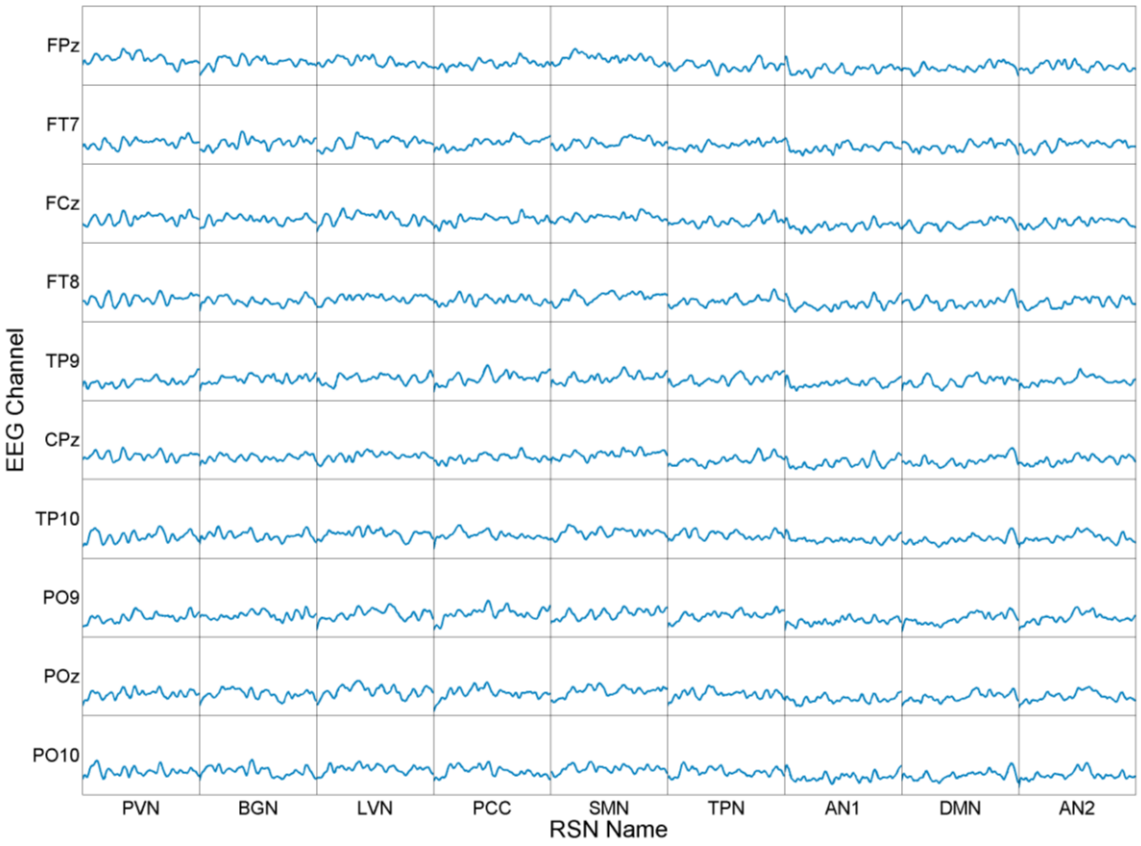

Figure 3.10: Montage of RSN-EEG coherence spectra averaged across all trials. Each element of the montage is consistently formatted; horizontal axes represent frequencies between [0.01 Hz, 0.25 Hz] while vertical axes represent coherence values between [0, 1]. Values across for all spectra are consistently low at around 0.3 and are universally statistically insignificant, suggesting that no particular frequency is of group-wide importance to RSN-EEG coupling.

3.5.3 - Single-Trial Coherence between RSN and EEG Signals

RSN-EEG coherence spectra exhibit variability across trials that is consistent with results from all other sections of this of this chapter. This explains why the group-averaged spectra from the previous section contain no significantly high coherence values or even any large deviations from the average value of approximately 0.3. Unlike those results, single-trail

coherence spectra like those displayed in Figure 3.11 regularly attain high values, often at multiple frequencies within a single spectrum. However, high variability exists not only between trials but between all other parameters as well, including RSNs and electrodes.

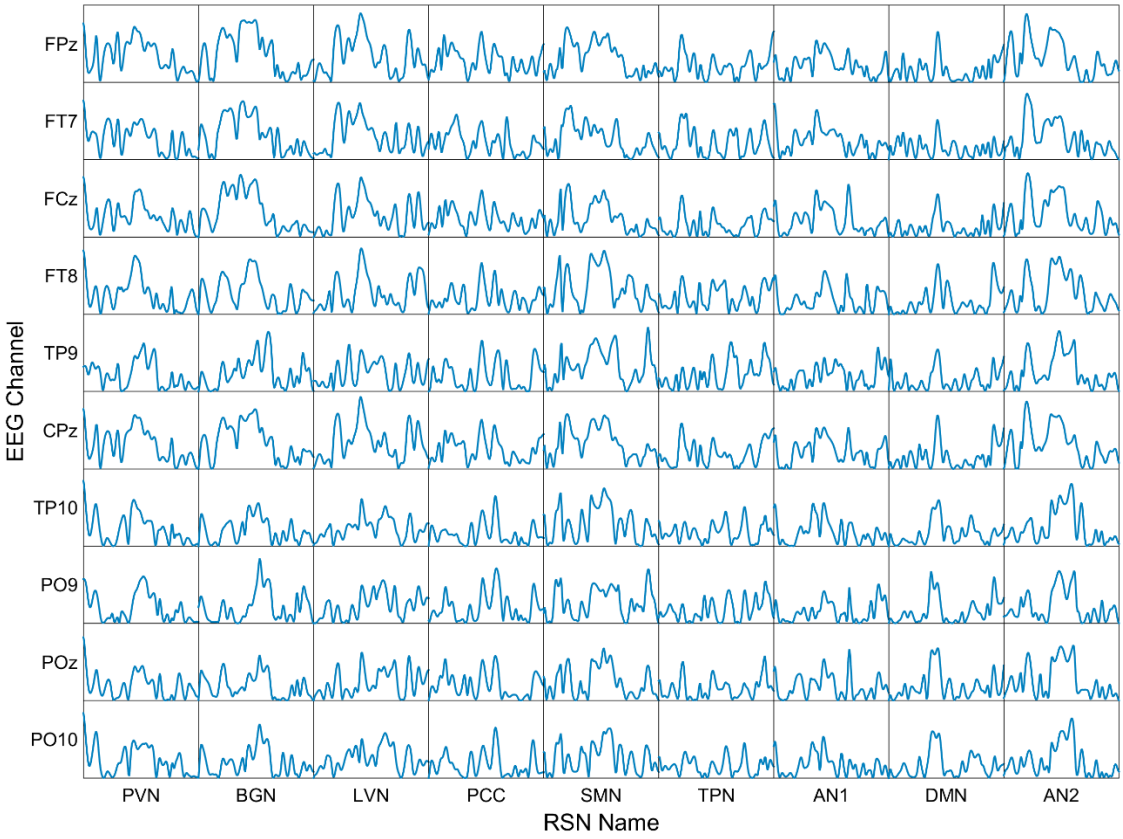

Figure 3.11: Montage of RSN-EEG coherence spectra for a single trial. Each element of the montage is formatted identically with those from Figure 3.10. Unlike those spectra, coherence here often attains high values. However, results are markedly different between trials and, within a trial such as this one, the frequency at which high values occur differs across both electrodes and RSNs. This explains why averaging across any parameter failed to produce significant results after FWER correction. These inconsistencies suggest a complicated and dynamic relationship between RSNs and EEG signals that changes over time, space, and frequency of oscillations.

Spectra are most consistent to one another across EEG electrodes, a feature that can easily be seen by comparing rows of the montage in Figure 3.11. Their similarities imply that the RSN-EEG relationship has widespread involvement from electrophysiology. However, the degree of consistency was also observed to change across RSNs. In some networks and trials, spectra were highly consistent across all ten electrodes. In others, spectra were consistent across most but not all channels. This suggests that RSN-EEG coupling involves varying spatial extents. Together, these observations are in good agreement with the results discussed in Section 3.4.

The individual spectra from single-trial results offer some additional insights. Most of them possess several high-valued peaks distributed across frequencies, strongly suggesting that RSN-EEG coupling occurs across multiple frequencies simultaneously. On a related note, both narrow and broad peaks are often visible in the results. If these spectra are truly reflecting an RSN-EEG relationship, then the coupling appears to be quite variable in the frequency domain, contributed to sometimes by one or more wide frequency ranges and other times by sharp peaks suggesting fewer frequencies of importance.

It is also worth mentioning that high coherence was commonly found in frequencies well above 0.08 Hz, which served as the lowpass cutoff frequency for our infraslow data throughout this study. It is unclear at this point whether or not those peaks in our data have physiological relevance. Early studies showed that the frequency range below 0.1 Hz is of principal importance to BOLD functional connectivity metrics (Cordes et al., 2000), but recent works have demonstrated that higher frequency hemodynamics are also informative (Boubela et al., 2013; H.-L. Lee et al., 2013). If the higher frequency peaks in our data are

not related to neuronal activity, they may be attributable to several factors. Some are likely harmonics of peaks at lower fundamental frequencies. Others may relate to the ICA signal reconstruction process, which presumably could introduce higher frequency imperfections while estimating component time series.

3.6 - Discussion and Conclusions

Throughout this chapter we presented our initial approaches to establishing and understanding the relationship between infraslow BOLD and EEG activities. These analyses quantified the similarities between signals of both modalities and provided a time-averaged glimpse into how one might relate to the other. To briefly summarize our results, we observed that strong correlations exist between the EEG data and certain well-known functional brain networks. We also found that the spatiotemporal characteristics of these correlations vary considerably between individual trials.

The high correlations seen across our data echo the findings of recent work done in both rats (Pan et al., 2013) and humans (Hiltunen et al., 2014), which altogether indicate that infraslow electrophysiology and hemodynamics are indeed related to one another. At the very least, the two signal types appear to contain one or more common components. It may therefore be tempting to conclude that these shared components represent a neuronal basis for BOLD functional connectivity, but unfortunately such a statement cannot be made with certainty. Prior studies suggest that scalp-recorded infraslow potentials can arise from both cortical pyramidal neurons (Birbaumer et al., 1990; He et al., 2008; Mitzdorf, 1985; Monto et al., 2008; Speckmann, 1997; Trimmel et al., 1990) as well as some non-neuronal

generators (Nita et al., 2004; Vanhatalo et al., 2003; Voipio et al., 2003). Consequently, the origins of the signal similarities found by others (Hiltunen et al., 2014; Pan et al., 2013) and by us here are not yet completely clear.

Disentangling the neuronal and non-neuronal sources of this correlation will likely require invasive recordings and in any case was beyond the reach of the present study. Nevertheless, indirect support favoring a neuronal origin for the infraslow BOLD-EEG relationship already exists. The fact that correlations are localizable to gray matter and RSN-like topographies provides some indication that they result from neuronal activity. Extensive work has gone into successfully linking BOLD RSNs to behavior (for reviews, see Rosazza and Minati, 2011; van den Heuvel and Hulshoff Pol, 2010), and the tendency of BOLD-EEG correlations to feature these networks is a clue that they too could be behaviorally relevant. Additionally, and perhaps relatedly, infraslow EEG signals have been linked to similar behaviors (see Section 1.4.3).

The variability that was found between trials and across the various analysis parameters highlights the potential complexity of the infraslow BOLD-EEG relationship. In particular, it seems that their coupling is temporally dynamic, or capable of changing across time, because analyses of separate trials from the same individual typically yielded inconsistent results. This finding may be related to similarly high inter-trial variability that has been observed in other simultaneous fMRI-EEG studies investigating higher frequency (>1 Hz) electrophysiology (Gonçalves et al., 2006; Meyer et al., 2013). To further complicate matters, our results suggest that the relationship is spectrally dynamic as well, meaning that the important frequencies contributing to BOLD-EEG correlations are variable. If so, the

data in Figure 3.11 would then imply that that these frequencies extend beyond just the infraslow passband. Based on prior works linking RSNs to higher frequency EEG power fluctuations (Mantini et al., 2007; Meyer et al., 2013), they may include all frequencies of EEG activity.

CHAPTER 4

TIME-VARYING DATA RELATIONSHIPS

4.1 - Introduction

Throughout Chapter 3 we saw some interesting and well known functional connectivity properties that appear to be reflected in the infraslow electrophysiological data. We have also seen some limited evidence that the BOLD-EEG relationship is much more complicated than the analysis methods of that chapter are capable of capturing. Indeed, this observation is directly related to a notion that is rapidly capturing the interest of the neuroimaging community: *dynamic* functional connectivity.

Studies of the time-invariant properties of functional connectivity have yielded a wealth of information on the trends or averages of brain behavior across both time and individuals. However, recent works have unequivocally shown that assumptions of stationarity are hiding large amounts of information about dynamic interactions both within and between brain networks (Chang and Glover, 2010; Grigg and Grady, 2010; Handwerker et al., 2012; Hutchison et al., 2013b; Keilholz, 2014; Leonardi and Ville, 2015; Liu and Duyn, 2013; Majeed, 2010; Majeed et al., 2011). Early attempts to tap into this hidden information have already established links to behavior (Thompson et al., 2013a), higher frequency electrophysiology (Chang et al., 2013; Tagliazucchi et al., 2012; Thompson et al., 2013b), and have found certain repeating patterns across individuals (Handwerker et al., 2012; Liu and Duyn, 2013; Majeed et al., 2011) that may be of special importance to healthy brain function.

The task of capturing temporal variability from an otherwise stationary metric has commonly been addressed using windowing methods. Generally speaking, these methods work by repeatedly performing static analyses on small segments of data in order to produce a time series of measurement changes. In doing so, they simultaneously exploit well-known methods and relax assumptions of stationarity. For a very well-known example of this principle, consider the short-time Fourier transform. Somewhat more directly related to the field of functional neuroimaging, however, windowed approaches have been applied to ICA of BOLD data (Karvanen and Theis, 2004; Kiviniemi et al., 2011), pattern finding (Liu and Duyn, 2013; Majeed, 2010; Majeed et al., 2011), and of course correlation (Allen et al., 2014; Handwerker et al., 2012; Hutchison et al., 2013a, 2013b; Keilholz, 2014; Leonardi and Ville, 2015; Thompson et al., 2013a, 2013b). Other approaches such as the wavelet transform have also been applied (Chang and Glover, 2010; Sato et al., 2006).

In this chapter, we explore the dynamic interactions between infraslow hemodynamics and electrophysiology using sliding window analyses. We examine estimates of the direct time-varying relationships between BOLD and EEG signals. We also examine how representative RSN signals and EEG may dynamically relate to each other.

4.2 - Mapping Dynamic Correlations between Infraslow EEG and BOLD Signals

The BOLD-EEG correlation results that were presented earlier (see Sections 3.3 and 3.4) suggested a relationship between infraslow electrophysiology and the resting state networks themselves. Indeed, we saw strong positive average correlations with task positive and sensorimotor network regions almost universally across electrodes. Many of

the averages exhibited sign inversions at larger time shifts that hinted at the possibility of periodic or quasiperiodic relationships. Furthermore, the single-trial results of all analyses showed us that trial-by-trial variability may be essential to the infraslow BOLD-EEG relationship.

4.2.1 - Sliding Window Correlation (SWC)

For the exploratory purposes of this segment of the study, it was decided that sliding window correlation (SWC) would be sufficient to evaluate the dynamic relationships between infraslow BOLD and EEG signals. Correlation is a standard metric for functional connectivity and its use with windowed segments of neuroimaging data has been more extensively documented than alternative approaches to date (Leonardi and Ville, 2015). It was therefore expected that SWC would afford the best possible means of comparing our results with earlier findings from both dynamic and stationary studies.

SWC is perhaps most easily understood through an algorithmic definition as opposed to a mathematically notated one. That is how we will present it here, although we also refer the interested reader to a good mathematical treatment of the topic (Leonardi and Ville, 2015) and an illustration of the process in Figure 4.1. Recall from Section 3.3.1 the calculation of a Pearson product-moment correlation coefficient (not cross-correlation, but that could be used as well). The essence of SWC between two signals is to partition each into an equal number of segments and then to calculate the *r* values between corresponding segments. This yields a series of correlation coefficients (i.e. a correlation signal) that varies as a function of window segment, which are bins of time.

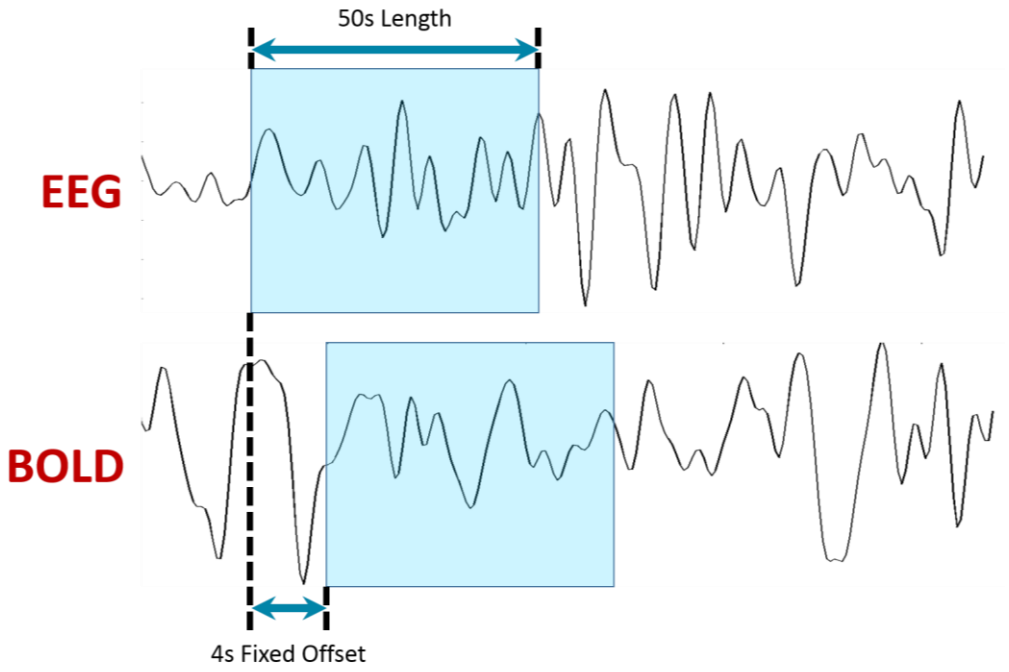

Figure 4.1: An illustration of the sliding window correlation (SWC) analysis using example infraslow BOLD and EEG data. Successive windows "slide" along each time series (maintaining the offset present), constructing a correlation signal at each increment until one or both signals are completely consumed.

The length of each signal segment that is being correlated is chosen by the researcher, but the decision is usually driven by the frequency content of the original signals. More specifically, window length is typically matched to the slowest frequency of interest in the data so that correlation estimates are influenced by the entire passband (Hutchison et al., 2013b; Leonardi and Ville, 2015; Smith et al., 2012). Related to this, the researcher can also control how much overlap exists between successive signal segments. This parameter influences the smoothness of the resulting correlation signal; higher amounts of overlap increase the number of sample points in the output and are more computationally

demanding, but also increase the chances of capturing transient events. Window segments may also be offset from one another to account for known delays between signal events.

Unfortunately, SWC has a number of pitfalls that complicate the interpretation of its results. The choice of window length can have a profound impact on results (Keilholz and Magnuson, 2013; Leonardi and Ville, 2015; Thompson et al., 2013b), and a method of determining an "ideal" length is not currently known. An ideal size may not exist at all if signal coupling is variable across frequencies at short intervals, which has already been shown to be true in neuroimaging data (Chang and Glover, 2010).

Additionally, testing SWC signals for statistical significance can be difficult. Data preprocessing in general has been known to impose correlations both within and between signals (see Section 3.3.4), and can thereby sharply reduce the degrees of freedom in the data. Inappropriately short window lengths in SWC may also increase the observation of high magnitude, spurious correlations, as has been shown in simulations (Leonardi and Ville, 2015). Combinations of these effects may be especially influential in permutation tests where both the real and null data distributions would be affected.

4.2.2 - SWC between Infraslow BOLD and EEG Signals

We computed SWC time series between all BOLD voxels of a trial and each of the ten members of the EEG electrode subset. Window length was fixed at 50s (50s = 1/(2 * 0.01 Hz), per (Sakoğlu et al., 2010)) for both BOLD and EEG data, and BOLD windows were offset 4s in the future relative to EEG windows to account for the hemodynamic delay time (Miezin et al., 2000). Successive windows along each time series were maximally (48s =

50s – 2s TR) overlapped with one another in an attempt to capture any short-lived events that might occur. Correlation coefficients at each time point were again converted to z-scores using the methods detailed in Section 3.3.4. However, unlike the results from that section, these correlation mappings cannot be averaged and have not been thresholded for statistical significance due to the concerns outlined in the previous section.

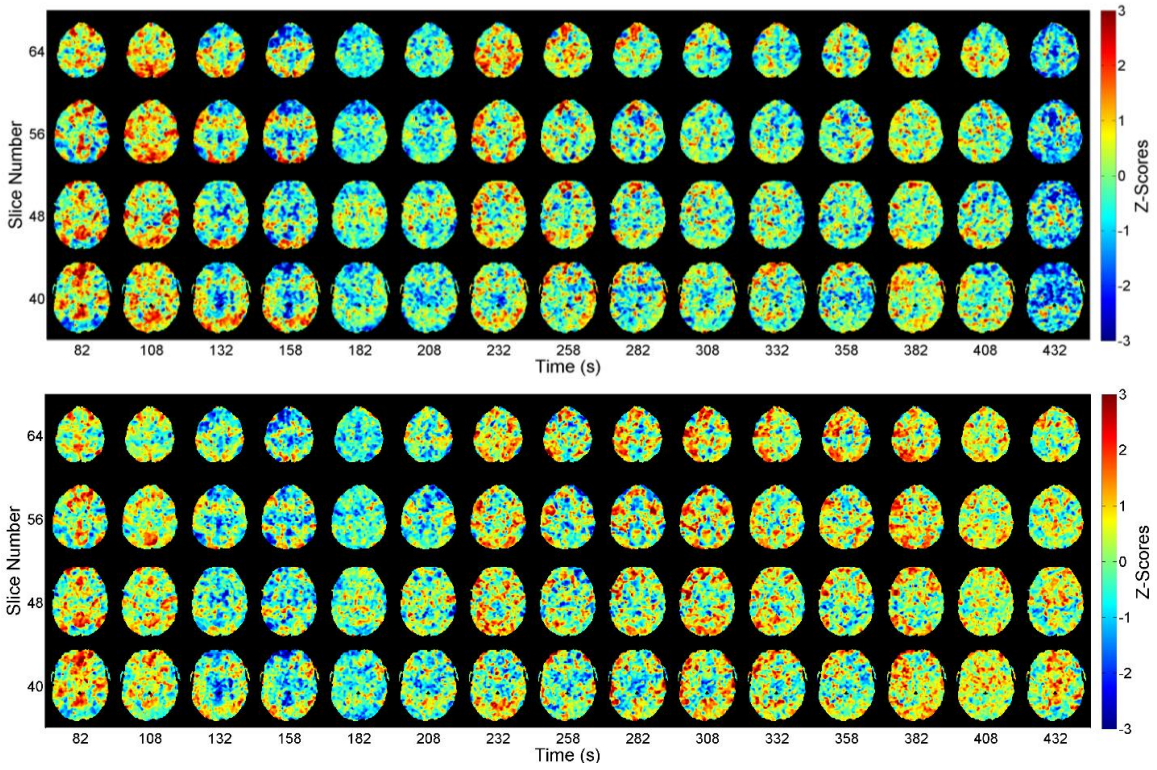

Figure 4.2: Example SWC volumes over time series from one trial. **Top:** This particular map represents dynamic correlations between infraslow BOLD and the electrode FT8. High magnitude correlations between electrophysiology and RSN nodes are visible at multiple time shifts, which is typical of these data. Temporal patterns are also visible. Correlation with DMN nodes starts strongly positive at 82s and shifts to strongly negative at 158s, then reappears positive at 258s. TPN correlation initially starts negative at 82s, shifts to positive by 158s, and then reappears positive and separate from the DMN at 232s. **Bottom:** BOLD-TP9 SWC series from the same trial. Correlation morphologies are mostly similar until approximately 282s, where they begin to diverge appreciably. Between 308s-382s, TP9 appears to correlate with lateralized components while FT8 appears uncorrelated.

This analysis produced one correlation mapping per electrode per trial, for a total of 120 separate SWC data sets. For obvious reasons, it is impossible to display images here that fit within the margins of this document while adequately summarizing the results. We have provided two example images in Figure 4.2 from a single trial with highly abbreviated time dimensions in order to illustrate some particular points. Later in this chapter, we provide references to movies of entire SWC time series that are combined with other results.

Images like the ones in Figure 4.2 were manually inspected for patterns and trends. The most salient feature of all images is the presence of strong correlation in regions corresponding with nodes of various resting state networks. Easily the most prevalent among them are the sensorimotor cortices, the IPS of the task positive network, and the various nodes of the default mode network. BOLD-EEG dynamic correlations are visible in these particular nodes at multiple time points in the example images. Other networks were also visible in other trials and electrodes.

Some additional features have been observed throughout the data that are worth mentioning here. RSN-like patterns were sometimes observed to invert in sign over time. Patterns were also observed to invert in sign over space (i.e. in a different electrode). Combinations of the two also have been seen, whereby a pattern disappears from one electrode and emerges in another with the opposite sign. However, the sign change is by no means universal; in many instances patterns do not change sign at all. That is, they may emerge and disappear at multiple time points while retaining the same sign, or they may appear to transition between electrodes without a sign change.

Not surprisingly given the results of Chapter 3, the between-trial correlation mappings are extremely variable. Any given pair of trials, even ones that originate from the same human subject, are distinctly unique. The perceived stability of RSN-like patterns is yet another variable contributing to their uniqueness. In at least three trials, patterns were observed to be stable for approximately 200s. In others, such as the example images in Figure 4.2, they vary much more rapidly (between approximately 25s-50s). Varying degrees of spatial stability have been witnessed, too. Segments of correlation mappings across nearly all electrodes exhibit very similar patterns in some trials. Other trials provide examples of differing patterns across electrodes. On this last point, however, it should be noted that this tends to only be observable in channels that are remote from one another on the electrode montage.

4.2.3 - Decomposing BOLD-EEG SWC Series with ICA

Throughout our examination of the infraslow BOLD-EEG SWC series, one detail consistently caught our attention across every individual mapping: the tendency of patterns to frequently and strongly resemble RSN topologies. Their ubiquitous presence bolstered our initial suspicions that infraslow EEG signals are dynamically coupled with the functional networks themselves, and we sought to test this hypothesis further.

However, visually inspecting unthresholded SWC images as we did for the previous section was a difficult endeavor. The presence of noise and the inability to effectively view and compare every time point of the data also made visual inspection an impractical approach for further testing. We therefore devised a simple test to provide more

information on whether or not the BOLD-EEG coupling occurs through resting state networks.

If functional brain networks are truly a link between infraslow BOLD and EEG signals, then we would expect RSN spatial patterns to constitute a mutually independent basis set of that link, just like they do for the BOLD data alone. Spoken plainly, we believed that if we decomposed our SWC series using group sICA, then we should see RSN patterns as the independent components. Performing this test using the same parameters from Section 3.4.3 yielded the results in Figure 4.3, which do appear very similar to RSNs established in literature (Damoiseaux et al., 2006; Rosazza and Minati, 2011; Veer et al., 2010).

Admittedly, while this test has practical value for the analysis to follow, it is likely incapable of providing conclusive meaning regardless of what the ICs look like. To understand why we must consider two related factors. First, it has been well established that RSNs represent separate brain regions whose BOLD signals are largely coherent over time. As a direct consequence, any EEG signal that is highly correlated with an RSN node by chance alone stands a much higher likelihood of being highly correlated with all nodes of that network. This can conceivably generate the appearance of strong correlation with one or more RSNs nodes at any time point in the SWC series. Also, because the SWC analysis utilized windowed segments of low-pass filtered data, and because successive windows maximally overlapped with previous ones, any false positives correlations with RSNs that were present would likely reappear at several successive time points.

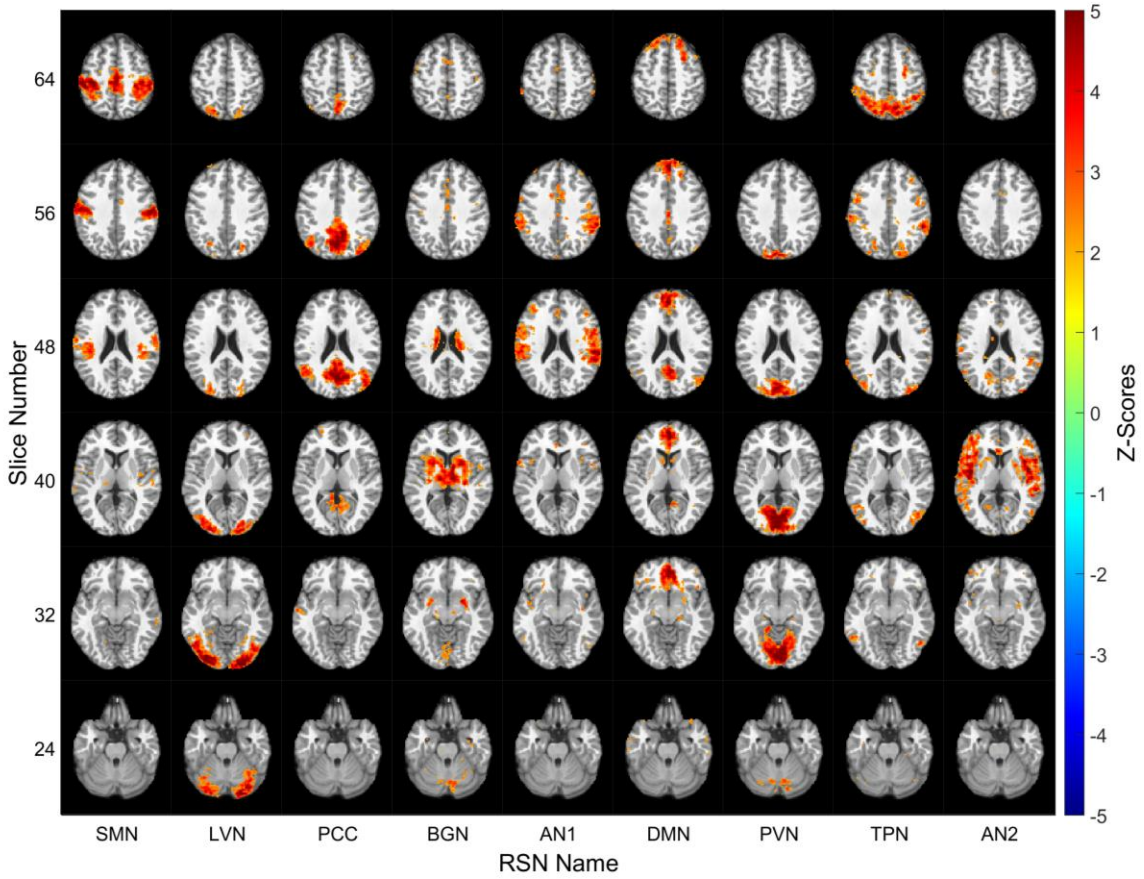

Figure 4.3: An example of the independent spatial components of BOLD-EEG SWC series. Group sICA decomposes the correlation volumes into components that strongly resemble RSNs, consistent with the notion that RSNs are coherent units of the infraslow BOLD-EEG coupling. Other networks including lateralized, salience, and precuneus components were also present but are not shown.

This is important to consider because it illustrates one of the major potential problems with SWC analyses as a whole. However, it is also receiving special emphasis here due to the extensive use of human visual inspection throughout this chapter. As we have noted, multiple sightings of RSN-like patterns over the SWC series are a particularly salient feature of the data, and in light of the issue just mentioned, we are compelled to advise caution lest we unintentionally fall victim to confirmation bias.

The second factor would have applied had the ICs *not* resembled complete RSNs. Recall that RSNs are *largely* coherent over time, inasmuch as they are coherent enough to be repeatedly found across individuals and species using time-invariant methods. However, it is now known that they are not *absolutely* coherent and do exhibit within-network fluctuations of connectivity metrics at the time scales of this SWC analysis (Allen et al., 2014; Hutchison et al., 2013b; Kiviniemi et al., 2011). Thus, had the ICA results of this section resembled separate nodes of RSNs, it may have been attributable to that factor.

Nevertheless, the sight of the networks in Figure 4.3 using the same parameters of past decompositions is consistent with the notion that RSNs are a fundamental unit of infraslow BOLD-EEG coupling. It also suggests that EEG tends to covary with the full topology of functional brain networks instead of individual nodes, at least for the SWC analysis parameters that were chosen. This is a critical foundation upon which the subsequent analysis was based.

4.3 - Mapping Dynamic Correlations between Infraslow RSN and EEG Signals

We have now repeatedly seen evidence that there is indeed a relationship between the infraslow signals of BOLD and EEG recorded in humans. The first analysis in this chapter shows how BOLD correlates of certain representative EEG signals dynamically vary as a function of time, space, and trial. Despite the high variability, correlation topologies at individual time points often bear a close resemblance to well-known RSNs. The previous section then suggested that the independently varying spatial patterns of BOLD-EEG correlations are indeed functional brain networks. What remains unclear is how this

relationship varies as a function of time, *electrode* space (as opposed to BOLD voxel space), and trial. It is this lack of knowledge that we address next.

4.3.1 - SWC between Infraslow RSN and EEG Signals

To get a sense of how the presumed RSN-EEG relationship spatiotemporally varies we combined the stationary analysis applied in Section 3.4 with the sliding window approach. Specifically, we generated SWC series between the RSN signals from the original ICA of our BOLD data and the infraslow EEG data. This is why the preceding section was informative, despite difficulties in interpreting the results; we justify the use of the original RSN signals by demonstrating that the spatial ICs of the SWC series are the full RSN topologies. Had they been only pieces or separate nodes of RSNs, the use of these signals would be invalid.

The results below complement our earlier BOLD-EEG SWC series by providing correlation mappings in electrode space. SWC between signals was performed with the same parameters used in Section 4.2.2: 50s window length, maximal window overlap, and 4s offset between RSN and EEG signals. Correlation coefficients were again converted to z-scores before images were produced. EEG signals from the full 68 channel montage were used in this analysis, unlike others that use only the representative subset of 10.

This analysis produced one mapping per trial, which greatly facilitated their inspection compared to the first SWC analysis. Still, space constraints in this document make it impossible to effectively display even a subset of the results. The image shown in Figure 4.4 is provided as a highly abbreviated example to illustrate some specific points. It also

results from the same trial as the BOLD-EEG mappings presented in Figure 4.2 in order to afford readers the opportunity for some limited comparisons.

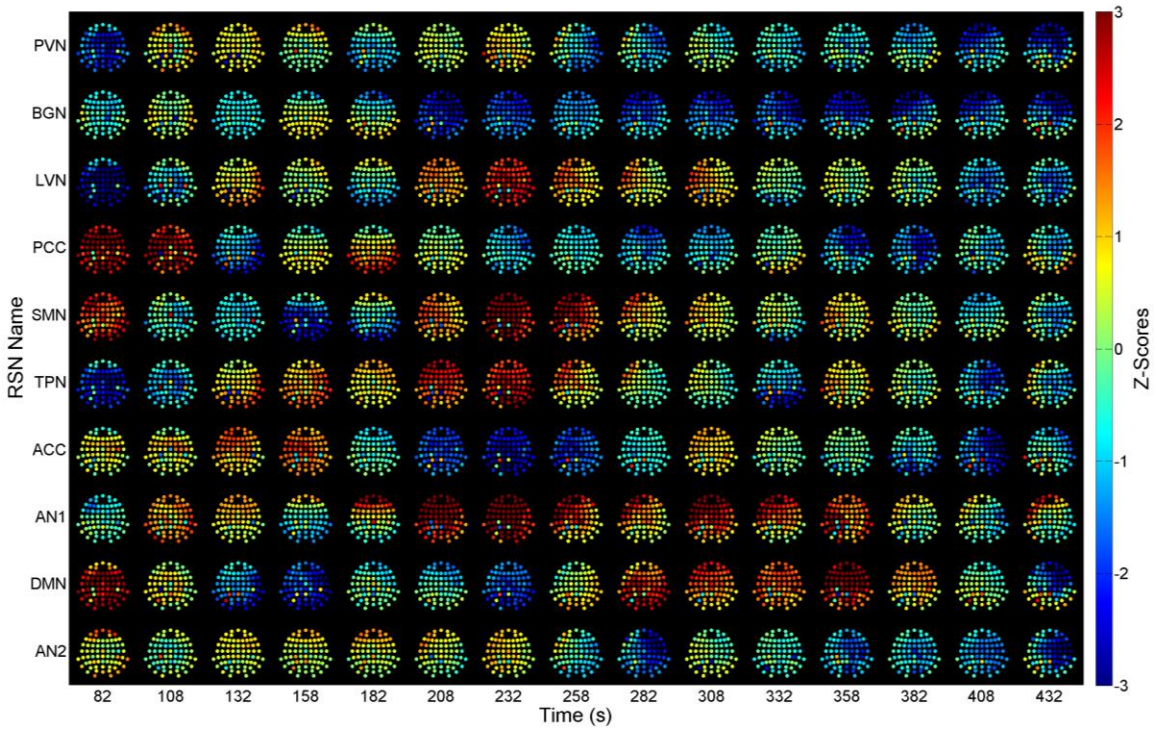

Figure 4.4: Example SWC series between infraslow BOLD RSN and EEG signals from one trial. This mapping shows how the correlation between RSNs and EEG change over time and electrode space. Each individual element of the montage is a spatial EEG channel mapping with a common orientation (nasion direction is up, left is truly left). The horizontal axis of the montage represents time and is highly condensed. The vertical montage axis labels the RSN signal that was correlated with infraslow EEG data. To facilitate comparisons, this mapping results from the same trial data as the BOLD-EEG SWC maps from Figure 4.2.

In keeping with the results of the rest of this study, mappings from this analysis are highly variable across trials. No two images, including those from the same subject, bear any resemblances to one another. However, they do all show that strong correlations with RSN

signals tend to occur in large groupings of electrodes across the scalp. In some instances, correlation appears uniform and nearly globally present in channels. In others, cluster size was observed to be restricted to half or fewer of all electrodes at multiple time points.

Several spatiotemporal features of the correlations are noteworthy as well and may be providing information about dynamic interactions between networks. One example that can be seen elsewhere in our results is a tendency for some correlations to fluctuate between positive and negative values over time. Mappings along the DMN and TPN rows in Figure 4.4, among others, exhibit this behavior here and even display some of their characteristic anticorrelations (Chai et al., 2012; Fox et al., 2009, 2005) with one another at select time points. Another interesting feature is how clusters of correlation can be seen to apparently move about the scalp over time (see the PVN in Figure 4.4, for example). Certain clusters can also appear complementary to others, either in the sign of the relationship or in scalp position. In Figure 4.4, correlations with the visual components PVN and LVN capture one instance of this occurring.

Generally speaking, the correlation patterns in electrode space (Figure 4.4) track those observed in voxel space (Figure 4.2) fairly well, although we did not quantify the extent to which they agree. Readers can better inspect this correspondence by viewing the movie provided in Figure 4.5. Unlike the other images in this chapter, the movie is capable of displaying every available time point in the SWC series. When viewing it and others, we observed that high-magnitude RSN-EEG correlations tended to similarly valued patterns in voxel space, especially when the former is roughly uniform and covers a majority of scalp electrodes. But this is not universally true; there are several instances, even in the

attached movie, where predictability appears to fall (see the period between approximately 350-400 s, for example).

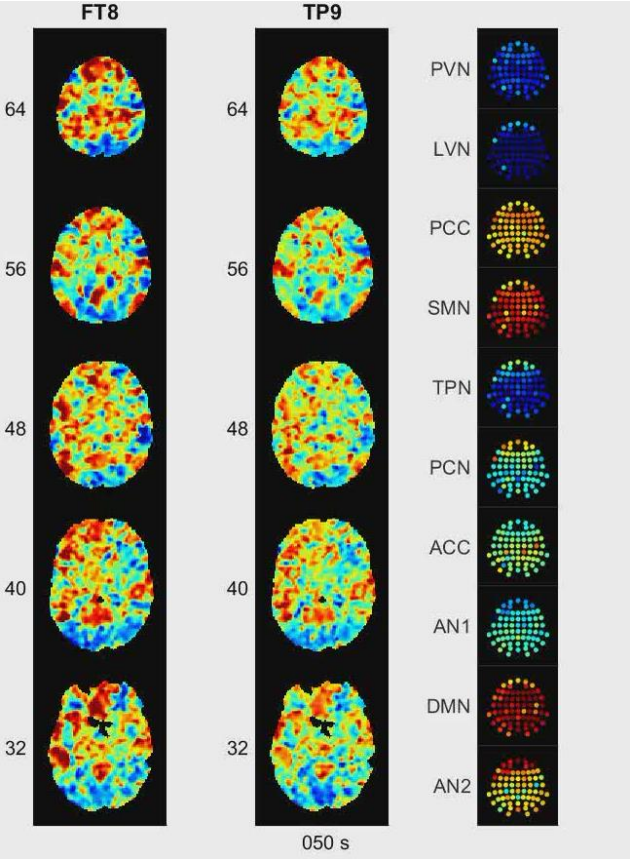

Figure 4.5: (BOLD-EEG Sliding Window Correlations.mp4, 4.31 MB)
Movie of SWC time series from BOLD-EEG and RSN-EEG analyses. This figure compares correlation results from BOLD voxel space (FT8 on the left, TP9 at center, both from Figure 4.2) with those from EEG electrode space (right, from Figure 4.4), showing every time point of correlation between the signals. The coloring of images changes with each frame of the movie, and a time index (in seconds) is centered on the bottom of each frame. The index starts at 50s to account for the window length used in the analyses and increments by 2s per frame. These results offer a view into the spatiotemporal dynamics of infraslow BOLD and EEG coupling over the course of a typical scan.

4.4 - Discussion and Conclusions

Throughout the preceding sections we presented our early attempts to investigate the time-varying behavior of the infraslow BOLD-EEG relationship. The analyses from Chapter 3 strongly suggested that this relationship is unstable over longer time periods and, although much work remains to be done before a complete understanding is developed, the results of this chapter are a clear indicator that infraslow electrophysiological and hemodynamic signals are not statically linked to one another. Instead their relationship appears to evolve across time and space throughout the duration of a typical scan. In further agreement with our previous discussions and recent findings (Hiltunen et al., 2014), BOLD functional networks are again a central feature of the relationship.

It is perhaps surprising to witness such a variable relationship because conventional theories suggest that infraslow BOLD and EEG signals are reflections of the same neuronal process (Drew et al., 2008; He et al., 2008; Hiltunen et al., 2014; Khader et al., 2008; Palva and Palva, 2012). If that were true, we might expect the signal correlations to be reasonably stationary in both time and space, an expectation that is obviously subverted by our results. Then why aren't the signals statically coupled? One obvious possibility is that the conventional thinking is incorrect; infraslow BOLD and EEG signals may not actually share a common neuronal component. If so, the correlations observed in this study could be the result of some other non-neuronal process that dynamically contributes to both signal types.

However, there is evidence to suggest that a neuronal mechanism links infraslow BOLD and EEG activity (Palva and Palva, 2012), and there may yet be an explanation for our findings that does not preclude its existence. First, consider the implications of the fact that the spatial origins of our infraslow EEG signals are unclear. Even if volume conduction is not a contributing factor, and it shouldn't be (see Section 2.4.2 and (Khader et al., 2008)), our EEG data are still a mixture of electrical activity across cortical regions of unknown size and overlap. This is a problem that is inherent to working in electrode space as opposed to brain space (Laufs et al., 2008). While we presume that localization is more accurate in infraslow data than in higher frequencies because of the lack of volume conduction, any given signal from our data reflects a regionally aggregated state that could depend significantly on the states of surrounding areas.

As regional measures, EEG signals are biased towards capturing the larger-scale, most proximal, and most active networks at any given time. Contributions from less active, smaller-scale, and deeper networks are probably obscured to varying degrees in the recordings. Consider also that the configuration of active brain networks can change substantially over brief intervals (see Figure 3.7), which likely has complicated effects on EEG readings if the two are truly related. It is therefore plausible that some non-stationarities in their relationship arise from the low spatial resolution of EEG, meaning that common components between the infraslow signals may change because scalp electrophysiology only reflects a dominant subset of network activity per time point.

It is also likely that infraslow EEG by itself cannot completely characterize the overall BOLD-EEG relationship. Others have noted evidence that the BOLD signal contains

information related to multiple frequency bands of neuronal activity (Chang et al., 2013; Keilholz, 2014; Laufs et al., 2006; Magri et al., 2012; Mantini et al., 2007; Meyer et al., 2013; Raichle, 2011) and that these different bands might coordinate activities across different distances (Buzsáki, 2006). Our coherence results from Section 3.5.3 suggested that such links might even variable within and between bands over time. If so, then the dynamics that have been observed in this study could represent yet another frequency scale that factors into this organizational scheme.

However, characterizing this spectral organization is currently being complicated by an uncertain relationship between the infraslow and higher frequency signals. Some studies in humans have found that the phases of infraslow EEG signals appear to be driven by the amplitudes of higher frequency ones (Monto et al., 2008; Vanhatalo et al., 2004). If infraslow EEG and BOLD are both just reflections of higher frequency activity and each other, then the infraslow scale might not factor into the organizational scheme at all. One recent study suggests that this is not the case, though. Using invasive electrophysiology in rat models, Thompson et al. provided evidence that fast and slow (including infraslow) electrophysiology contribute differently to spontaneous BOLD fluctuations (Thompson et al., 2014).

Although the correlations seen throughout this chapter serve as an indicator of when and possibly where coupling occurs between the BOLD and EEG data, it is not clear how they might indicate the activities of the networks themselves. From a practical standpoint, it is interesting to consider whether or not any patterns might be present that would be useful for predicting RSN activity or brain state, which could impact future behavioral and clinical

studies. The RSN-EEG correlation series shown here seem well suited to this kind of endeavor due to their ability to summarize the potential link between multiple networks and neurophysiology. In previous work, topographies of coherent slow cortical potentials recorded by ECoG have already been found to be similar to those of RSNs (He et al., 2008). Additionally, RSN activities have been found to statically correlate with certain microstates derived from higher frequency EEG data (Britz et al., 2010; Yuan et al., 2012). Before such a feat becomes possible, however, additional work would need to be done to assess the uniqueness of correlation topographies as well as their repeatability.

CHAPTER 5

CONCLUSIONS

5.1 - On the Relationship between Infraslow Hemodynamics and Electrophysiology

We conclude our investigation of the infraslow BOLD-EEG relationship by stating simply that it does appear to exist, but its complex nature exceeds the ability of our methods to fully characterize it. There is much that that was presented here that we do not yet understand, and many questions need to be resolved before the deeper significance behind some results becomes clear. However, our findings do suggest several starting points on which future studies might be based. Additional work will be critical in order to unravel the connection between hemodynamics and electrophysiology, and by extension the relationship between functional connectivity and neuronal activity.

Chapter 3 examined the relationship under the assumption that it is temporally stationary, or time-invariant. We found that strong correlations exist between infraslow EEG signals and spatial patterns of BOLD signals that resemble well-known large-scale functional brain networks. Comparing representative signals of those networks with EEG signals again demonstrated that they are well-correlated in all available trials. However, the high degree of variability present across individual trials leads to incoherent averaging when attempting to examine any group-wide trends in correlation. We therefore concluded that this is evidence of a direct relationship between the signal types, but that this relationship cannot be considered spatially or temporally static over times similar to our scanning duration.

Chapter 4 investigated these conclusions without the assumption of temporal stationarity. In agreement with our earlier results, correlations between BOLD and EEG signals were found to vary appreciably over time scales much smaller than the trial duration. Additional analyses revealed that RSNs are a central feature of the dynamic and that representative signals of these networks are also variably linked with changing topographies of EEG electrodes. These results lead us to conclude that EEG and fMRI signals are linked together in large part by the activity of large-scale brain networks. We further suspect that the dynamic coupling between them might be the consequence of a relationship that depends on more parameters than can be considered by sliding window correlation. Namely, it could be evidence of a relationship that extends across multiple frequency scales.

5.2 - Limitations of This Study

Despite our best efforts to mitigate them, several limitations affected this study and are worth mentioning here. Usually, they took the form of gaps in knowledge that interfered with our ability to meaningfully interpret results, but in a few instances they also interfered with our ability to fully meet the goals of our study. Regardless, readers should keep the limitations discussed here in mind while considering our findings and when designing new experiments that are related to them.

Perhaps the single biggest limiting factor is the small sample population that was simultaneously imaged. Our study originally called for 26 healthy adult participants, but only 12 were ultimately scanned. Out of those, 4 were rejected from over concerns with the quality of their data (see Section 2.4.1), leaving us with 8 test subjects in which to probe

the infraslow BOLD-EEG relationship. A sample size of 8 is admittedly low and almost certainly had a negative impact on the statistical power available to us. Unfortunately, this was a consequence of unforeseen cuts to project funding while we were still in the early stages of data collection. Although many of our findings are predicated on un-averaged, single-trial analyses, the inclusion of additional subjects might have allowed us to better explore group-wide trends in BOLD-EEG coupling. For example, the averages presented in Chapter 3 might have refined appearances and could have achieved statistical significance more often, which in turn could have led us towards other theories and analyses that we did not pursue. A higher sample size would also have afforded us the opportunity to witness more variability in cases where averaging was to be incoherent anyway. This would be helpful for gauging the extent of ordinary variability in general, but might have been especially useful in the time-varying analyses of Chapter 4. Having additional subjects for that section of the study could have allowed us to investigate for common patterns of correlation between trials and individuals.

Another limitation derives from our experimental protocol, which did not include the recording of respiratory signals from participants. Respiration is typically is of higher frequency (~0.3 Hz) but is aliased down into the infraslow passband when long TRs are used (Bhattacharyya and Lowe, 2004; Lowe et al., 1998), making them a source of noise in data such as ours. Worse still, respiratory-related fluctuations have been shown to correlate with BOLD signals and spuriously influence functional connectivity metrics (Birn et al., 2006; Shmueli et al., 2007; Wise et al., 2004). Respiration may also be influencing infraslow EEG signals through motion and by changing blood CO_2 concentrations (discussed below). If both BOLD and EEG are being influenced by the same

noise source, then there is an increased likelihood of observing erroneous correlations between them. Yet without recordings of respiratory activity from each subject, we were unable to control for this confound.

Our ability to understand some results is also limited by a general lack of knowledge on infraslow EEG. This study demonstrates that infraslow EEG tends to correlate best with BOLD signals derived from cortical gray matter, but it is still difficult to disentangle the non-neuronal and neuronal contributors to this correlation. Because our sensitivity with EEG is largely limited to the cortex, the term non-neuronal here refers to glial or physiological signals that are present in the cortex. That is, we are referring to phenomena such as blood flow and not to subcortical signals originating from deeper brain structures. Infraslow EEG in particular is susceptible to noise from numerous sources including variations in CO_2 concentrations (Voipio et al., 2003) and blood volume (Vanhatalo et al., 2003). While animal work is helpful in sorting this issue out (Pan et al., 2013), the connection to neural processing can also be made by performing tasks while simultaneous fMRI and EEG is recorded. Task-based results would strengthen those seen throughout this study.

5.3 - Future Directions

This study has provided some insight into the relationship between infraslow BOLD and EEG activities, but there are many questions that remain to be answered before their link is completely understood. Future work that is based on this project should focus on refining several of the aspects that were given only cursory treatment or were not addressed directly.

Some examples include further characterizing the static and dynamic properties of the infraslow BOLD-EEG relationship, determining whether or not the relationship can be linked to behavioral and disease states, and working towards fully understanding infraslow EEG recordings alone.

While the temporally stationary analyses used throughout Chapter 3 are known to hide nuanced interactions, they still describe the dominant trends of the BOLD-EEG relationship over time and can serve purposes that were not explored here. One way in which these analyses may yet prove useful would be to consider nonlinear couplings between the data. Our methods investigated only for the presence of covariance, or linear similarities, between the waveforms, but there are other mechanisms by which the data could be related.

Information theory, and in particular mutual information, has been leveraged in the past to describe higher order statistical dependencies between electrophysiology and BOLD (Magri et al., 2012) and between functionally connected BOLD signals (Hlinka et al., 2011). Although Hlinka et al. reported that linear correlation misses only a small fraction of functional relationships described by mutual information in BOLD data alone (Hlinka et al., 2011), it is not yet clear how applicable their finding is to relationships between BOLD and EEG data. In that particular relationship, neurovascular coupling could conceivably be introducing nonlinearities.

Another area where static analyses would be helpful is in determining whether or not the infraslow BOLD-EEG relationship can be used to predict behaviors or task performance.

We originally attempted to record two scans of task performance per individual subject in order to partially address this question, but technical problems and an abrupt loss of project funding meant that the amount of usable data was ultimately too low. Future studies could work on linking the results that were found here to task performance, likely by using the same psychomotor vigilance task that we proposed. It is already known that static functional connectivity metrics can be used as a predictors of vigilance (Drummond et al., 2005; Singh and Fawcett, 2008; Thompson et al., 2013a). Similarly, it has been shown that infraslow cortical potentials can be predictive of both vigilance (Helps et al., 2010; Trimmel et al., 1990) and the functional connectivity that was just mentioned (Hlinka et al., 2010). We therefore suspect that the two are related, especially given that our results suggest a relationship between spontaneous data. Other task paradigms should be considered too. Additional knowledge on this front could be used to document new standalone EEG-based performance metrics, which would be useful to some research that is unable to concurrently record fMRI.

The BOLD-EEG link may also be useful as a marker for certain diseases. BOLD-based metrics have repeatedly been demonstrated to predict a number of neurological disorders (Arbabshirani, 2014; Bonnelle et al., 2012; Garrity et al., 2007; Greicius et al., 2007; Sheline and Raichle, 2013; Tian et al., 2006; Veer et al., 2010). Comparatively little research has been done to directly relate infraslow EEG to disease states, but spontaneous scalp fluctuations have been linked with attentional disorders (Helps et al., 2008, 2010). Future studies could work towards establishing links with other diseases for which BOLD already has predictive and diagnostic value. They could also examine how the relationship between infraslow EEG and functional brain networks might be used to similar ends. For

example, one recent study found that patterns of BOLD-EEG coupling were shifted in frequency in patients with schizophrenia compared to healthy controls (Razavi et al., 2013). Considering all of the direct and indirect evidence that now exists relating these phenomena, we believe that infraslow EEG could become a valuable tool for research and clinical work on various brain disorders.

Our static analyses strongly suggested that the infraslow BOLD-EEG relationship is dynamic at timescales less than the trial duration, and the analyses of Chapter 4 afforded us a preliminary glimpse at how coupling may be dynamic over space and time. The suggested directions for future work that were made earlier in this apply here as well. Eventually, researchers should investigate how the dynamics of functional connectivity and its relationship to electrophysiology relate to behavioral and pathological states. However, the results of Chapter 4 highlight several points on which our knowledge is decidedly poor. These may deserve more immediate attention from the research community.

One such point concerns the theory that BOLD is coupled with multiple frequency scales of electrophysiological activity. Prior evidence is suggestive of this scheme (Jann et al., 2010; Keilholz, 2014; Magri et al., 2012; Mantini et al., 2007; Meyer et al., 2013; Raichle, 2011; Tagliazucchi et al., 2012) and some results suggest that the relationship could vary between bands of frequencies over time (Chang and Glover, 2010; Chang et al., 2013). Our findings from Chapter 3 (see Figure 3.11) also indicate that this might be true by demonstrating that coherence can occur across a range of frequencies that is not exclusive to the infraslow band and is highly variable, even in trials from the same individual. To

date, though, no studies have analyzed full-band EEG in conjunction with fMRI, which will be a necessary step in order to test that hypothesis directly in humans. Until this is done, interpreting the results from Chapter 4 will remain a difficult endeavor because spectrally dynamic behaviors cannot be completely accounted for.

Another point is related to the dynamic analysis techniques themselves. Sliding window correlation has so far been a popular means of observing both time-varying functional connectivity and time-varying relationships between BOLD and EEG (Leonardi and Ville, 2015), but there are problems with this approach. It is not only difficult to assess statistical significance when using it (see Section 4.2.1), but it is difficult and potentially impossible to correctly choose certain parameters when applying it. Consider, for example, the relationship between BOLD and EEG at any frequency scale. If their coupling occurs variably across the frequency spectrum, and evidence presented earlier suggests that it does, then there cannot be an ideal SWC window length. Moreover, if the coupling relies on multiple frequencies simultaneously, then the problem is compounded. Future studies can avoid these problems altogether by utilizing other methods for assessing time-varying relationships. The use of wavelets seems particularly promising in solving these issues due to their ability to account for multiple temporal and spectral scales (Torrence and Compo, 1998).

The results of this project serve as a strong incentive to learn more about the infraslow EEG signals themselves. For example, it is not currently known to what degree non-neuronal sources contribute to the scalp recorded potentials. Answering this question will likely be difficult and involve invasive recordings that can be compared with surface ones.

However, without this knowledge it is unclear how much of the BOLD-EEG relationship can be attributed to neuronal activity. Similar experiments may also be carried out to assess the influences of volume conduction at infraslow frequencies. We expected that volume conduction was not a major contributor in our data based on a simple test for its presence (see Section 2.4.2) and indirect evidence (Birbaumer et al., 1990), but direct investigations would strengthen that assertion.

It is also unclear how the infraslow EEG signals might relate to higher frequency data. As we discussed in Chapter 4, Monto et al. found that infraslow fluctuations are tightly coupled with faster activities (Monto et al., 2008). Considering the support for a BOLD-EEG relationship at infraslow frequencies, this implies that BOLD might only be reflecting the higher frequencies and infraslow electrophysiology is just an intermediary. However, the later study by Thompson et al. suggests that high and low frequencies contribute separately (Thompson et al., 2014). Further experimentation is necessary to determine the true nature of their connection. Doing so could also bring us a step closer to understanding how functional networks relate to more rapid cognitive processes that hemodynamics are too slow to explain alone.

REFERENCES

Acharjee, P., Phlypo, R., Wu, L., Calhoun, V., Adali, T., 2015. Independent Vector Analysis for Gradient Artifact Removal in Concurrent EEG-fMRI Data. IEEE Trans. Biomed. Eng. 9294, 1–1.

Aladjalova, N. a, 1957. Infra-slow rhythmic oscillations of the steady potential of the cerebral cortex. Nature 179, 957–959.

Aladjalova, N.A., 1964. Infraslow potential oscillations in the cerebral cortex. Prog. Brain Res. Slow Electr. Process. Brain 7, 39–58.

Allen, E. a, Erhardt, E.B., Damaraju, E., Gruner, W., Segall, J.M., Silva, R.F., Havlicek, M., Rachakonda, S., Fries, J., Kalyanam, R., Michael, A.M., Caprihan, A., Turner, J. a, Eichele, T., Adelsheim, S., Bryan, A.D., Bustillo, J., Clark, V.P., Feldstein Ewing, S.W., Filbey, F., Ford, C.C., Hutchison, K., Jung, R.E., Kiehl, K. a, Kodituwakku, P., Komesu, Y.M., Mayer, A.R., Pearlson, G.D., Phillips, J.P., Sadek, J.R., Stevens, M., Teuscher, U., Thoma, R.J., Calhoun, V.D., 2011. A baseline for the multivariate comparison of resting-state networks. Front. Syst. Neurosci. 5, 2.

Allen, E. a., Damaraju, E., Plis, S.M., Erhardt, E.B., Eichele, T., Calhoun, V.D., 2014. Tracking whole-brain connectivity dynamics in the resting state. Cereb. Cortex 24, 663–676.

Arbabshirani, M.R., 2014. Functional network connectivity in human brain and its applications in automatic diagnosis of brain disorders.

Bauer, H., Korunka, C., Leodolter, M., 1989. Technical requirements for high-quality scalp DC recordings. Electroencephalogr. Clin. Neurophysiol. 72, 545–547.

Bell, A.J., Sejnowski, T.J., 1995. Information-Maximization Approach to Blind Separation and Blind Deconvolution. Neural Comput. 7, 1129–1159.

Belliveau, J.W., Kennedy, D.N., McKinstry, R.C., Buchbinder, B.R., Weisskoff, R.M., Cohen, M.S., Vevea, J.M., Brady, T.J., Rosen, B.R., 1991. Functional mapping of the human visual cortex by magnetic resonance imaging. Science (80-.). 254, 716 – 719.

Belliveau, J.W., Rosen, B.R., Kantor, H.L., Rzedzian, R.R., Kennedy, D.N., McKinstry, R.C., Vevea, J.M., Cohen, M.S., Pykett, I.L., Brady, T.J., 1990. Functional cerebral imaging by susceptibility-contrast NMR. Magn. Reson. Med. 14, 538–546.

Berger, H., 1929. Über das elektroenkephalogramm des menschen. Achte mitteilung. Arch. Psychiatr. Nervenkr.

Bhattacharyya, P.K., Lowe, M.J., 2004. Cardiac-induced physiologic noise in tissue is a direct observation of cardiac-induced fluctuations. Magn. Reson. Imaging 22, 9–13.

Bianciardi, M., Fukunaga, M., van Gelderen, P., Horovitz, S.G., de Zwart, J. a, Shmueli, K., Duyn, J.H., 2009. Sources of functional magnetic resonance imaging signal fluctuations in the human brain at rest: a 7 T study. Magn. Reson. Imaging 27, 1019–29.

Birbaumer, N., Elbert, T., Canavan, A.G., Rockstroh, B., 1990. Slow potentials of the cerebral cortex and behavior. Physiol Rev 70, 1–41.

Birn, R.M., Diamond, J.B., Smith, M. a., Bandettini, P. a., 2006. Separating respiratory-variation-related fluctuations from neuronal-activity-related fluctuations in fMRI. Neuroimage 31, 1536–1548.

Biswal, B., 1995. Functional connectivity in the motor cortex of resting human brain using echo-planar mri. Magn. Reson. … 537–541.

Biswal, B.B., Van Kylen, J., Hyde, J.S., 1997. Simultaneous assessment of flow and BOLD signals in resting-state functional connectivity maps. NMR Biomed. 10, 165–170.

Bollimunta, A., Chen, Y., Schroeder, C.E., Ding, M., 2008. Neuronal mechanisms of cortical alpha oscillations in awake-behaving macaques. J. Neurosci. 28, 9976–9988.

Bonnelle, V., Ham, T.E., Leech, R., Kinnunen, K.M., Mehta, M. a, Greenwood, R.J., Sharp, D.J., 2012. Salience network integrity predicts default mode network function after traumatic brain injury. Proc. Natl. Acad. Sci. U. S. A. 109, 4690–5.

Born, J., Whipple, S.C., Stamm, J., 1982. Spontaneous cortical slow-potential shifts and choice reaction time performance. Electroencephalogr. Clin. Neurophysiol. 54, 668–76.

Boubela, R.N., Kalcher, K., Huf, W., Kronnerwetter, C., Filzmoser, P., Moser, E., 2013. Beyond Noise: Using Temporal ICA to Extract Meaningful Information from High-Frequency fMRI Signal Fluctuations during Rest. Front. Hum. Neurosci. 7, 168.

Britz, J., Van De Ville, D., Michel, C.M., 2010. BOLD correlates of EEG topography reveal rapid resting-state network dynamics. Neuroimage 52, 1162–70.

Buckner, R.L., Andrews-Hanna, J.R., Schacter, D.L., 2008. The brain's default network: Anatomy, function, and relevance to disease. Ann. N. Y. Acad. Sci. 1124, 1–38.

Buckner, R.L., Vincent, J.L., 2007. Unrest at rest: Default activity and spontaneous network correlations. Neuroimage 37, 1091–1096.

Buxton, R.B., 2009. Introduction to Functional Magnetic Resonance Imaging, Book.

Buzsáki, G., 2006. Rhythms of the Brain, Rhythms of the Brain.

Buzsáki, G., Anastassiou, C. a., Koch, C., 2012. The origin of extracellular fields and currents — EEG, ECoG, LFP and spikes. Nat. Rev. Neurosci. 13, 407–420.

Buzsáki, G., Silva, F.L. Da, 2012. High frequency oscillations in the intact brain. Prog. Neurobiol. 98, 241–249.

Calhoun, V., Adali, T., 2001. Spatial and temporal independent component analysis of functional MRI data containing a pair of task-related waveforms. Hum. brain … 53, 43–53.

Calhoun, V., Adali, T., 2006. Unmixing fMRI with independent component analysis. … Med. Biol. Mag. IEEE 79–90.

Calhoun, V., Adali, T., Hansen, L., Larsen, J., Pekar, J., 2003. ICA of functional MRI data: an overview 281–288.

Calhoun, V.D., Adali, T., Pearlson, G.D., Pekar, J.J., 2001. A method for making group inferences from functional MRI data using independent component analysis. Hum. Brain Mapp. 14, 140–51.

Calhoun, V.D., Liu, J., Adali, T., 2009. A review of group ICA for fMRI data and ICA for joint inference of imaging, genetic, and ERP data. Neuroimage 45, S163–72.

Canolty, R.T., Knight, R.T., 2010. The functional role of cross-frequency coupling. Trends Cogn. Sci. 14, 506–515.

Carvajal-Rodríguez, A., de Uña-Alvarez, J., Rolán-Alvarez, E., 2009. A new multitest correction (SGoF) that increases its statistical power when increasing the number of tests. BMC Bioinformatics 10, 209.

Castellanos, F.X., Margulies, D.S., Kelly, C., Uddin, L.Q., Ghaffari, M., Kirsch, A., Shaw, D., Shehzad, Z., Di Martino, A., Biswal, B., Sonuga-Barke, E.J.S., Rotrosen, J., Adler, L. a., Milham, M.P., 2008. Cingulate-Precuneus Interactions: A New Locus of Dysfunction in Adult Attention-Deficit/Hyperactivity Disorder. Biol. Psychiatry 63, 332–337.

Caton, R., 1875. The Electric Currents of the Brain. Brit Med J.

Chai, X.J., Castañán, A.N., Öngür, D., Whitfield-Gabrieli, S., 2012. Anticorrelations in resting state networks without global signal regression. Neuroimage 59, 1420–1428.

Chai, X.J., Whitfield-Gabrieli, S., Shinn, A.K., Gabrieli, J.D.E., Nieto Castañón, A., McCarthy, J.M., Cohen, B.M., Ongür, D., 2011. Abnormal medial prefrontal cortex resting-state connectivity in bipolar disorder and schizophrenia. Neuropsychopharmacology 36, 2009–2017.

Chang, C., Glover, G.H., 2010. Time-frequency dynamics of resting-state brain connectivity measured with fMRI. Neuroimage 50, 81–98.

Chang, C., Liu, Z., Chen, M.C., Liu, X., Duyn, J.H., 2013. EEG correlates of time-varying BOLD functional connectivity. Neuroimage 72, 227–236.

Clark, C.M., Kessler, R., Buchsbaum, M.S., Margolin, R.A., Holcomb, H.H., 1984. Correlational methods for determining regional coupling of cerebral glucose metabolism: a pilot study. Biol. Psychiatry 19, 663–78.

Comon, P., 1994. Independent component analysis, A new concept? Signal Processing 36, 287–314.

Cordes, D., Haughton, V.M., Arfanakis, K., Carew, J.D., Turski, P.A., Moritz, C.H., Quigley, M.A., Meyerand, M.E., 2001. Frequencies contributing to functional connectivity in the cerebral cortex in "resting-state" data. Am. J. Neuroradiol. 22, 1326–1333.

Cordes, D., Haughton, V.M., Arfanakis, K., Wendt, G.J., Turski, P.A., Moritz, C.H., Quigley, M.A., Meyerand, M.E., 2000. Mapping functionally related regions of brain with functional connectivity MR imaging. Am. J. Neuroradiol. 21, 1636–1644.

Cox, R.W., 1996. AFNI: software for analysis and visualization of functional magnetic resonance neuroimages. Comput. Biomed. Res. 29, 162–173.

Damoiseaux, J.S., Rombouts, S.A.R.B., Barkhof, F., Scheltens, P., Stam, C.J., Smith, S.M., Beckmann, C.F., 2006. Consistent resting-state networks across healthy subjects. Proc. Natl. Acad. Sci. U. S. A. 103, 13848–13853.

Darvas, F., Pantazis, D., Kucukaltun-Yildirim, E., Leahy, R.M., 2004. Mapping human brain function with MEG and EEG: methods and validation. Neuroimage 23 Suppl 1, S289–99.

Davey, C.E.C., Grayden, D.D.B., Egan, G.G.F., Johnston, L.L. a, 2013. Filtering induces correlation in fMRI resting state data. Neuroimage 64, 728–40.

De Luca, M., Beckmann, C.F., De Stefano, N., Matthews, P.M., Smith, S.M., 2006. fMRI resting state networks define distinct modes of long-distance interactions in the human brain. Neuroimage 29, 1359–67.

Debener, S., Mullinger, K.J., Niazy, R.K., Bowtell, R.W., 2008. Properties of the ballistocardiogram artefact as revealed by EEG recordings at 1.5, 3 and 7 T static magnetic field strength. Int. J. Psychophysiol. 67, 189–199.

Delorme, A., Makeig, S., 2004. EEGLAB: An open source toolbox for analysis of single-trial EEG dynamics including independent component analysis. J. Neurosci. Methods 134, 9–21.

Dinges, D.F., Powell, J.W., 1985. Microcomputer analyses of performance on a portable, simple visual RT task during sustained operations. Behav. Res. Methods, Instruments, Comput. 17, 652–655.

Drew, P.J., Duyn, J.H., Golanov, E., Kleinfeld, D., 2008. Finding coherence in spontaneous oscillations. Nat. Neurosci. 11, 991–3.

Drummond, S.P. a, Bischoff-Grethe, A., Dinges, D.F., Ayalon, L., Mednick, S.C., Meloy, M.J., 2005. The neural basis of the psychomotor vigilance task. Sleep 28, 1059–1068.

Eichele, T., Calhoun, V., Debener, S., 2009. Mining EEG–fMRI using independent component analysis. Int. J. … 73, 53–61.

Eichele, T., Calhoun, V.D., Moosmann, M., Specht, K., Jongsma, M.L. a, Quiroga, R.Q., Nordby, H., Hugdahl, K., 2008a. Unmixing concurrent EEG-fMRI with parallel independent component analysis. Int. J. Psychophysiol. 67, 222–34.

Eichele, T., Debener, S., Calhoun, V.D., Specht, K., Engel, A.K., Hugdahl, K., von Cramon, D.Y., Ullsperger, M., 2008b. Prediction of human errors by maladaptive changes in event-related brain networks. Proc. Natl. Acad. Sci. U. S. A. 105, 6173–8.

Eichele, T., Moosmann, M., Wu, L., Gutberlet, I., Debener, S., 2010. Removal of MRI Artifacts from EEG Recordings, in: Ullsperger, M., Debener, S. (Eds.), Simultaneous EEG and fMRI: Recording, Analysis, and Application. Oxford University Press, pp. 95–104.

Elbert, T., 1993. Slow cortical potentials reflect the regulation of cortical excitability. Physiol. … 235–251.

Engel, a K., Fries, P., Singer, W., 2001. Dynamic predictions: oscillations and synchrony in top-down processing. Nat. Rev. Neurosci. 2, 704–716.

Esposito, F., Scarabino, T., Hyvarinen, A., Himberg, J., Formisano, E., Comani, S., Tedeschi, G., Goebel, R., Seifritz, E., Di Salle, F., 2005. Independent component analysis of fMRI group studies by self-organizing clustering. Neuroimage 25, 193–205.

Esposito, F., Seifritz, E., Formisano, E., Morrone, R., Scarabino, T., Tedeschi, G., Cirillo, S., Goebel, R., Di Salle, F., 2003. Real-time independent component analysis of fMRI time-series. Neuroimage 20, 2209–2224.

Faro, S., Mohamed, F., 2010. BOLD fMRI: A Guide to Functional Imaging for Neurocientists.

Filippov, I. V, Gladyshev, A. V, Williams, W.C., 2002. Role of infraslow (0–) potential oscillations in the regulation of brain stress response by the locus coeruleus system. Neurocomputing.

Fisher, R.A., 1915. Frequency distribution of the values of the correlation coefficient in samples from an indefinitely large population. Biometrika.

Fox, M.D., Raichle, M.E., 2007. Spontaneous fluctuations in brain activity observed with functional magnetic resonance imaging. Nat. Rev. Neurosci. 8, 700–711.

Fox, M.D., Snyder, A.Z., Vincent, J.L., Corbetta, M., Van Essen, D.C., Raichle, M.E., 2005. The human brain is intrinsically organized into dynamic, anticorrelated functional networks. Proc. Natl. Acad. Sci. U. S. A. 102, 9673–8.

Fox, M.D., Snyder, A.Z., Zacks, J.M., Raichle, M.E., 2006. Coherent spontaneous activity accounts for trial-to-trial variability in human evoked brain responses. Nat. Neurosci. 9, 23–25.

Fox, M.D., Zhang, D., Snyder, A.Z., Raichle, M.E., 2009. The global signal and observed anticorrelated resting state brain networks. J. Neurophysiol. 101, 3270–3283.

Fransson, P., 2005. Spontaneous low-frequency BOLD signal fluctuations: an fMRI investigation of the resting-state default mode of brain function hypothesis. Hum. Brain Mapp. 26, 15–29.

French, C.C., Beaumont, J.G., 1984. A critical review of EEG coherence studies of hemisphere function. Int. J. Psychophysiol.

Fries, P., Reynolds, J.H., Rorie, a E., Desimone, R., 2001. Modulation of oscillatory neuronal synchronization by selective visual attention. Science 291, 1560–1563.

Friston, K., 2011. Functional and effective connectivity: a review. 1.

Friston, K.J., Frith, C.D., Liddle, P.F., Frackowiak, R.S., 1993. Functional connectivity: the principal-component analysis of large (PET) data sets. J. Cereb. Blood Flow Metab. 13, 5–14.

Frostig, R.D., Gottlieb, Y., Vaadia, E., Abeles, M., 1983. The effects of stimuli on the activity and functional connectivity of local neuronal groups in the cat auditory cortex. Brain Res. 272, 211–221.

Ganzetti, M., Mantini, D., 2013. Functional connectivity and oscillatory neuronal activity in the resting human brain. Neuroscience 240, 297–309.

Garrity, A.G., Pearlson, G.D., McKiernan, K., Lloyd, D., Kiehl, K.A., Calhoun, V.D., 2007. Aberrant "default mode" functional connectivity in schizophrenia. Am. J. Psychiatry.

Gerstein, G.L., 1970. Functional association of neurons: detection and interpretation. Neurosci. Second Study Progr. 648–661.

Goense, J.B.M., Logothetis, N.K., 2008. Neurophysiology of the BOLD fMRI Signal in Awake Monkeys. Curr. Biol. 18, 631–640.

Goldman, R., Stern, J., Jr, J.E., Cohen, M., 2002. Simultaneous EEG and fMRI of the alpha rhythm. Neuroreport 13, 2487–2492.

Gonçalves, S.I., De Munck, J.C., Pouwels, P.J.W., Schoonhoven, R., Kuijer, J.P. a, Maurits, N.M., Hoogduin, J.M., Van Someren, E.J.W., Heethaar, R.M., Lopes Da Silva, F.H., 2006. Correlating the alpha rhythm to BOLD using simultaneous EEG/fMRI: Inter-subject variability. Neuroimage 30, 203–213.

Greicius, M., 2008. Resting-state functional connectivity in neuropsychiatric disorders. Curr. Opin. Neurol. 21, 424–430.

Greicius, M.D., Flores, B.H., Menon, V., Glover, G.H., Solvason, H.B., Kenna, H., Reiss, A.L., Schatzberg, A.F., 2007. Resting-State Functional Connectivity in Major Depression: Abnormally Increased Contributions from Subgenual Cingulate Cortex and Thalamus. Biol. Psychiatry 62, 429–437.

Greicius, M.D., Krasnow, B., Reiss, A.L., Menon, V., 2003. Functional connectivity in the resting brain: a network analysis of the default mode hypothesis. Proc. Natl. Acad. Sci. U. S. A. 100, 253–8.

Grigg, O., Grady, C.L., 2010. Task-related effects on the temporal and spatial dynamics of resting-state functional connectivity in the default network. PLoS One 5, e13311.

Gutberlet, I., 2010. Recording EEG Signals Inside the MRI, in: Ullsperger, M., Debener, S. (Eds.), Simultaneous EEG and fMRI: Recording, Analysis, and Application. Oxford University Press, New York, pp. 69–81.

Hampson, M., Driesen, N., Roth, J.K., Gore, J.C., Constable, R.T., 2010. Functional connectivity between task-positive and task-negative brain areas and its relation to working memory performance. Magn. Reson. Imaging 28, 1051–7.

Handwerker, D. a, Roopchansingh, V., Gonzalez-Castillo, J., Bandettini, P. a, 2012. Periodic changes in fMRI connectivity. Neuroimage 63, 1712–9.

Harrison, A.H., Noseworthy, M.D., Reilly, J.P., Connolly, J.F., 2014. Ballistocardiogram correction in simultaneous EEG / fMRI recordings : a comparison of average artifact subtraction and optimal basis set methods using two popular software tools. Crit. Rev. Biomed. Eng. 42, 95–107.

He, B.J., Raichle, M.E., 2009. The fMRI signal, slow cortical potential and consciousness. Trends Cogn. Sci. 13, 302–309.

He, B.J., Snyder, A.Z., Zempel, J.M., Smyth, M.D., Raichle, M.E., 2008. Electrophysiological correlates of the brain's intrinsic large-scale functional architecture. Proc. Natl. Acad. Sci. U. S. A. 105, 16039–44.

Helps, S., James, C., Debener, S., Karl, A., Sonuga-Barke, E.J.S., 2008. Very low frequency EEG oscillations and the resting brain in young adults: a preliminary study of localisation, stability and association with symptoms of inattention. J. Neural Transm. 115, 279–85.

Helps, S.K., Broyd, S.J., James, C.J., Karl, A., Chen, W., Sonuga-Barke, E.J.S., 2010. Altered spontaneous low frequency brain activity in attention deficit/hyperactivity disorder. Brain Res. 1322, 134–43.

Helps, S.K., Broyd, S.J., James, C.J., Karl, A., Sonuga-Barke, E.J.S., 2009. The Attenuation of Very Low Frequency Brain Oscillations in Transitions from a Rest State to Active Attention. J. Psychophysiol. 23, 191–198.

Hiltunen, T., Kantola, J., Abou Elseoud, A., Lepola, P., Suominen, K., Starck, T., Nikkinen, J., Remes, J., Tervonen, O., Palva, S., Kiviniemi, V., Palva, J.M., 2014. Infra-slow EEG fluctuations are correlated with resting-state network dynamics in fMRI. J. Neurosci. 34, 356–62.

Hlinka, J., Alexakis, C., Diukova, A., Liddle, P.F., Auer, D.P., 2010. Slow EEG pattern predicts reduced intrinsic functional connectivity in the default mode network: an inter-subject analysis. Neuroimage 53, 239–46.

Hlinka, J., Palus, M., Vejmelka, M., Mantini, D., Corbetta, M., 2011. Functional connectivity in resting-state fMRI: is linear correlation sufficient? Neuroimage 54, 2218–25.

Horwitz, B., 2003. The elusive concept of brain connectivity. Neuroimage 19, 466–470.

Horwitz, B., Duara, R., Rapoport, S.I., 1984. Intercorrelations of glucose metabolic rates between brain regions: application to healthy males in a state of reduced sensory input. J. Cereb. Blood Flow Metab. 4, 484–499.

Horwitz, B., Grady, C.L., Haxby, J. V, Schapiro, M.B., Rapoport, S.I., Ungerleider, L.G., Mishkin, M., 1992. Functional Associations among Human Posterior Extrastriate Brain Regions during Object and Spatial Vision. J. Cogn. Neurosci. 4, 311–22.

Horwitz, B., McIntosh, A.R., Haxby, J. V, Furey, M., Salerno, J.A., Schapiro, M.B., Rapoport, S.I., Grady, C.L., 1995. Network analysis of PET-mapped visual pathways in Alzheimer type dementia. Neuroreport 6, 2287–92.

Huettel, S., Song, A., McCarthy, G., 2009. Functional magnetic resonance imaging, 2nd ed. Sinauer Associates.

Huster, R.J., Debener, S., Eichele, T., Herrmann, C.S., 2012. Methods for Simultaneous EEG-fMRI: An Introductory Review. J. Neurosci. 32, 6053–6060.

Hutchison, R.M., Womelsdorf, T., Allen, E. a., Bandettini, P. a., Calhoun, V.D., Corbetta, M., Della Penna, S., Duyn, J.H., Glover, G.H., Gonzalez-Castillo, J., Handwerker, D. a., Keilholz, S., Kiviniemi, V., Leopold, D. a., de Pasquale, F., Sporns, O., Walter, M., Chang, C., 2013a. Dynamic functional connectivity: Promise, issues, and interpretations. Neuroimage 80, 360–378.

Hutchison, R.M., Womelsdorf, T., Gati, J.S., Everling, S., Menon, R.S., 2013b. Resting-state networks show dynamic functional connectivity in awake humans and anesthetized macaques. Hum. Brain Mapp. 34, 2154–2177.

Hyde, J.S., Li, R., 2014. Functional connectivity in rat brain at 200 μm resolution. Brain Connect. 4, 470–80.

Ives, J.R., Warach, S., Schmitt, F., Edelman, R.R., Schomer, D.L., 1993. Monitoring the patient's EEG during echo planar MRI. Electroencephalogr. Clin. Neurophysiol. 87, 417–20.

Jann, K., Koenig, T., Dierks, T., Boesch, C., Federspiel, A., 2010. Association of individual resting state EEG alpha frequency and cerebral blood flow. Neuroimage 51, 365–372.

Jerbi, K., Vidal, J.R., Ossandon, T., Dalal, S.S., Jung, J., Hoffmann, D., Minotti, L., Bertrand, O., Kahane, P., Lachaux, J.-P., 2010. Exploring the electrophysiological correlates of the default-mode network with intracerebral EEG. Front. Syst. Neurosci. 4, 27.

Jiang, T., He, Y., Zang, Y., Weng, X., 2004. Modulation of Functional Connectivity during the Resting State and the Motor Task. Hum. Brain Mapp. 22, 63–71.

Karvanen, J., Theis, F.J., 2004. Spatial ICA of fMRI data in time windows. Bayesian Inference Maximum Entropy Methods Sci. Eng.

Keilholz, S., Magnuson, M., 2013. Dynamic properties of functional connectivity in the rodent. Brain … 1–31.

Keilholz, S.D., 2014. Review Article: The Neural Basis of Time-Varying Resting State Functional Connectivity. Brain Connect. 4, 1–32.

Kelly, a M.C., Uddin, L.Q., Biswal, B.B., Castellanos, F.X., Milham, M.P., 2008. Competition between functional brain networks mediates behavioral variability. Neuroimage 39, 527–37.

Khader, P., Schicke, T., Röder, B., Rösler, F., 2008. On the relationship between slow cortical potentials and BOLD signal changes in humans. Int. J. Psychophysiol. 67, 252–61.

Kiviniemi, V., Vire, T., Remes, J., Elseoud, A.A., Starck, T., Tervonen, O., Nikkinen, J., 2011. A sliding time-window ICA reveals spatial variability of the default mode network in time. Brain Connect. 1, 339–47.

Klimesch, W., 1999. EEG alpha and theta oscillations reflect cognitive and memory performance: a review and analysis. Brain Res. Brain Res. Rev. 29, 169–195.

Koch, C., 2009. The SCP is not specific enough to represent conscious content. Trends Cogn. Sci. 13, 367.

Koenig, T., Prichep, L., Lehmann, D., Sosa, P.V., Braeker, E., Kleinlogel, H., Isenhart, R., John, E.R., 2002. Millisecond by millisecond, year by year: normative EEG microstates and developmental stages. Neuroimage 16, 41–48.

Koenig, T., Studer, D., Hubl, D., Melie, L., Strik, W.K., 2005. Brain connectivity at different time-scales measured with EEG. Philos. Trans. R. Soc. Lond. B. Biol. Sci. 360, 1015–1023.

Kornhuber, H.H., Deecke, L., 1965. Changes inthe brain potential in voluntary movements and passive movements in man: readiness potential and reafferent potentials. Pflugers Arch. Gesamte Physiol. Menschen Tiere 284, 1–17.

Kwong, K.K., Belliveau, J.W., Chesler, D.A., Goldberg, I.E., Weisskoff, R.M., Poncelet, B.P., Kennedy, D.N., Hoppel, B.E., Cohen, M.S., Turner, R., 1992. Dynamic magnetic resonance imaging of human brain activity during primary sensory stimulation. Proc. Natl. Acad. Sci. U. S. A. 89, 5675–5679.

Laufs, H., Daunizeau, J., Carmichael, D.W., Kleinschmidt, A., 2008. Recent advances in recording electrophysiological data simultaneously with magnetic resonance imaging. Neuroimage 40, 515–28.

Laufs, H., Holt, J.L., Elfont, R., Krams, M., Paul, J.S., Krakow, K., Kleinschmidt, a., 2006. Where the BOLD signal goes when alpha EEG leaves. Neuroimage 31, 1408–1418.

Laufs, H., Kleinschmidt, a, Beyerle, a, Eger, E., Salek-Haddadi, a, Preibisch, C., Krakow, K., 2003a. EEG-correlated fMRI of human alpha activity. Neuroimage 19, 1463–1476.

Laufs, H., Krakow, K., Sterzer, P., Eger, E., Beyerle, a, Salek-Haddadi, a, Kleinschmidt, a, 2003b. Electroencephalographic signatures of attentional and cognitive default modes in spontaneous brain activity fluctuations at rest. Proc. Natl. Acad. Sci. U. S. A. 100, 11053–11058.

Lauterbur, P.C., 1973. Image formation by induced local interactions: Examples employing nuclear magnetic resonance. Nature 242, 190–191.

Lee, H.-L., Zahneisen, B., Hugger, T., LeVan, P., Hennig, J., 2013. Tracking dynamic resting-state networks at higher frequencies using MR-encephalography. Neuroimage 65, 216–22.

Lee, M.H., Smyser, C.D., Shimony, J.S., 2013. Resting-state fMRI: A review of methods and clinical applications. Am. J. Neuroradiol. 34, 1866–1872.

Lehmann, D., Strik, W.K., Henggeler, B., Koenig, T., Koukkou, M., 1998. Brain electric microstates and momentary conscious mind states as building blocks of spontaneous thinking: I. Visual imagery and abstract thoughts. Int. J. Psychophysiol. 29, 1–11.

Lenoski, B., Baxter, L.C., Karam, L.J., Maisog, J., Debbins, J., 2008. On the performance of autocorrelation estimation algorithms for fMRI analysis. IEEE J. Sel. Top. Signal Process. 2, 828–838.

Leonardi, N., Ville, D. Van De, 2015. On spurious and real fluctuations of dynamic functional connectivity during rest. Neuroimage 104, 430–436.

Liao, R., Krolik, J.L., McKeown, M.J., 2005. An information-theoretic criterion for intrasubject alignment of FMRI time series: Motion corrected independent component analysis. IEEE Trans. Med. Imaging 24, 29–44.

Liu, J., Calhoun, V., 2007. Parallel independent component analysis for multimodal analysis: application to fMRI and EEG data. Biomed. Imaging From Nano to Macro, … 1028–1031.

Liu, X., Duyn, J.H., 2013. Time-varying functional network information extracted from brief instances of spontaneous brain activity. Proc. Natl. Acad. Sci. U. S. A. 110, 4392–7.

Logothetis, N.K., Pauls, J., Augath, M., Trinath, T., Oeltermann, A., 2001. Neurophysiological investigation of the basis of the fMRI signal. Nature.

Logothetis, N.K., Wandell, B. a, 2004. Interpreting the BOLD signal. Annu. Rev. Physiol. 66, 735–69.

Lowe, M.J., Dzemidzic, M., Lurito, J.T., Mathews, V.P., Phillips, M.D., 2000. Correlations in low-frequency BOLD fluctuations reflect cortico-cortical connections. Neuroimage 12, 582–587.

Lowe, M.J., Mock, B.J., Sorenson, J. a, 1998. Functional connectivity in single and multislice echoplanar imaging using resting-state fluctuations. Neuroimage 7, 119–32.

Magri, C., Schridde, U., Murayama, Y., Panzeri, S., Logothetis, N.K., 2012. The amplitude and timing of the BOLD signal reflects the relationship between local field potential power at different frequencies. J. Neurosci. 32, 1395–407.

Majeed, W., 2010. Spatiotemporal Dynamics of Low Frequency Fluctuations in BOLD fMRI.

Majeed, W., Magnuson, M., Hasenkamp, W., Schwarb, H., Schumacher, E.H., Barsalou, L., Keilholz, S.D., 2011. Spatiotemporal dynamics of low frequency BOLD fluctuations in rats and humans. Neuroimage 54, 1140–50.

Majeed, W., Magnuson, M., Keilholz, S.D., 2009. Spatiotemporal dynamics of low frequency fluctuations in BOLD fMRI of the rat. J. Magn. Reson. Imaging 30, 384–93.

Mantini, D., Perrucci, M.G., Del Gratta, C., Romani, G.L., Corbetta, M., 2007. Electrophysiological signatures of resting state networks in the human brain. Proc. Natl. Acad. Sci. U. S. A. 104, 13170–5.

McKeown, M., Makeig, S., Brown, G., 1997. Analysis of fMRI data by blind separation into independent spatial components.

Metter, E.J., Riege, W.H., Kuhl, D.E., Phelps, M.E., 1984. Cerebral metabolic relationships for selected brain regions in healthy adults. J. Cereb. Blood Flow Metab. 4, 1–7.

Meyer, M.C., van Oort, E.S.B., Barth, M., 2013. Electrophysiological correlation patterns of resting state networks in single subjects: a combined EEG-fMRI study. Brain Topogr. 26, 98–109.

Michel, C.M., Murray, M.M., Lantz, G., Gonzalez, S., Spinelli, L., Grave de Peralta, R., 2004. EEG source imaging. Clin. Neurophysiol. 115, 2195–222.

Miezin, F.M., Maccotta, L., Ollinger, J.M., Petersen, S.E., Buckner, R.L., 2000. Characterizing the hemodynamic response: effects of presentation rate, sampling procedure, and the possibility of ordering brain activity based on relative timing. Neuroimage 11, 735–59.

Mitzdorf, U., 1985. Current source-density method and application in cat cerebral cortex: investigation of evoked potentials and EEG phenomena. Physiol. Rev. 65, 37–100.

Møller, A.R., 2011. Intraoperative Neurophysiological Monitoring, 3rd ed.

Monto, S., Palva, S., Voipio, J., Palva, J.M., 2008. Very slow EEG fluctuations predict the dynamics of stimulus detection and oscillation amplitudes in humans. J. Neurosci. 28, 8268–72.

Moosmann, M., Ritter, P., Krastel, I., Brink, A., Thees, S., Blankenburg, F., Taskin, B., Obrig, H., Villringer, A., 2003. Correlates of alpha rhythm in functional magnetic resonance imaging and near infrared spectroscopy. Neuroimage 20, 145–158.

Moosmann, M., Schönfelder, V.H., Specht, K., Scheeringa, R., Nordby, H., Hugdahl, K., 2009. Realignment parameter-informed artefact correction for simultaneous EEG-fMRI recordings. Neuroimage 45, 1144–1150.

Mullinger, K., Bowtell, R., 2010. Influence of EEG Equipment on MR Image Quality, in: Ullsperger, M., Debener, S. (Eds.), Simultaneous EEG and fMRI: Recording, Analysis, and Application. Oxford University Press, pp. 107–116.

Mullinger, K.J., Havenhand, J., Bowtell, R., 2013. Identifying the sources of the pulse artefact in EEG recordings made inside an MR scanner. Neuroimage 71, 75–83.

Murakami, S., Okada, Y., 2006. Contributions of principal neocortical neurons to magnetoencephalography and electroencephalography signals. J. Physiol. 575, 925–936.

Musso, F., Brinkmeyer, J., Mobascher, A., Warbrick, T., Winterer, G., 2010. Spontaneous brain activity and EEG microstates. A novel EEG/fMRI analysis approach to explore resting-state networks. Neuroimage 52, 1149–61.

Nair, D.G., 2005. About being BOLD. Brain Res. Brain Res. Rev. 50, 229–43.

Neuner, I., Arrubla, J., Felder, J., Shah, N.J., 2013. Simultaneous EEG-fMRI acquisition at low, high and ultra-high magnetic fields up to 9.4 T: Perspectives and challenges. Neuroimage 102, 71–79.

Niazy, R.K., Beckmann, C.F., Iannetti, G.D., Brady, J.M., Smith, S.M., 2005. Removal of FMRI environment artifacts from EEG data using optimal basis sets. Neuroimage 28, 720–737.

Nir, Y., Mukamel, R., Dinstein, I., Privman, E., Harel, M., Fisch, L., Gelbard-Sagiv, H., Kipervasser, S., Andelman, F., Neufeld, M.Y., Kramer, U., Arieli, A., Fried, I., Malach, R., 2008. Interhemispheric correlations of slow spontaneous neuronal fluctuations revealed in human sensory cortex. Nat. Neurosci. 11, 1100–1108.

Nita, D. a, Vanhatalo, S., Lafortune, F.-D., Voipio, J., Kaila, K., Amzica, F., 2004. Nonneuronal origin of CO2-related DC EEG shifts: an in vivo study in the cat. J. Neurophysiol. 92, 1011–1022.

Norton, S., Jewett, R.E., 1965. Frequencies of slow potential oscillations in the cortex of cats. Electroencephalogr. Clin. Neurophysiol. 19, 377–86.

Ogawa, S., Lee, T., 1990. Brain magnetic resonance imaging with contrast dependent on blood oxygenation. Proc. … 87, 9868–72.

Ogawa, S., Tank, D.W., Menon, R., Ellermann, J.M., Kim, S.G., Merkle, H., Ugurbil, K., 1992. Intrinsic signal changes accompanying sensory stimulation: functional brain mapping with magnetic resonance imaging. Proc Natl Acad Sci U S A 89, 5951–5955.

Palva, J.M., Monto, S., Kulashekhar, S., Palva, S., 2010. Neuronal synchrony reveals working memory networks and predicts individual memory capacity. Proc. Natl. Acad. Sci. U. S. A. 107, 7580–7585.

Palva, J.M., Palva, S., 2012. Infra-slow fluctuations in electrophysiological recordings, blood-oxygenation-level-dependent signals, and psychophysical time series. Neuroimage 62, 2201–11.

Palva, S., Linkenkaer-Hansen, K., Näätänen, R., Palva, J.M., 2005. Early neural correlates of conscious somatosensory perception. J. Neurosci. 25, 5248–5258.

Pan, W.-J., Thompson, G.J., Magnuson, M.E., Jaeger, D., Keilholz, S., 2013. Infraslow LFP correlates to resting-state fMRI BOLD signals. Neuroimage 74, 288–97.

Peraza, L.R., Asghar, A.U.R., Green, G., Halliday, D.M., 2012. Volume conduction effects in brain network inference from electroencephalographic recordings using phase lag index. J. Neurosci. Methods 207, 189–99.

Petersson, K.M., Nichols, T.E., Poline, J.B., Holmes, a P., 1999. Statistical limitations in functional neuroimaging. I. Non-inferential methods and statistical models. Philos. Trans. R. Soc. Lond. B. Biol. Sci. 354, 1239–1260.

Picchioni, D., Horovitz, S.G., Fukunaga, M., Carr, W.S., Meltzer, J. a, Balkin, T.J., Duyn, J.H., Braun, A.R., 2011. Infraslow EEG oscillations organize large-scale cortical-subcortical interactions during sleep: a combined EEG/fMRI study. Brain Res. 1374, 63–72.

Poldrack, R.A., Mumford, J.A., Nichols, T.E., 2011. Handbook of functional MRI data analysis. Cambridge University Press, New York.

Prado, J., Weissman, D.H., 2011. Heightened interactions between a key default-mode region and a key task-positive region are linked to suboptimal current performance but to enhanced future performance. Neuroimage 56, 2276–82.

Raichle, M.E., 2011. The Restless Brain. Brain Connect. 1, 3–12.

Raichle, M.E., MacLeod, a M., Snyder, a Z., Powers, W.J., Gusnard, D. a, Shulman, G.L., 2001. A default mode of brain function. Proc. Natl. Acad. Sci. U. S. A. 98, 676–82.

Rauch, A., Rainer, G., Logothetis, N.K., 2008. The effect of a serotonin-induced dissociation between spiking and perisynaptic activity on BOLD functional MRI. Proc. Natl. Acad. Sci. U. S. A. 105, 6759–6764.

Razavi, N., Jann, K., Koenig, T., Kottlow, M., Hauf, M., Strik, W., Dierks, T., 2013. Shifted coupling of EEG driving frequencies and fMRI resting state networks in schizophrenia spectrum disorders. PLoS One 8, e76604.

Rosazza, C., Minati, L., 2011. Resting-state brain networks: Literature review and clinical applications. Neurol. Sci. 32, 773–785.

Rösler, F., Heil, M., Röder, B., 1997. Slow negative brain potentials as reflections of specific modular resources of cognition. Biol. Psychol. 45, 109–141.

Rytty, R., Nikkinen, J., Paavola, L., Abou Elseoud, A., Moilanen, V., Visuri, A., Tervonen, O., Renton, A.E., Traynor, B.J., Kiviniemi, V., Remes, A.M., 2013. GroupICA dual regression analysis of resting state networks in a behavioral variant of frontotemporal dementia. Front. Hum. Neurosci. 7, 461.

Sakoğlu, Ü., Pearlson, G.D., Kiehl, K. a., Wang, Y.M., Michael, A.M., Calhoun, V.D., 2010. A method for evaluating dynamic functional network connectivity and task-modulation: Application to schizophrenia. Magn. Reson. Mater. Physics, Biol. Med. 23, 351–366.

Sato, J.R., Junior, E.A., Takahashi, D.Y., de Maria Felix, M., Brammer, M.J., Morettin, P.A., 2006. A method to produce evolving functional connectivity maps during the course of an fMRI experiment using wavelet-based time-varying Granger causality. Neuroimage 31, 187–96.

Scheeringa, R., Bastiaansen, M.C.M., Petersson, K.M., Oostenveld, R., Norris, D.G., Hagoort, P., 2008. Frontal theta EEG activity correlates negatively with the default mode network in resting state. Int. J. Psychophysiol. 67, 242–51.

Shah, A.S., Bressler, S.L., Knuth, K.H., Ding, M., Mehta, A.D., Ulbert, I., Schroeder, C.E., 2004. Neural Dynamics and the Fundamental Mechanisms of Event-related Brain Potentials. Cereb. Cortex 14, 476–483.

Sharma, R., 2012. Functional Magnetic Resonance Imaging - Advanced Neuroimaging Applications.

Sheline, Y.I., Raichle, M.E., 2013. Resting state functional connectivity in preclinical Alzheimer's disease. Biol. Psychiatry 74, 340–7.

Shiavi, R., 2007. Introduction to Applied Statistical Signal Analysis, 3rd ed. Academic Press.

Shmuel, A., Augath, M., Oeltermann, A., Logothetis, N.K., 2006. Negative functional MRI response correlates with decreases in neuronal activity in monkey visual area V1. Nat. Neurosci. 9, 569–577.

Shmueli, K., van Gelderen, P., de Zwart, J. a, Horovitz, S.G., Fukunaga, M., Jansma, J.M., Duyn, J.H., 2007. Low-frequency fluctuations in the cardiac rate as a source of variance in the resting-state fMRI BOLD signal. Neuroimage 38, 306–20.

Singh, K.D., Fawcett, I.P., 2008. Transient and linearly graded deactivation of the human default-mode network by a visual detection task. Neuroimage 41, 100–112.

Smith, S.M., Miller, K.L., Moeller, S., Xu, J., Auerbach, E.J., Woolrich, M.W., Beckmann, C.F., Jenkinson, M., Andersson, J., Glasser, M.F., Van Essen, D.C., Feinberg, D. a, Yacoub, E.S., Ugurbil, K., 2012. Temporally-independent functional modes of spontaneous brain activity. Proc. Natl. Acad. Sci. U. S. A. 109, 3131–6.

Speckmann, E.J., 1997. Generation of field potentials in the brain. J. Clin. Pharmacol. 37, 8S–10S.

Stam, C.J., Nolte, G., Daffertshofer, A., 2007. Phase lag index: assessment of functional connectivity from multi channel EEG and MEG with diminished bias from common sources. Hum. Brain Mapp. 28, 1178–93.

Stamm, J.S., Whipple, S.C., Born, J., 1987. Effects of spontaneous cortical slow potentials on semantic information processing. Int. J. Psychophysiol. 5, 11–8.

Steriade, M., 2001. Impact of network activities on neuronal properties in corticothalamic systems. J. Neurophysiol. 86, 1–39.

Steriade, M., 2006. Grouping of brain rhythms in corticothalamic systems. Neuroscience 137, 1087–1106.

Tagliazucchi, E., von Wegner, F., Morzelewski, A., Brodbeck, V., Laufs, H., 2012. Dynamic BOLD functional connectivity in humans and its electrophysiological correlates. Front. Hum. Neurosci. 6, 339.

Tallgren, P., 2006. DC-EEG for routine clinical use: methods and clinical impact.

Tallgren, P., Vanhatalo, S., Kaila, K., Voipio, J., 2005. Evaluation of commercially available electrodes and gels for recording of slow EEG potentials. Clin. Neurophysiol. 116, 799–806.

Thomas, C.G., Harshman, R. a, Menon, R.S., 2002. Noise reduction in BOLD-based fMRI using component analysis. Neuroimage 17, 1521–1537.

Thompson, G.J., Magnuson, M.E., Merritt, M.D., Schwarb, H., Pan, W.-J., McKinley, A., Tripp, L.D., Schumacher, E.H., Keilholz, S.D., 2013a. Short-time windows of correlation between large-scale functional brain networks predict vigilance intraindividually and interindividually. Hum. Brain Mapp. 34, 3280–98.

Thompson, G.J., Merritt, M.D., Pan, W.-J., Magnuson, M.E., Grooms, J.K., Jaeger, D., Keilholz, S.D., 2013b. Neural correlates of time-varying functional connectivity in the rat. Neuroimage 83, 826–36.

Thompson, G.J., Pan, W.-J., Billings, J.C.W., Grooms, J.K., Shakil, S., Jaeger, D., Keilholz, S.D., 2014. Phase-amplitude coupling and infraslow (<1 Hz) frequencies in the rat brain: relationship to resting state fMRI. Front. Integr. Neurosci. 8, 41.

Tian, L., Jiang, T., Wang, Y., Zang, Y., He, Y., Liang, M., Sui, M., Cao, Q., Hu, S., Peng, M., Zhuo, Y., 2006. Altered resting-state functional connectivity patterns of anterior cingulate cortex in adolescents with attention deficit hyperactivity disorder. Neurosci. Lett. 400, 39–43.

Tohka, J., Foerde, K., Aron, A.R., Tom, S.M., Toga, A.W., Poldrack, R. a, 2008. Automatic independent component labeling for artifact removal in fMRI. Neuroimage 39, 1227–45.

Torrence, C., Compo, G.P., 1998. A Practical Guide to Wavelet Analysis. Bull. Am. Meteorol. Soc. 79, 61–78.

Trimmel, M., Mikowitsch, A., Groll-Knapp, E., Haider, M., 1990. Occurrence of infraslow potential oscillations in relation to task, ability to concentrate and intelligence. Int. J. Psychophysiol. 9, 167–170.

Trimmel, M., Strässler, F., Knerer, K., 2001. Brain DC potential changes of computerized tasks and paper/pencil tasks. Int. J. Psychophysiol. 187–194.

Uddin, L.Q., Kelly, a M., Biswal, B.B., Castellanos, F.X., Milham, M.P., 2009. Functional connectivity of default mode network components: correlation, anticorrelation, and causality. Hum. Brain Mapp. 30, 625–37.

Van de Ven, V.G., Formisano, E., Prvulovic, D., Roeder, C.H., Linden, D.E.J., 2004. Functional connectivity as revealed by spatial independent component analysis of fMRI measurements during rest. Hum. Brain Mapp. 22, 165–78.

Van den Heuvel, M.P., Hulshoff Pol, H.E., 2010. Exploring the brain network: A review on resting-state fMRI functional connectivity. Eur. Neuropsychopharmacol. 20, 519–534.

Van Dijk, K.R. a, Hedden, T., Venkataraman, A., Evans, K.C., Lazar, S.W., Buckner, R.L., 2010. Intrinsic functional connectivity as a tool for human connectomics: theory, properties, and optimization. J. Neurophysiol. 103, 297–321.

Vanhatalo, S., Palva, J.M., Holmes, M.D., Miller, J.W., Voipio, J., Kaila, K., 2004. Infraslow oscillations modulate excitability and interictal epileptic activity in the human cortex during sleep. Proc. Natl. Acad. Sci. U. S. A. 101, 5053–7.

Vanhatalo, S., Tallgren, P., Andersson, S., Sainio, K., Voipio, J., Kaila, K., 2002. DC-EEG discloses prominent, very slow activity patterns during sleep in preterm infants. Clin. Neurophysiol. 113, 1822–1825.

Vanhatalo, S., Tallgren, P., Becker, C., Holmes, M.., Miller, J.., Kaila, K., Voipio, J., 2003. Scalp-recorded slow EEG responses generated in response to hemodynamic changes in the human brain. Clin. Neurophysiol. 114, 1744–1754.

Vanhatalo, S., Voipio, J., Kaila, K., 2005. Full-band EEG (FbEEG): an emerging standard in electroencephalography. Clin. Neurophysiol. 116, 1–8.

VanRullen, R., Carlson, T., Cavanagh, P., 2007. The blinking spotlight of attention. Proc. Natl. Acad. Sci. U. S. A. 104, 19204–19209.

VanRullen, R., Koch, C., 2003. Is perception discrete or continuous? Trends Cogn. Sci. 7, 207–213.

Veer, I.M., Beckmann, C.F., van Tol, M.-J., Ferrarini, L., Milles, J., Veltman, D.J., Aleman, A., van Buchem, M. a, van der Wee, N.J., Rombouts, S. a R.B., 2010.

Whole brain resting-state analysis reveals decreased functional connectivity in major depression. Front. Syst. Neurosci. 4, 1–10.

Voipio, J., Tallgren, P., Heinonen, E., Vanhatalo, S., Kaila, K., 2003. Millivolt-scale DC shifts in the human scalp EEG: evidence for a nonneuronal generator. J. Neurophysiol. 89, 2208–14.

Walter, W., Cooper, R., Aldridge, V., 1964. Contingent negative variation: an electric sign of sensorimotor association and expectancy in the human brain. Nature.

Wang, K., Liang, M., Wang, L., Tian, L., Zhang, X., Li, K., Jiang, T., 2007. Altered functional connectivity in early Alzheimer's disease: A resting-state fMRI study. Hum. Brain Mapp. 28, 967–978.

Wendel, K., Väisänen, O., Malmivuo, J., Gencer, N.G., Vanrumste, B., Durka, P., Magjarević, R., Supek, S., Pascu, M.L., Fontenelle, H., Grave de Peralta Menendez, R., 2009. EEG/MEG source imaging: methods, challenges, and open issues. Comput. Intell. Neurosci. 2009, 656092.

Whitfield-Gabrieli, S., Thermenos, H.W., Milanovic, S., Tsuang, M.T., Faraone, S. V, McCarley, R.W., Shenton, M.E., Green, A.I., Nieto-Castanon, A., LaViolette, P., Wojcik, J., Gabrieli, J.D.E., Seidman, L.J., 2009. Hyperactivity and hyperconnectivity of the default network in schizophrenia and in first-degree relatives of persons with schizophrenia. Proc. Natl. Acad. Sci. U. S. A. 106, 1279–1284.

Wise, R.G., Ide, K., Poulin, M.J., Tracey, I., 2004. Resting fluctuations in arterial carbon dioxide induce significant low frequency variations in BOLD signal. Neuroimage 21, 1652–1664.

Womelsdorf, T., Fries, P., Mitra, P.P., Desimone, R., 2006. Gamma-band synchronization in visual cortex predicts speed of change detection. Nature 439, 733–736.

Worsley, K., Friston, K., 1995. Analysis of fMRI time-series revisited—again. Neuroimage.

Yeo, B.T.T., Krienen, F.M., Sepulcre, J., Sabuncu, M.R., Lashkari, D., Hollinshead, M., Roffman, J.L., Smoller, J.W., Zöllei, L., Polimeni, J.R., Fischl, B., Liu, H., Buckner, R.L., 2011. The organization of the human cerebral cortex estimated by intrinsic functional connectivity. J. Neurophysiol. 106, 1125–1165.

Yuan, H., Zotev, V., Phillips, R., Drevets, W.C., Bodurka, J., 2012. Spatiotemporal dynamics of the brain at rest - Exploring EEG microstates as electrophysiological signatures of BOLD resting state networks. Neuroimage 60, 2062–2072.

Zarahn, E., Aguirre, G., D'Esposito, M., 1997. Empirical analyses of BOLD fMRI statistics. Neuroimage 212, 199–212.

Zeki, S., Watson, J.D., Lueck, C.J., Friston, K.J., Kennard, C., Frackowiak, R.S., 1991. A direct demonstration of functional specialization in human visual cortex. J. Neurosci. 11, 641–649.